Design of Multi-band, Broadband Passive Circuits and their application in RF Power Amplifiers

THIS THESIS IS SUBMITTED IN PARTIAL FULFILMENT OF THE REQUIREMENTS FOR THE DEGREE OF

DOCTOR OF PHILOSOPHY

By

Antra Saxena

PhD16108

Under the supervision of

Prof Mohammad S. Hashmi

Department of Electronics and Communication Engineering

Indraprastha Institute of Information Technology Delhi, New Delhi- 110020

December, 2022

I would like to dedicate this thesis to my loving family

and

supporting husband Deepayan . . .

Certificate

December 14, 2022

This is to certify that the thesis submitted by Antra Saxena (PhD16108) entitled "Design of Multi-band, Broadband Passive Circuits and their application in RF Power Amplifiers" in fulfilment for the award of Doctor of Philosophy is a record of original research work carried out by her during the academic year 2016 - 2022 under my supervision

The thesis has not formed the basis for the award of any degree or other title in this or any other university. I hereby confirm the originality of the work.

Prof Mohammad S. Hashmi

Declaration

I, at this moment, declare that except where specific reference is made to the work of others, the contents of this dissertation are original and have not been submitted in part or full for consideration for any other degree or qualification in this or any other university. This dissertation is my work and contains nothing about the outcome of work done in collaboration with others, except as specified in the text and Acknowledgements.

Antra

Antra Saxena

December 2022

Acknowledgements

First of all, I would like to thank and praise Almighty God; this thesis would not be completed without his grace. I want to express my sincere gratitude to my supervisor, Prof Mohammad S. Hashmi, for his constant guidance, motivation and support throughout my research journey.

Besides my supervisor, my sincere thanks go to my internal thesis committee members, including Dr Vivek Bohara and Dr Sujay Deb, for their immense encouragement and support. Also, I would like to thank other faculty members, Dr Shobha Sundar Ram and Dr Sanat Biswas, who encouraged and motivated me several times during this research period.

My sincere thanks go to Prof Fadhel M. Ghannouchi, Alberta Innovates/the Canada Research Chair, and the Founding Director of the Intelligent RF Radio Technology Laboratory (iRadio Lab) and Prof Mohamed Helaoui, Department of Electrical and Computer Engineering, University of Calgary, Calgary, Canada for offering visiting research scholar opportunity at iRadio Lab and providing a platform to work on diverse fields. Also, I would like to thank Dr Karun Rawat for providing measurement setups and immense knowledgeable discussion that encouraged me to think creatively, technically and spiritually.

I would also like to extend my heartfelt obligations to my parents, in-laws, my sister Ms Ekta Saxena, and brother-in-law Mr Abhik Ray who constantly support, encourage and teach me the lesson of perseverance that always help me to get motivated. I am incredi-

bly thankful to my husband, Dr Deepayan Banerjee, who unconditionally supported and motivated me through this journey. I want to thank my niece Viana Ray for her love and unconscious support, which helped me during tough times. I am thankful to my friend Ms Sufia Khatoon, Ms Khujasta Afreen, and Dr Asma Iqbal for their remarkable support, as they were always there to help me whenever I felt depressed from a long distance. I want to give special thanks to Ms Dilnashin Anwar, who also provides technical and spiritual support.

Also last but not least, I would like to thank all seniors, juniors, lab staff and non-technical staff for their cooperation during this research period.

Abstract

The last two years have shown a different life scenario when the pandemic hit every part of the world. It reshaped the life of humans rapidly by forcing work from home, online education, online shopping and more. The pandemic has put brakes on this constantly fast-moving world. However, technology bridged the gap of physical distancing by providing everything online, from medical assistance to non-essential items, from family video-calling to online schooling and many more. The internet has played a preeminent role in the last two years, and technology in the hand of every human, from kids to adults, assists in overcoming stressful situations. The technologies that will formulate the next-generation wireless systems are being defined today.

The primary motivation of this research was the increased complexity of mobile devices, resulting in more significant challenges and stringent requirements in the design of all front-end components, including filters, power dividers, matching networks and power amplifiers (PAs). Inevitably, RF front-end solutions for different applications, including telecommunication, aerospace, military and others, have moved from the discrete solution with one or more single-band circuits, including PA modules, matching networks etc., towards the ultimate multi-band solutions. In this approach, one module will support all existing standards while covering different frequency bands of operation.

This doctoral dissertation focused on the challenges and considerations in designing different components in any RF front-end module. The main contribution of this thesis is to develop dual-band/broadband architectures for passive devices, including matching networks and

power dividers, as well as their applications in active devices such as harmonically tuned power amplifiers. Various design methods have been discussed and analyzed to provide different architectures with practical solutions. Design and analysis of distinct matching networks are proposed. The theoretical basis for designing the dual-band matching networks, closed-form equations, analysis, additional case studies and fabrication of prototypes for validation purposes is contributed. Different scenarios discussed include real-to-real matching, real-to-complex matching and complex-to-complex matching, depending on the nature of the source and load type. Also, broadband power dividers have been studied rigorously to operate over a wide range of frequencies with DC blocking capability, which is a primary demand in any RF front end. Two different broadband power dividers operating over a wide range of frequencies, including their design and analysis, are proposed. Other methods are presented with inherent DC-blocking capabilities that are useful in many practical applications. Along with passive circuits, the multi-band matching network is utilized to design power amplifiers that can provide desirable performance in terms of efficiency and gain. Two methodologies are proposed, which are simple and supported by closed-form equations that maintain easy fabrication and are pragmatic in implementation. It considers the application of multi-band matching networks in designing high-efficiency RF power amplifiers.

Thus the key findings of this thesis include different multi-band/broadband passive devices, including matching networks and power dividers which are accompanied by closed-form equations to obtain mathematical formulations for easy designing and prototyping. The application of matching networks in active devices, i.e. power amplifiers, is explored. The harmonically tuned power amplifier, accompanied by formulations and design procedures to obtain optimum performance, is verified with design examples and case studies.

Table of contents

List of figures **xv**

List of tables **xxi**

1 Introduction **1**

1.1 Motivation 2

1.2 Impedance Matching Networks 6

1.2.1 Resistance 8

1.2.2 Impedance 9

1.2.3 Admittance 11

1.2.4 Characteristic Impedance 12

1.2.5 Impedance Matching Techniques 14

1.3 Power Dividers 22

1.4 Power Amplifiers 24

2 Literature Review **31**

2.1 Background 31

2.1.1 Impedance Matching Networks 32

2.1.2 Power Dividers 37

2.1.3 Power Amplifiers 40

3 Impedance Matching Networks - Dual-Band with FDCL **45**

3.1 Introduction 45

3.2 Analysis of Dual-Band Impedance Matching Network - Design 1 48

3.2.1 Proposed Matching Network 49

3.2.2 Design Example and Case studies 52

3.3 Analysis of Dual-Band Impedance Matching Network - Design 2 56

3.3.1 Proposed Matching Network 56

3.3.2 Design Example and Case studies 60

3.4 Analysis of Dual-Band Impedance Matching Network - Design 3 64

3.4.1 Proposed Matching Network 65

3.4.2 Design Equations 66

3.4.3 Design Examples, Prototype, and Results 68

3.5 Summary 72

4 Power Dividers - Broadband Frequency Response **73**

4.1 Introduction 73

4.2 Broadband Power Divider - Design 1 74

4.2.1 Design and Analysis 74

4.2.2 Case-studies, Results and Analysis 84

4.2.3 Wideband DC Isolated WPD 87

4.3 DC Isolated Broadband Power Divider - Design 2 94

4.3.1 Circuit Topology and Analysis 94

4.3.2 Frequency Response Analysis 98

4.3.3 Case Studies, Simulation and Measurement 102

4.4 Summary 107

5 Harmonic Tuned Power Amplifier - Application of Matching Networks **109**

5.1 Introduction 109
5.2 Design of Harmonic Tuned Power Amplifier - Design 1 111
5.2.1 Circuit Design and Analysis 111
5.2.2 Case Study and Experimental Evaluation 117
5.3 Design of a Harmonically Tuned RF Power Amplifier - Design 2 122
5.3.1 Circuit Design and Analysis 124
5.3.2 Experimental Validation and Results 127
5.4 Summary 130

6 Conclusions and Future Work **131**
6.1 Conclusion 131
6.2 Future Work 132

References **135**

Publications **157**

List of figures

1.1 5G: new standard for number of applications [8] 3
1.2 RF front end with multiple devices to operate at different bands 4
1.3 RF front end with multi-band or broadband circuitry for multiple bands of operation 5
1.4 Multi-band power amplifier operating at different frequencies of application [14] 6
1.5 Block diagram representing RF power transferring from input to output . . 7
1.6 Concept of resistance 8
1.7 Impedance containing both resistance and reactance 9
1.8 Circuit with resistor 10
1.9 Circuit with inductor 10
1.10 Circuit with capacitor 11
1.11 Transmission line model over an infinitesimal length Δx 12
1.12 Block diagram representing impedance matching network between source and load network 15
1.13 Matching scenario for resistive unequal source and load 15
1.14 Matching scenario for resistive source and reactive load 16
1.15 Matching scenario for reactive source and load 16
1.16 Multi-band matching scenario for resistive unequal source and load 17

1.17 Multi-band matching scenario for resistive source and reactive load varying with frequency 18
1.18 Multi-band matching scenario for reactive source and load both varying with frequency 18
1.19 Representation of darlington theorem 19
1.20 Power division by power divider 22
1.21 Schematic of Wilkinson power divider 23
1.22 RF power amplifier with amplification of RF input signal 24
1.23 3W power amplifier from acquitek 25
1.24 Block diagram showing RF power amplifier components 26

2.1 Block diagram of RF front end transceiver 31

3.1 Quarter-wave transformer 45
3.2 Smith chart tool to match source impedance to load impedance 46
3.3 Block diagram depicting different modules of RF front end with single matching network 47
3.4 Block diagram depicting different modules with cascaded matching networks 48
3.5 Proposed dual-band impedance transformer 49
3.6 S_{11}(dB) for different cases listed in table 3.1 53
3.7 Fabricated prototype for real load of 250Ω 53
3.8 Fabricated prototype for FDCL of 100-j35.4Ω and 150-j6.4Ω 54
3.9 EM simulation vs measured results for real load of 250 Ω 54
3.10 EM simulation vs measured results for load=100-j35.4 @0.9GHz 55
3.11 EM simulation vs measured results for load=150-j6.4 @2.4GHz 55
3.12 Proposed dual-band impedance transformer 57
3.13 Section-A cancelling the imaginary value of load 58
3.14 Section-B matching the unequal real value to source 59

3.15 Architecture for matching of unequal real loads 61
3.16 S_{11}(dB) for different cases listed in table 3.5 62
3.17 Fabricated prototype with load-A @ 1 GHz: Load A-50+j80 62
3.18 Fabricated prototype with load-B @ 1 GHz: Load B-60+j120 63
3.19 EM simulation vs measured results 63
3.20 EM simulation vs measured results 63
3.21 Block diagram of a typical dual-band front-end 65
3.22 Proposed dual-band matching network 65
3.23 Design of section-A 66
3.24 Design of section-C 68
3.25 S11(dB) for different cases listed in table 3.8 69
3.26 Prototype of dual-band matching network 69
3.27 Result for load = 30+j*100 and source = 60-j*130 at freq=1 GHz (Case 1) . 70
3.28 Result for load = 40+j*120 and source = 80+j*150 at freq=1.8 GHz (Case 1) 70

4.1 Schematic of the proposed wideband WPD 75
4.2 Even-mode half-circuit 76
4.3 Transfer characteristics of the proposed network 79
4.4 Transfer characteristics of Chebyshev band pass filter 80
4.5 Odd-mode half-circuit 81
4.6 Transformed odd-mode half-circuit 81
4.7 Relation between isolation resistor values 82
4.8 Simulated S-parameter for $\theta_c = 55^\circ$ 83
4.9 Simulated S-parameters for $\theta_c = 60^\circ$ 83
4.10 Simulated S-parameters for $\theta_c = 65^\circ$ 84
4.11 Fabricated prototype of the proposed WPD 85
4.12 Measurement setup for (A): S_{11} (B): S_{21} for $\theta_c = 55^\circ$ 85

4.13 EM vs measured S-parameters for S_{11} for $\theta_c = 55^\circ$ 86
4.14 EM vs measured S-parameters for S_{23}, S_{22} for $\theta_c = 55^\circ$ 86
4.15 EM vs measured S-parameters for (A) S_{21} (B) S_{31} for $\theta_c = 55^\circ$ 86
4.16 Schematic of the proposed DC isolated wideband WPD 87
4.17 Even-mode analysis of half-network 87
4.18 Relation between R_1 and R_2 for different θ_c 89
4.19 Variation of S_{23}(dB) for $\theta_c = 55^\circ$ with different isolation resistors 90
4.20 EM vs measured S-parameters for (A) S_{21} (B) S_{31} for $\theta_c = 55^\circ$ 91
4.21 Simulated S-parameters for $\theta_c = 65^\circ$ 91
4.22 Fabricated prototype of the proposed DC isolated WPD 91
4.23 Measurement setup for (A): S_{23} (B): S_{21} for $\theta_c = 55^\circ$ 92
4.24 EM vs measured S-parameters for (A) S_{21} (B) S_{31} for $\theta_c = 55^\circ$ 92
4.25 EM vs measured S-parameters for (A) S_{21} (B) S_{31} for $\theta_c = 55^\circ$ 92
4.26 Schematic representation of proposed WPD 94
4.27 Even-mode representation of proposed WPD 95
4.28 (a) Odd-mode circuit of proposed WPD (b) revised equivalent circuit 97
4.29 Transfer characteristics of proposed WPD 99
4.30 Insertion loss characteristics of proposed WPD 100
4.31 Filtering characteristics of theoretical bandpass filter 101
4.32 Isolation resistor variation 102
4.33 $S_{11}(dB)$ vs frequency (GHz) with varying θ_c 103
4.34 $S_{21}(dB)$ vs frequency (GHz) with varying θ_c 104
4.35 $S_{22}(dB)$ vs frequency (GHz) with varying θ_c 104
4.36 $S_{23}(dB)$ vs frequency (GHz) with varying θ_c 105
4.37 Fabricated prototype (top and bottom view) 105
4.38 Simulated vs measured S_{11}(dB) and S_{21} (dB) 106

4.39 Simulated vs measured S_{22}(dB) and S_{23} (dB) 107

5.1 Current and voltage waveform with zero overlapping area 110
5.2 Schematic of the proposed two-port output network 112
5.3 Drain bias network 113
5.4 Impedance looking at the drain bias network at fundamental frequency, second and third harmonic 113
5.5 Impedance trajectories at the drain of the transistor 118
5.6 Dependence of drain efficiency on θ_1 for different frequency 118
5.7 Dependence of drain efficiency on θ_2 for different frequency 119
5.8 Drain efficiency vs fundamental load 119
5.9 Schematic of the measurement setup 120
5.10 Drain efficiency and gain for input power sweep 121
5.11 The prototype, PAE and power delivered for input power sweep 121
5.12 Voltage and current waveforms at the intrinsic plane of transistor 121
5.13 Schematic of the PA with different drain bias network 123
5.14 Schematic of the proposed two-port output network 125
5.15 Section - A: All-pass coupled line with dual-band stub 126
5.16 Section - B: π-structure based real-to-real dual-band transformer 127
5.17 Power added efficiency and gain vs input power(dBm) and prototype 128
5.18 Drain efficiency and power delivered vs input power(dBm) 129
5.19 Voltage and current waveform at the CG plane 129

List of tables

3.1 Design parameters for different loads at different frequencies 52
3.2 Design parameters for fabricated prototypes 54
3.3 Simulation & measured results for FDCL load 55
3.4 Comparison with the other state-of-the-art 56
3.5 Design parameters for different loads at different frequencies 61
3.6 Simulation & measured results 62
3.7 Comparison with the current state-of-the-art 64
3.8 Comparison with the other architectures 69
3.9 Design parameters for different loads at different frequencies 71

4.1 Design parameters of wideband WPD 82
4.2 Design parameters of DC isolated wideband WPD 89
4.3 Comparison with previous wideband WPDs 93
4.4 Parameters of the different case studies with varying θ_c 103
4.5 Comparison with the previous wide-band WPDs 106

5.1 Optimum impedances at the drain of the transistor 117
5.2 Design parameters of matching network 117
5.3 Comparison with the previous 3.5 GHz PA design 120
5.4 Impedances at the drain terminal with obtained PAE 124

5.5 Optimum impedances at the drain of the transistor 128

5.6 Design parameters of the proposed output network 128

5.7 Comparison with previous high efficiency PAs 129

Chapter 1

Introduction

In its current form, modern electromagnetic laid down its foundation on Maxwell's equations. Understanding the two most peculiar forces that exist in nature - Electricity, Magnetism and their relationship is possible only through these four influential equations. These equations made the basis for the most significant advances in humankind, from the study of black holes to quantum mechanics, from giant telescopes to small smartphones etc. In 1931, on the 100^{th} anniversary of Maxwell's birth, Einstein stated that development in the creation of reality in physics that resulted from Maxwell's work as **"the most profound and fruitful that physics has accomplished since the time of Newton".** [1].

The last two decades have seen remarkable advancements in the communication field- either wired or wireless. In the early 16th century, before the invention of electromagnetic telephones, mechanical devices were used for transmitting speech over a distance. However, after the successful demonstration of wired telephones for voice transmission, the era of communication changed. Technically, the telephones were diverse initially. Some comprise water microphones, some with metallic diaphragm for inducing currents, and some utilize vibrated coil of wire of permanent magnet [2]. Later, an induction coil was used that acts as an impedance matching transformer to make it compatible with the impedance of the

line. Hence, the critical requirement for transmitting the speech is efficiently transferring power from the source to the load. Similarly, another pillar of modern civilization includes electricity, which relies on the maximum power to be transferred from source to load side. In brief, this is referred to as Impedance Matching [3]. The impedance matching can be achieved considering the matching theorem for both real as well as reactive sources and load. The theorem states that if the source and load are real, the load resistance should equal the source resistance to maximize the power transfer. However, for the reactive loads, the impedance of the load should be the complex conjugate of the source [4].

1.1 Motivation

In the last decade, the cellular system has evolved from an uncomplicated calling and messaging device to one that connects the entire world using different platforms. The ubiquitous nature of this evolving technology in commercial, industrial, aerospace, and military applications has reconstructed cellular technology from a personal hand-held device to a flexible wireless system. Wireless technologies such as mobile handsets have seen the transformation from single-function devices to multi-function devices. It incorporates advancements such as reduction in size, cost and technology, including Bluetooth, Wi-Fi, GPS and many more multimedia functions in a single device [5]-[6]. Considering a 5G enabled smartphone which includes all of the following frequency bands or more operating simultaneously in a single portable device, as shown in Fig. 1.1 [7]:

- **Wi-Fi** - 1 GHz, 2.4 GHz, 3.6 GHz, 4.9 GHz, 5 GHz, 5.9 GHz, 6 GHz and 60 GHz [9]
- **GPS** - L1- L5 bands
- **2G-GSM** - 900 MHz or 1800 MHz
- **3G-GSM** - 900 MHz or 1800 MHz or 2100 MHz

- **4G-LTE** - 2100, 1800, 850, 750, 1900 MHz
- **5G** - 26 GHz and 40 GHz

Fig. 1.1 5G: new standard for number of applications [8]

Thus mobile handsets must operate at different frequency bands with discrete characteristics. In order to support multiple frequencies wireless connections, the RF front end should be capable of handling multi-mode signals. In the last decade, network technologies have evolved through generations, such as" 2G"," 3G"," 4G", and current "5G". In any transceiver unit of an RF system, there is a conglomeration of individual units that operate at different frequency bands, as shown in Fig. 1.2. As wireless standards are evolving rapidly, it dictates the need for a multi-band multi-mode RF front end. RF front end with variable characteristics attracts researchers in the mobile telecommunication field. Mobile telecommunication systems with variable RF front end operating at different frequency bands enhance their functionality and performance and help make the device more compact and cheap, as shown in Fig. 1.3 [10]-[11].

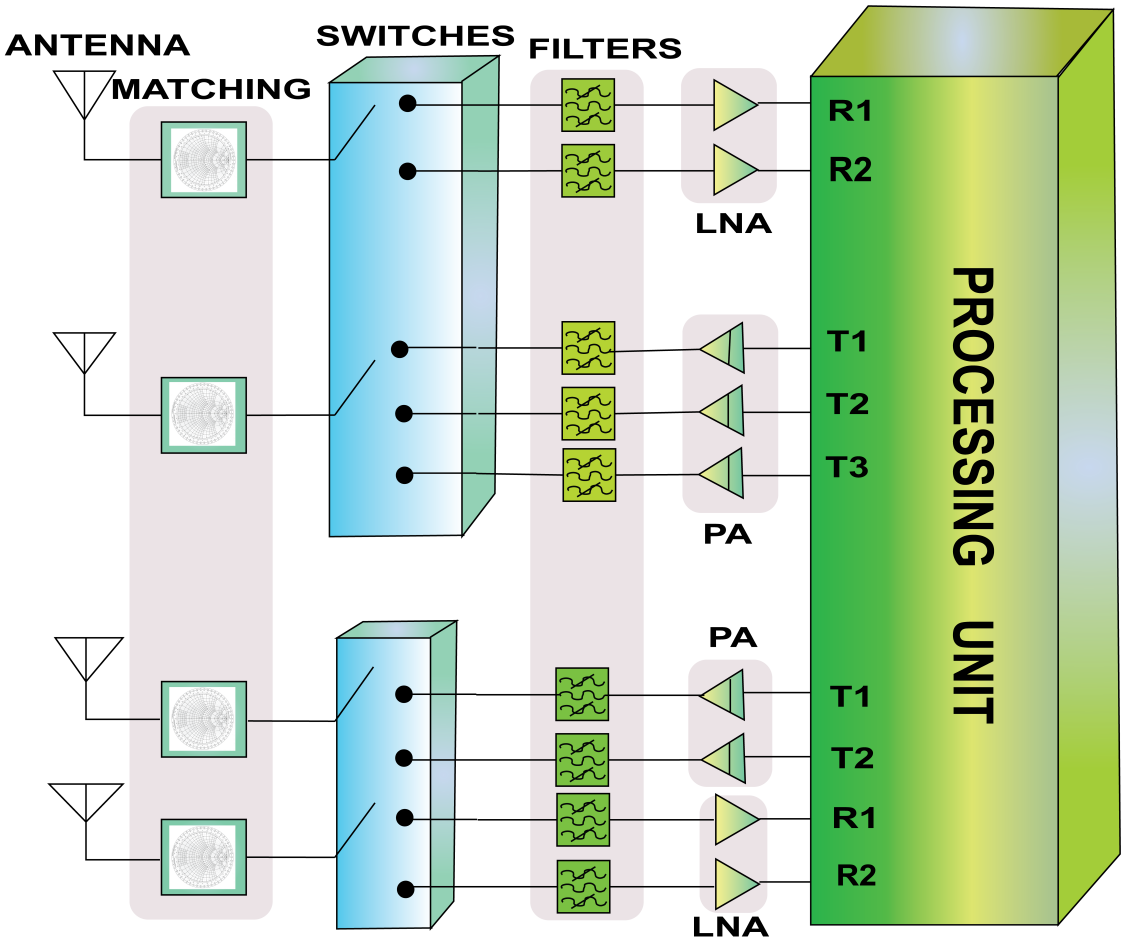

Fig. 1.2 RF front end with multiple devices to operate at different bands

The above-stated reasons necessitate the interest in finding innovative ideas for integrating RF hardware to be more compact with optimal performance. Thus instead of replicating the same transceiver for each new standard or frequency band, making them reconfigurable is a feasible solution. Since reconfigurable RF front ends require circuits such as filters, impedance matching networks, LNAs, antennas etc., with variable characteristics. It has been a challenge for researchers to implement a tunable RF front end that can vary its characteristics with corresponding variations in wireless standards. If all RF front-end circuits are individually tuned at different frequency bands, it reduces the RF circuit's need to implement individually. As seen from Fig. 1.2, an individual RF transceiver unit increases the overall weight of the system and cost, which is unenviable for mobile applications.

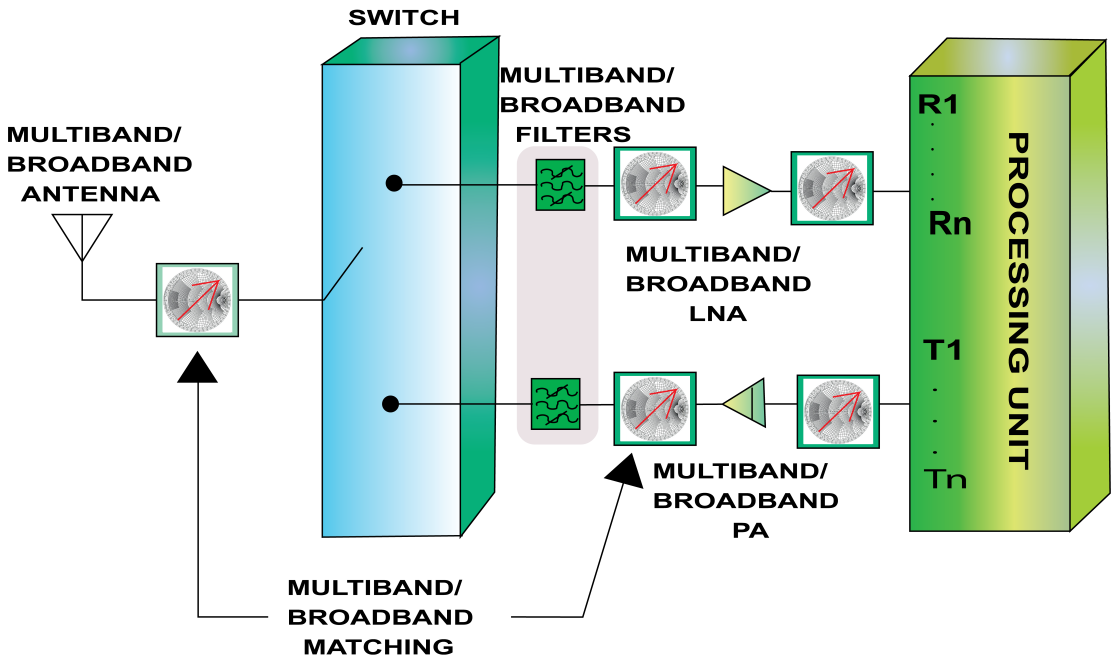

Fig. 1.3 RF front end with multi-band or broadband circuitry for multiple bands of operation

Fig. 1.3 shows a reconfigurable RF system for multi-mode standards in a single unit rather than replicating individual units for each new standard. In order to support multi-mode and multiband operation, RF circuitry such as Duplexer, Filter, PA, Impedance Matching Network, Antenna etc. needs to be reconfigurable [12]. Tunability in antenna provides many advantages, such as operating at different bands and filtering out interference signals using multiband and broadband circuitry. The need of reconfigurable devices also require the components that can be designed or modified for other applications as well. The different applications have different frequency ranges, hence the design of different components should be independent of frequencies selected. Tunability in impedance matching network provides required susceptance for antenna to compensate for changes such as frequency and the detuning effects [13]. Since reconfigurable RF front end requires different units, there is a need for a multiband Power Amplifier (PA) and multiband matching networks that will work on multiple bands and multi-modes. Fig. 1.4 represents the application of multiband PA operating at different bands of frequencies to make its use in varieties of

applications like smartphones, automotive industry, biomedical and many more [14]. As above discussed the motivation of this research was increased complexity, challenges and considerations in designing different circuits in any RF front-end module. In addition to the design and analysis of any active or passive circuit, the major design feature is to have frequency independent designs i.e. instead of selecting individual frequencies, the frequency ratio should be considered. This will ease the selection of the frequency of operation for any application. Thus this research includes the design of passive and active components found in any RF front end operating at different frequencies concurrently reducing the complexity, size and overall cost of the system.

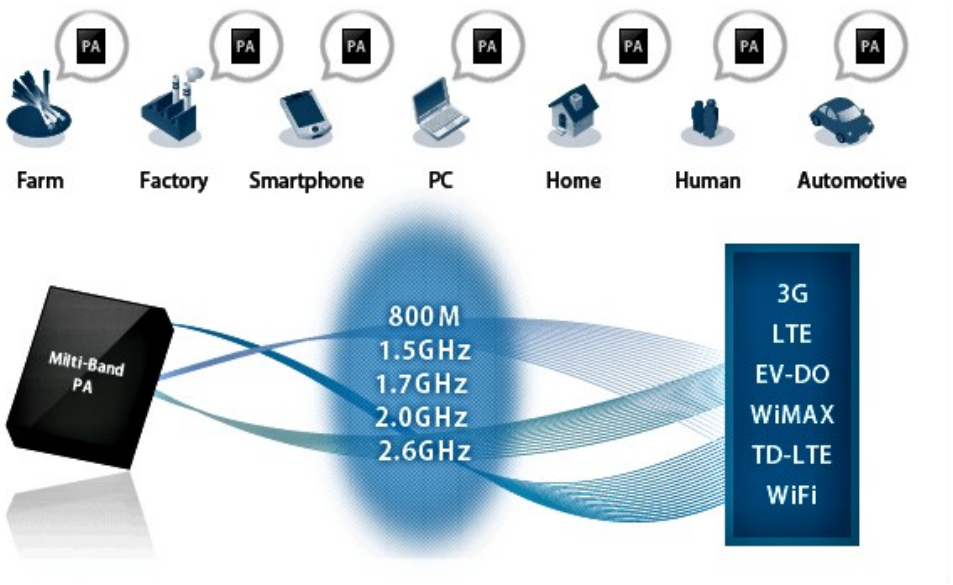

Fig. 1.4 Multi-band power amplifier operating at different frequencies of application [14]

1.2 Impedance Matching Networks

In any wireless system, electromagnetic (EM) radiation is transmitted through space in the form of waves. These EM waves carry the information within an RF circuit from one location to another and then radiate in space with the aid of an antenna. These radiations can be characterized in terms of wavelength and frequency. It is worth noting that while transferring

the power from the input side, the total energy should be carried to the output side of the circuit. Hence, the matching circuits are needed for transferring the maximum power from the input to the output side, which holds for both the large scale systems, including power stations or small RF circuits such as smartphones etc as presented in Fig. 1.5.

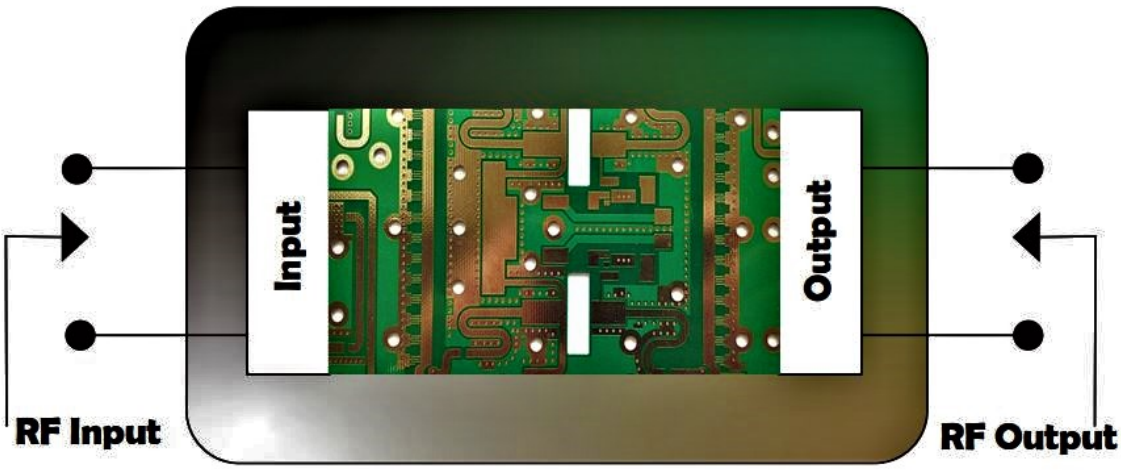

Fig. 1.5 Block diagram representing RF power transferring from input to output

As mentioned, at a single frequency, the problem of maximizing the power from resistive or reactive source to resistive or reactive load can be solved by taking the complex conjugate of each other. However, for variable frequency, the complex conjugate method fails, and reflection from the load results in the loss of power [3].

To understand the circuit's behaviour for maximizing the power, a fundamental concept related to the electric network, is the derivation of its transfer function. Also, the driving point impedance function is used to synthesize and analyze the circuit. However, for a brief understanding of these circuit realizations, it is necessary to define the terms: resistance, impedance, admittance and characteristic impedance. The difference between these terms allows for designing circuits with mathematical formulations. For a comprehensive understanding of impedance matching, these terms related to it should be reviewed.

1.2.1 Resistance

The resistance is the traditional term in electrical engineering relating the voltage and current.

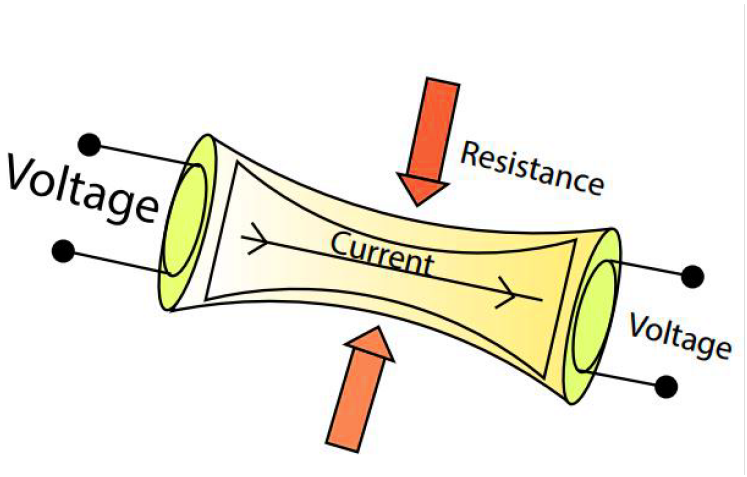

Fig. 1.6 Concept of resistance

It measures the opposition to the current flow in an electrical circuit, as illustrated in Fig. 1.6. The term was coined by Georg Simon Ohm, describing the relationship between current and voltage in terms of Ohm's Law [4].

Mathematically, it is defined as the ratio of voltage across the circuit and current flowing through it at any given time 't'.

$$R(t) = \frac{V(t)}{I(t)} \tag{1.1}$$

In any electric circuit consisting of resistors only, the resistance can be calculated by considering the equivalent resistance of the circuit $R_{eq}(t)$. Hence, the resistance can be defined in terms of $R_{eq}(t)$ rather than R(t). This definition of resistance is valid for DC currents where current is taken as constant. However, for AC circuits containing reactive elements such as inductors and capacitors, the term resistance is inadequate to use. Another term defining the opposition of current with reactive elements is introduced to ease this problem, "Impedance".

1.2.2 Impedance

In an electrical circuit, the term impedance is defined as the opposition of the current produced by an integration of resistance and reactance as presented in Fig. 1.7 [4]. Reactance is the

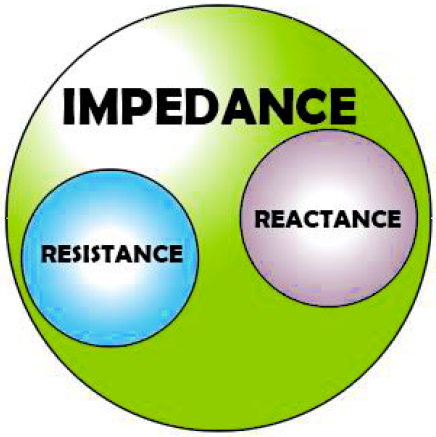

Fig. 1.7 Impedance containing both resistance and reactance

opposition provided to the alternating current by reactive elements such as inductor(L) and capacitor(C). Oliver Heaviside coined the term impedance. In addition to resistance, the effect of induction voltage between conductors, i.e. inductance and charge between the conductors, i.e. capacitance, is considered in AC circuits.

The impedance is represented in phasor form in terms of magnitude and phase angle, $Z = Z_o\phi^z$. Mathematically, impedance can be represented in terms of resistor, inductor and capacitor for a sinusoidal current as follows.

Resistor:

Considering a voltage $V(t) = V_o sin(\omega t)$ across circuit containing a resistor R as depicted in Fig. 1.8, the impedance is defined as:

$$Z(t) = \frac{V_o sin(\omega t)}{I_o sin(\omega t)} = R \tag{1.2}$$

Here, the impedance Z(t) is simply defined as the resistance across the circuit.

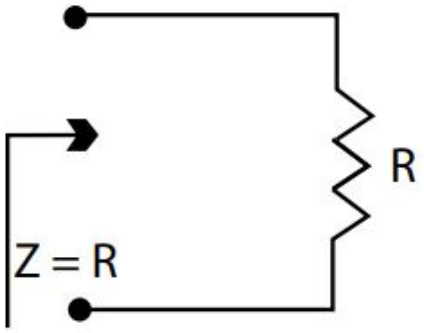

Fig. 1.8 Circuit with resistor

Inductor:

In a circuit shown in Fig. 1.9 containing the inductor 'L', the voltage and current across the circuit is $V(t) = V_o sin(\omega t)$ and $I(t) = I_o sin(\omega t)$ respectively, then impedance Z is defined as:

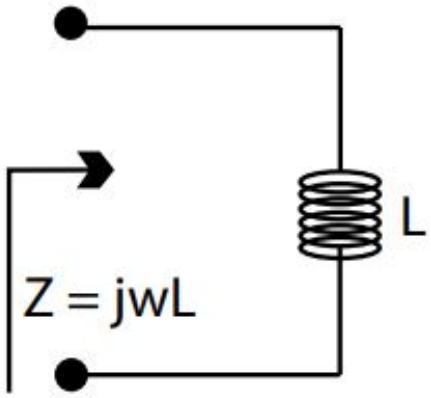

Fig. 1.9 Circuit with inductor

$$v(t) = L\frac{dI(t)}{dt} = L\frac{d(I_o sin(\omega t))}{dt} \tag{1.3a}$$

$$v(t) = \omega L I_o cos(\omega t) = j\omega L I(t) \tag{1.3b}$$

$$Z = \frac{v(t)}{I(t)} = j\omega L \tag{1.3c}$$

The impedance Z across the inductor varies with frequency and hence for DC current, impedance offered by ideal inductor is zero and can be considered as short-circuit.

Capacitor:

Similarly, a circuit containing the another reactive element capacitor 'C' as shown in Fig. 1.10, the voltage and current across the circuit is $V(t) = V_o sin(\omega t)$ and $I(t) = I_o sin(\omega t)$ respectively, then impedance Z is defined as:

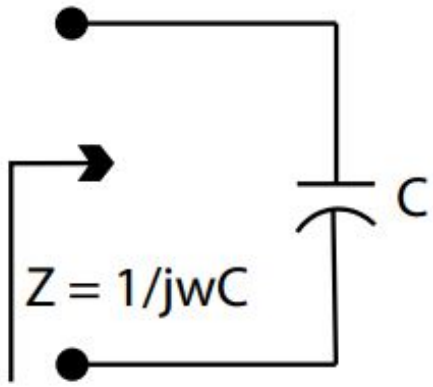

Fig. 1.10 Circuit with capacitor

$$I(t) = C\frac{dV(t)}{dt} = C\frac{d(V_o sin(\omega t))}{dt} \tag{1.4a}$$

$$I(t) = \omega C V_o cos(\omega t) = j\omega C V(t) \tag{1.4b}$$

$$Z = \frac{v(t)}{I(t)} = \frac{1}{j\omega C} \tag{1.4c}$$

The impedance Z across the capacitors also varies with frequency and hence for DC current, impedance offered by ideal capacitor is infinite and can be considered as open-circuit.

1.2.3 Admittance

Unlike impedance, admittance is considered to be the measurement of the amount of current flow through any material. Thus it can be defined as the reciprocal of the impedance. Oliver

Heaviside coined the term admittance.

$$Y = \frac{1}{Z} \tag{1.5}$$

Here, Y and Z are admittance and impedance respectively. Similarly, to impedance, the admittance is defined including both resistive and reactive elements. However, it is defined in terms of conductivity as below:

$$Y = G + jB \tag{1.6}$$

Here, G is the conductance and B is the susceptance, both measured in Ohms.

1.2.4 Characteristic Impedance

The above-defined terms are applied to electrical circuits with resistance and reactive elements for measuring their performance in terms of conductivity and resistivity. However, a new term was introduced for calculating the impedance in a transmission line known as Characteristic Impedance of the line [3].

It is considered the ratio of voltage and current in an infinite transmission line with no reflections. It is denoted by Z_o Ω. The characteristic impedance of the transmission line is calculated over an infinitesimal length Δx, which can be modelled as the combination of resistive and reactive elements as shown in Fig. 1.11 [15].

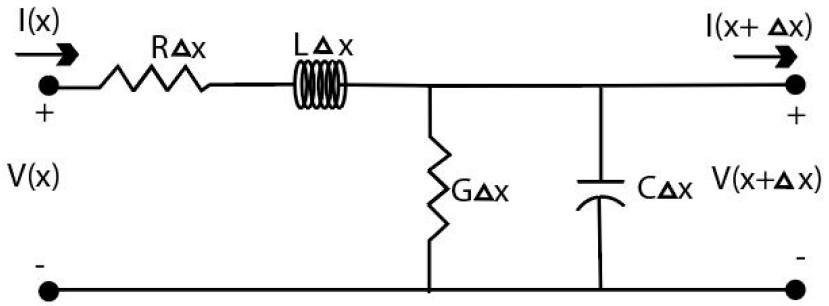

Fig. 1.11 Transmission line model over an infinitesimal length Δx

Here, R is the series resistance per unit length in Ω/m, L in the series inductance per unit length in H/m, G is the shunt conductance per unit length in S/m and C is the shunt capacitance pr unit length in F/m. By analyzing the defined model and applying the mathematical formulations, the two equations in terms of voltage and current can be written as:

$$V(x+\Delta x) - V(x) = -R\Delta x I(x) - j\omega L\Delta x I(x) \tag{1.7a}$$

$$I(x+\Delta x) - I(x) = -G\Delta x V(x) - j\omega C\Delta x V(x) \tag{1.7b}$$

Taking second-order differential equation with respect to x and considering Δ x tending towards zero results in :

$$\frac{d^2V(x)}{dx^2} - (R+j\omega L)(G+j\omega C)V = 0 \tag{1.8a}$$

$$\frac{d^2I(x)}{dx^2} - (R+j\omega L)(G+j\omega C)I = 0 \tag{1.8b}$$

Investigating these two equations for solutions in terms of V and I results in two waves, forward travelling and backward travelling wave as follows [15]:

$$V(x) = V_o^+ e^{-\gamma x} + V_o^- e^{+\gamma x} \tag{1.9a}$$

$$I(x) = I_o^+ e^{-\gamma x} + I_o^- e^{+\gamma x} \tag{1.9b}$$

where,

$$\gamma = \sqrt{(R+j\omega L)(G+j\omega C)}$$

The characteristic impedance of the transmission line is defined as the ratio of the forward travelling voltage wave to the forward current wave or the backward travelling voltage wave to the backward current wave.

$$Z_o = \frac{V_o^+}{I_o^+} = -\frac{V_o^-}{I_o^-} \tag{1.10}$$

By mathematical analysis, the characteristic impedance of transmission line in terms of lumped elements R, L, G and C is given as:

$$Z_o = \sqrt{\frac{R + j\omega L}{G + j\omega C}} \tag{1.11}$$

From (1.11), for a lossless transmission line, the characteristic impedance is purely resistive. It can be noted that if the transmission line is terminated at the load with the impedance equal to the line's characteristic impedance, then there will be no reflections, and the concept of impedance matching is introduced. The terms impedance and characteristic impedance are used interchangeably in the transmission line.

1.2.5 Impedance Matching Techniques

As mentioned before in circuit theory, the maximum power transfer theorem is one of the most significant theorem since it is the motivation behind the "Impedance Matching Network". According to this theorem, the maximum power can be transferred between a source and any load at a particular frequency if the load impedance is a complex conjugate of source impedance, i.e. $Z_L = Z_S^*$. However, for circuits where the frequency of operation is variable or circuits that match at one or more frequencies, maximum power transfer is challenging. For different loads, which can be constant or variable, a black box can be placed between the load and source that can transform the load impedance precisely to the same as desired to have maximum power transfer from the source. This black box can be termed as "Impedance Matching Network" as shown in Fig 1.12.

Considered a voltage source V_G with a input impedance of Z_S and has a load with impedance Z_L. Generally, the impedance matching between these arbitrary source and load can be categorized into following categories:

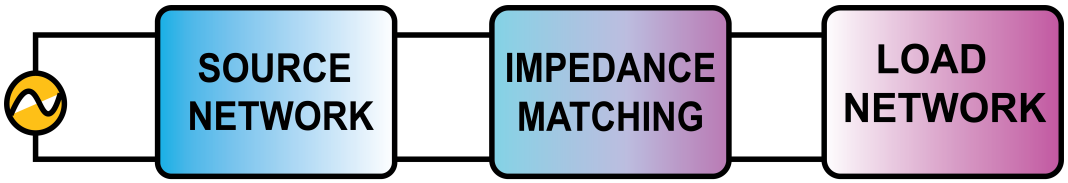

Fig. 1.12 Block diagram representing impedance matching network between source and load network

- **Source and Load - Both Real but unequal** - This is the most simple scenario, the input impedance Z_S and load impedance Z_L both are real and hence resistive at single frequency as shown in Fig.1.13. The matching between these two impedance is straightforward by using quarter-wave transformer.

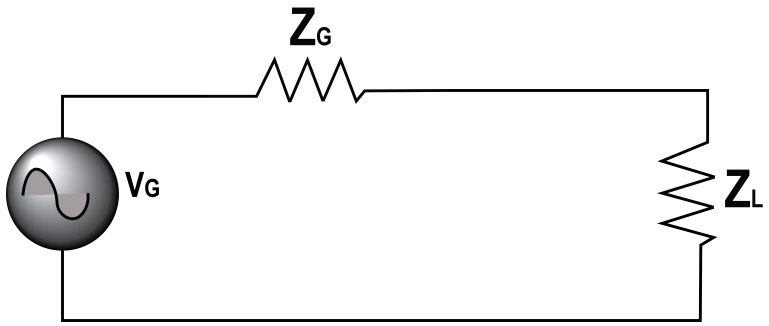

Fig. 1.13 Matching scenario for resistive unequal source and load

- **Source - Real and Load - Reactive or Complex** - In this scenario, the input impedance Z_S is real while load impedance Z_L is complex at a single frequency as shown in Fig. 1.14. The matching between these two impedance done by either lumped elements or transmission lines using tools such as Smith Chart.

- **Source and Load - Both Reactive or Complex** - This scenario is the most common in applications such as Power Amplifier (PA) connected to an antenna in any RF front end. As PA drain impedance is always complex because of parasitic, the input impedance is complex, while the impedance seen into an antenna is also complex. It is presented in Fig.1.15. The input and load impedance's are unequal but operate at a single frequency. For providing the maximum power between the source and load, the

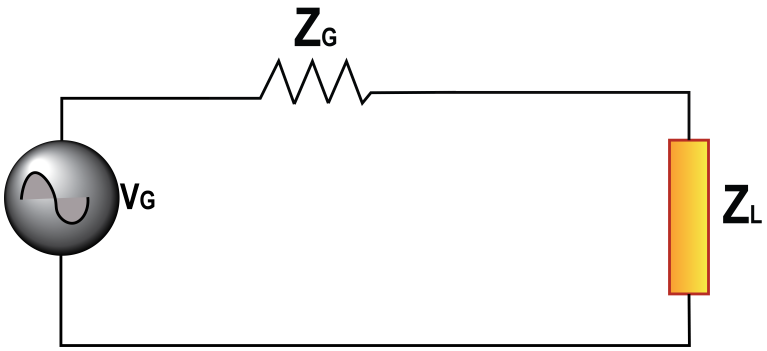

Fig. 1.14 Matching scenario for resistive source and reactive load

impedance matching network should be considered, which can provide impedance that is a complex conjugate of load impedance. This type of matching can be done by the Smith Chart tool.

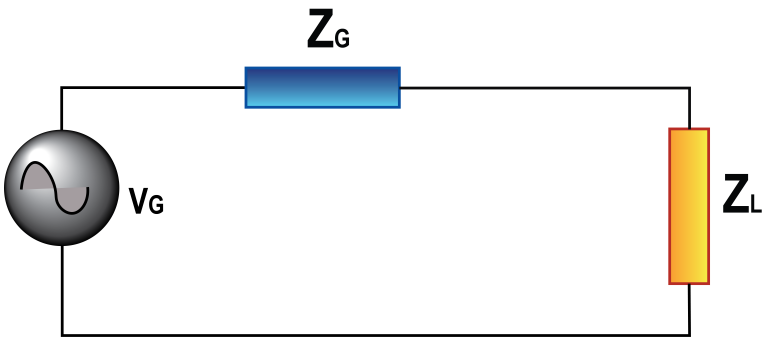

Fig. 1.15 Matching scenario for reactive source and load

The design methods for above three categories is quite straightforward and productive, but with following limitations:

1. Matching is provided at a single frequency only.
2. Narrow operating bandwidth (Quarter-wave transformer)
3. Load impedance should not vary with frequency.

However, in a pragmatic framework, the RF front end receives multiple frequencies at a time, and hence impedance matching network should also be capable of providing matching

at multi-frequencies consecutively. Another scenario can be considered where the load is frequency-dependent complex load (FDCL). The solutions to these problems have been a part of research in the last decade by providing either the multi-band or broadband impedance matching network.

Multi-band Matching Network

There has always been a demand for multi-standard RF transceivers in this wireless era, focusing mainly on size and cost reduction. In addition, these systems operate in a wide range to operate in dynamic environments. In any RF front end, to ensure the multi-standard transceivers can transmit and receive distinct signals at different frequencies simultaneously, reconfigurability of each block, including power amplifier, low noise amplifier, mixers and matching networks, is necessary. It is well known that the matching networks have been known for years for transferring maximum power from the source to load; the traditional method of using quarter-wave transformers, smith charts and other tools are familiar. However, the research in the multi-band matching networks, including dual-/tri-/multi-band, has gained much attention worldwide. In the design and implementation of multi-band matching networks, there are three categories based on source and load impedances as follows:

- When the source and load both are resistive but unequal and variant with respect to frequency as shown in Fig. 1.16.

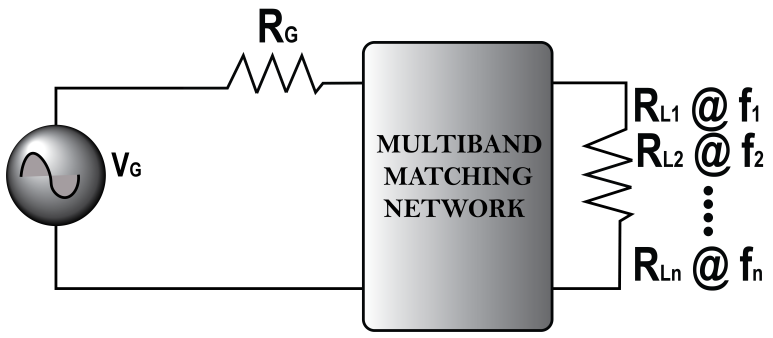

Fig. 1.16 Multi-band matching scenario for resistive unequal source and load

- When the source is resistive, load is complex and variant with respect to frequency as shown in Fig. 1.17.

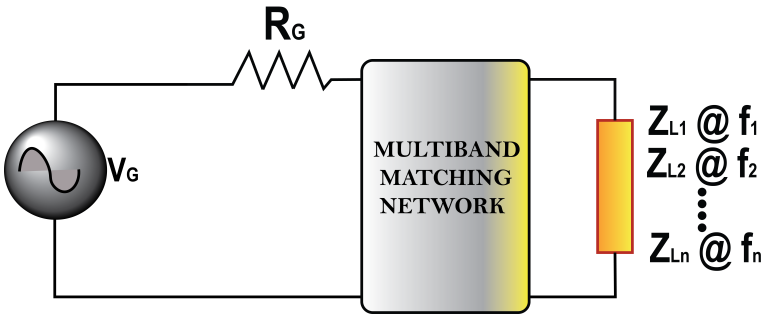

Fig. 1.17 Multi-band matching scenario for resistive source and reactive load varying with frequency

- When the source and load both unequal and complex and also, variant with respect to frequency as illustrated in Fig. 1.18.

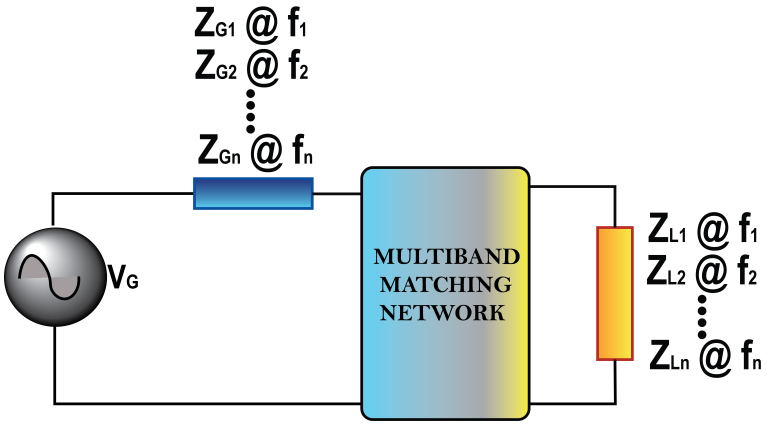

Fig. 1.18 Multi-band matching scenario for reactive source and load both varying with frequency

Broadband Matching Network

The term broadband matching network implies transferring maximum power from the source to load over a wide frequency band. The simple method of conjugate matching has limitations when matching is to be carried out over a broad frequency range. Before 1948, there was no

well-defined technique for broadband impedance matching in a microwave device and no practical procedure for defining the mathematical formulations for designing the matching network.

In 1945, an analytic broadband matching theory was given by Bode with gain-bandwidth limitations on any single-match network having a parallel RC load [16]. The work carried out by Bode was significant, although it considers a simple combination of resistor and capacitor, as it provides for the first time the gain-bandwidth formulation for a given load.

Initially, the integral theorem considered for designing broadband matching networks was Darlington theorem (1939) [17]. This theorem states that any impedance function of a random element, including resistance and reactance, can be represented by a simple reactive network consisting of loss-less L and C network terminated by 1-Ω resistance as shown in Fig. 1.19. Hence converting the impedance matching network problem into a filter design problem.

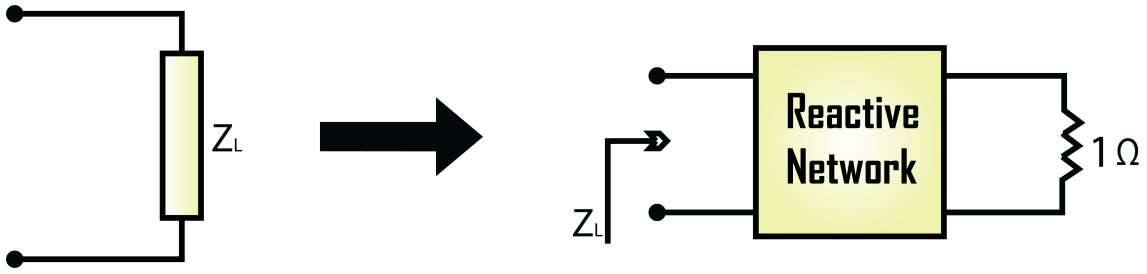

Fig. 1.19 Representation of darlington theorem

Extending this theorem and combining the work carried by Bode, Robert Fano in 1948 provided a simple approach to design a broadband matching network [18]. Fano replaces a defined load impedance Z_L with Darlington's defined network terminated by 1-Ω resistance resulting in a filter with resonators on both ends. The next step is to design a simple Chebyshev or elliptic equal-ripple doubly-terminated filter. The gain-bandwidth limitation is further investigated and later known as the Bode-Fano criterion, which states that for lossless matching networks for some standard loads with a resistor, R, in parallel with a capacitor, C,

there is a limit on the reflection loss, given by:

$$\int_0^{\infty} \ln \frac{1}{|\Gamma_{IN}(\omega)|} d\omega \leq \frac{\pi}{\tau} \tag{1.12}$$

Here, τ is the time constant RC and L/R for different load combinations, $\Gamma_{IN}(w)$ is the reflection coefficient seen into matching network. Considering, desired frequency range from w_1 to w_2, the reflection-coefficient can be calculated as:

$$\int_{\omega_1}^{\omega_2} \ln \frac{1}{|\Gamma|} d\omega \leq \frac{\pi}{\tau} \tag{1.13a}$$

$$(\omega_2 - \omega_1) \ln \frac{1}{|\Gamma|} d\omega \leq \frac{\pi}{\tau} \tag{1.13b}$$

This ideal results in trade-off between a good-match over a narrow band and poorer match over a wide band.

In practice, certain metrics are used to characterize the performance of impedance matching networks. They are elaborated briefly in the following section:

- ***Return and Insertion Loss:*** Return loss in any matching network is the important measuring parameter as it determines how much power is being reflected from the output port of the circuit due to a mismatch of transmission line characteristic impedance and load. Similarly, insertion loss is defined as the loss incurred during the transmission of a signal from input to output port. Return and Insertion loss are defined in terms of S-parameters as S_{11}(dB) and S_{21} (dB), where '1' and '2' represents the input and output ports respectively.

- ***Frequency Ratio:*** Frequency Ratio is the most significant performance measuring metric in any multi-band circuit and essentially defines the maximum obtainable band separation without degrading other measuring parameters. In literature, designs have

been reported either as frequency-based or frequency ratio based. Frequency-based designs consider the case of operation at discrete frequencies such as 900MHz, 3.5GHz and 5.8GHz. This limits the design flexibility as the same structure cannot be reused for other frequencies with the same frequency ratio. While frequency ratio-based design operates on ratios, such a device operating on 1, 2, and 4 GHz should also be able to operate successfully at 1.5, 3 and 6 GHz.

- ***Impedance Transformation Ratio:*** Another important defining performance measuring metric for multi-band devices is the impedance transformation ratio or the impedance gradient. It is the ratio of the load impedance at the output port of the device to the source impedance at its input port. In most conventional designs reported in the literature, the load impedance does not differ from the source impedance by a considerable value. This parameter is of utmost importance, especially in impedance transformation networks, as designing the same becomes challenging when the load impedance becomes high.

- ***Per-band Bandwidth:*** For a device operating at multiple frequencies, it is essential to determine the bandwidth attainable at each of the bands of interest. This parameter is not absolute as the bandwidth requirement per band depends upon the application the device is serving. For example, for a highly selective military radio operating at three bands of interest, the bandwidth per band needs to be as narrow as possible to make it highly selective (with a high Q-factor). On the other hand, the bandwidth requirement per operating band is very high in high-speed transmitting systems. Generally, the bandwidth is specified below a particular level of reflection coefficient, mostly -10, -15 or -20 dB.

1.3 Power Dividers

Another important passive device found extensively in any RF circuit is the power divider used for power dividing and combining. As presented in Fig. 1.20, a power divider is used to divide the input power into outputs that can be equal power or unequal power, depending upon the application. It is also essential in any power divider to have excellent isolation between the two output ports. The most commonly used power divider was the T-junction power divider; however, it suffers the poor isolation between two output ports and is hence not valuable for applications where isolation between ports is required, e.g. Doherty Power Amplifier.

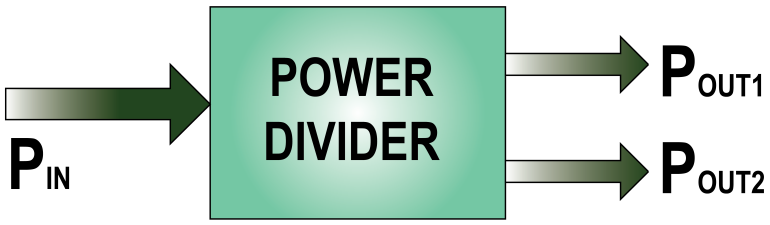

Fig. 1.20 Power division by power divider

The most popular power divider was introduced by Wilkinson in 1960 [19]. The proposed power divider divides the power into N equal magnitude and phase signals. The famous Wilkinson Power divider represents a two-way single band 3-dB power divider with N = 2. It has excellent isolation between the two output ports with perfect return loss, as illustrated in Fig. 1.21. However, it suffers the disadvantage of narrow bandwidth because of using a quarter-wave transformer.

The Wilkinson power divider is designed to split the output ports equally. However, the unequal power dividers were developed later to divide the power unequally with the' K' ratio. There are other types of power dividers, such as multi-way power dividers, including radial, multi-section designs etc., which will be discussed in Chapter 2. The design restrictions of all

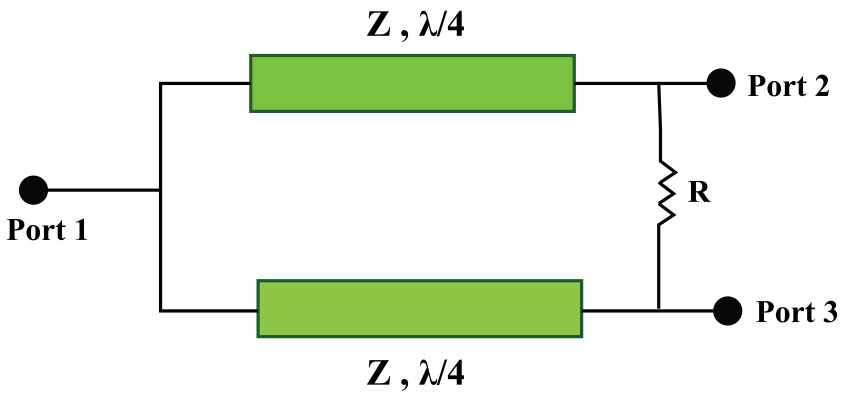

Fig. 1.21 Schematic of Wilkinson power divider

the discussed power dividers are single frequency operations. As described, the multi-band RF front end needs every component should operate at different frequencies simultaneously or over a wide frequency band. Hence, multi-band power dividers and broadband power dividers were investigated extensively in the last decade.

The most important parameters reviewed while designing a power divider are discussed below:

- ***Return Loss:*** Return loss is defined as the reflected power from the output port because of discontinuity or mismatch at the end of the transmission line. It is measured in terms of dB and denoted by S_{11} in terms of S-parameters. Here '1' is represented by port 1.

- ***Insertion Loss:*** Insertion loss is defined as the loss which occurs when the signal is transmitted through a transmission line. It is also defined as attenuation in terms of dB. It is denoted by S_{12}, where '1' and '2' are input and output ports, respectively. It is defined as a positive number in terms of gain and a negative number in terms of attenuation.

- ***Isolation:*** Isolation is defined as the mutually isolated output ports. In any power divider, power entering port two must not interfere with port 3 (in the case of a two-port power divider) and vice-versa. In terms of S-parameters, it is denoted by S_{23} (dB).

1.4 Power Amplifiers

A power amplifier is an essential system component that plays an essential role in many applications such as satellite communication, microwave and millimetre wave system [20]. It can be said that the imagination of the user limits applications of the power amplifier since it is a very crucial block in telecommunication, military systems, aerospace and other important applications. As power amplifier applications found diversity in different fields, specifications of power amplifiers also vary depending on the requirement, i.e. operating condition, technology used and application design strategy. Consequently, a wide variety of PA realizations results, from travelling-wave tube amplifiers in satellite payloads to solid-state amplifiers for personal wireless communication handsets. The main task of PA is to increase the power level of the signal at its input, and up to a certain level at its output within a particular frequency band, as shown in Fig. 1.22 [21].

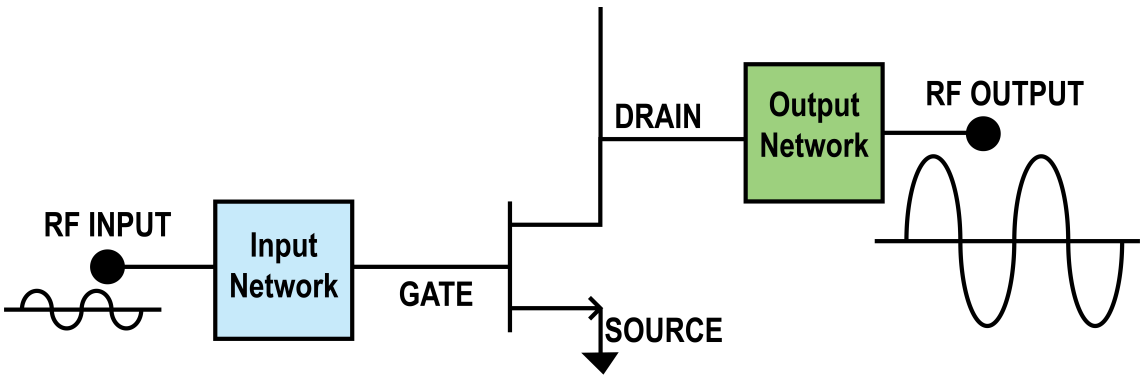

Fig. 1.22 RF power amplifier with amplification of RF input signal

Unlike linear amplifiers that include small-signal analysis to find out the small-signal gain, power amplifiers are often specified in terms of power gain and its power-added efficiency. It

determines the primary performance of a power amplifier. Fig. 1.23 represents the 3W RF power amplifier from Acquitek [22].

Fig. 1.23 3W power amplifier from acquitek

Different classes are defined to enhance the efficiency of a power amplifier. The PAs operating as Class-A, B, AB, and C are defined by controlling the current conduction angle. Theoretically, the class-A amplifier can achieve maximum 50% drain efficiency with both current and voltage waveforms as sinusoidal. However, to increase the efficiency, the current and voltage waveforms need to be reshaped. To reshape the waveforms, drain voltage may contain a number of harmonics while maintaining the current waveform as sinusoidal or vice versa. However, practically, it is impossible to alter infinite harmonics, but it is possible to achieve efficiency greater than 75 % by controlling the first three harmonics. It is also widely acknowledged that highly efficient RF power amplifier configurations such as switched-mode PAs are often constrained in the choice of the frequency of operation. This could be attributed to parasitic capacitance and inductance at the drain of the transistors.

In a design of RF power amplifier, the critical blocks are: active device [23], input matching network, output matching network, DC biasing network etc., as shown in Fig.1.24. Since, in telecommunication, the RF front end operates at different frequencies, there is a

need for either a multi-band or broadband power amplifier. For designing of multi-band or broadband power amplifier, all blocks present should be multi-band or broadband, e.g. multi-band or broadband input and output matching network, DC biasing network etc.

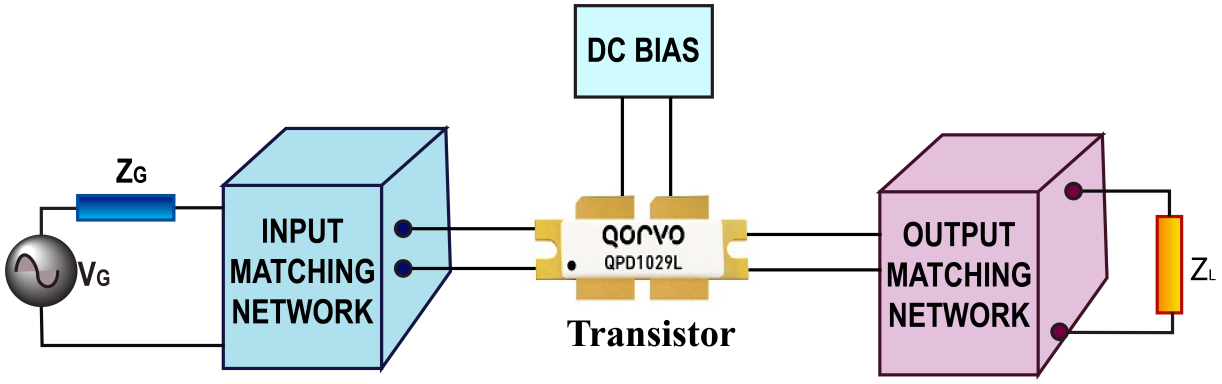

Fig. 1.24 Block diagram showing RF power amplifier components

In order to characterize the performance of a RF power amplifier, some important metrics are considered. These are discussed briefly in the following section:

- ***Power Gain*** P_{gain}***:*** It is defined as the ratio of output power P_{out} to input power P_{in}.

$$P_{gain} = \frac{P_{out}}{P_{in}} \tag{1.14}$$

  A power gain in any power amplifier mainly depends on the input signal drive, i.e. for small drive levels, the amplifier behaves linearly; thus, the gain is known as Linear Gain. When input level drive is increased, output voltages and currents will be saturated by the device's non-linearities; thus, gain start decreasing towards zero.

- ***Gain Compression:*** As mentioned above, power gain depends on input power. When input power is increased, due to non-linearities of the device, gain decreases from its linear value to zero. It is known as gain compression. One parameter known as the -1 dB compression point is defined as the output power level variation from the corresponding ideal linear behaviour. Thus, this merit is the border between the device's almost linear and non-linear behaviour.

- ***Drain Efficiency:*** Power amplifier is a device that amplifies the low power input signal to high output power. A parameter known as drain efficiency is defined as the ratio between amplified RF output power and DC power supplied to it. This is the most important key parameter since it determines the DC power budget.

$$\eta = \frac{P_{out}}{P_{DC}} \tag{1.15}$$

- ***Power Added Efficiency:*** If DC supply is fixed, then to improve overall system performance, high efficiency allows high transmitted power. As the power amplifier has an active device component, with an increase in frequency, amplifier gain starts decreasing due to parasitic and other constituents who come into the picture as frequency increases. Thus, output power coming from the input signal cannot be ignored as it contributes a significant portion of the total output power. Thus, another parameter is to be defined, known as Power Added Efficiency. It is defined as the ratio between power added (i.e. increase in signal power from power amplifier input to its output) to the supplied DC power.

$$\eta_{added} = \frac{P_{out} - P_{in}}{P_{DC}} \tag{1.16}$$

  To increase the overall efficiency of the power amplifier, power dissipation should be minimal. Thus, high efficiency results in lower dissipation power, thus reducing thermal issues.

- ***Harmonic Distortion:*** Due to the non-linear behaviour of the power amplifier, efficiency and output power both are restricted by compression. Harmonic generation at even and odd frequencies distorts a two-tone input signal. Thus harmonic distortion is defined as the ratio between output power at harmonic frequencies to the output power at the fundamental frequency.

- ***Intercept Point:*** Since practical signals are not signal tones, thus considering a two-tone signal at the input of the non-linear power amplifier, it results in several harmonics at its output whose components lead to the distorted output. Thus, power amplifier output contains a series of harmonic frequencies and can be out of the band and in-band components. These components are known as Inter-modulation Components. Third-order intercept point is the hypothetical extension of the third-order components power curve that meets the power curve of the fundamental power. It is the most significant parameter in terms of characterizing the device's performance [24].

Thesis Overview and Organization

This thesis presented the different methods for designing both active and passive devices in any RF front end. The passive devices discussed include primarily dual-band matching networks and broadband power divider, which is practical in implementation. Also, a harmonic power amplifier for high efficiency and gain is analyzed.

The thesis is organized as follows: *Chapter 2* will presents the literature review of the research work related to matching networks and power dividers from multi-band to broadband, the evolution of power amplifiers from simple harmonic tuned to present complex architectures. *Chapter 3* develops the theoretical basis for designing the dual-band matching networks, closed-form equations, analysis, different case studies and fabrication of prototypes for validation purposes. It includes three types of methods with variations in source and load type. *Chapter 4* discusses another important passive device, a power divider that is designed to work over a wider frequency range. The two different methods are presented with inherent DC-blocking capabilities that are useful in many practical applications. *Chapter 5* considers the application of discussed multi-band matching networks in designing highly efficient RF power amplifiers. The design part incorporates designing an output matching network and drain bias network to match the drain impedance of the transistor to the load by harmonic

tuning. *Chapter 6* finally summarizes the dissertation and proposes a future direction of research in this field.

Chapter 2

Literature Review

2.1 Background

In any transceiver, the RF front end mainly consists of circuits between the antenna and other digital blocks used to transfer and receive information without distortion, as shown in Fig. 2.1. The blocks preceding mixers are power amplifiers and matching networks on the transmitter side.

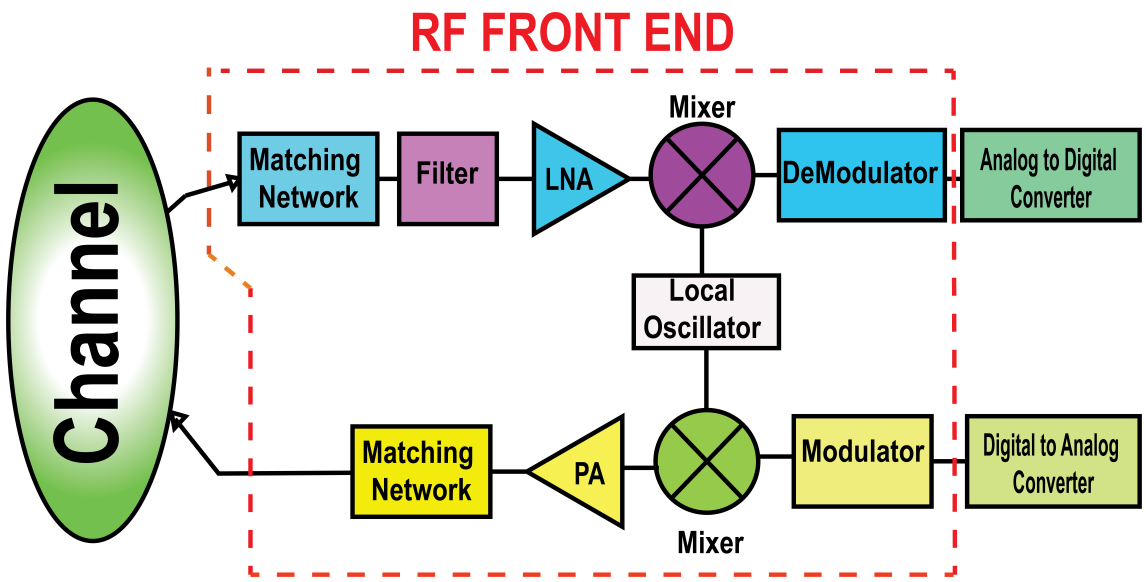

Fig. 2.1 Block diagram of RF front end transceiver

These are the two most crucial blocks in the transmitter chain as the power amplifier can boost the input power levels while the matching network is utilized to maintain the maximum power transfer. Chapter 1 discusses the emergence of a multi-band RF front end, which often requires multi-band or broadband circuitry, including power dividers, couplers, oscillators, etc. In this thesis, research mainly focuses on the design of multi-band or broadband passive devices and their application in power amplifiers; this chapter will discuss the existing literature study related to these ubiquitous blocks of any RF front end.

2.1.1 Impedance Matching Networks

The matching network is the crucial block in any RF/microwave system, and it found applications in many RF circuits. With the recent advancement in wireless technology, wireless standards are evolving rapidly. With the evolution of new wireless communication systems, different frequency bands are coming into use. Since matching network is omnipresent in almost all RF/microwave devices, different conventional matching networks exist, such as $\lambda/4$ quarter-wave transmission line, stub matching transformer (either single or double stub) and many more. $\lambda/4$ quarter-wave transmission line is the simplest but only limited to a single frequency. The above discussed matching networks have their limitations which many researchers reported [25]-[30]. Earlier, wireless standards were restricted, and frequency bands were also limited.

Nowadays, the RF front end incorporates concurrent operation of various frequency bands and thus, there is an immediate necessity for multi-frequency circuits. This framework the need for multi-frequency matching impedance transformers as well. New design challenges include dual-/tri-/multi frequency impedance matching networks. As of now, literature is replete with dual-band matching networks, but tri-band and quad-band matching networks are still in their early research stage. Literature has had many dual-band matching network architectures in the last decade, a handful of tri-band and virtually no multi-band matching

network topologies. Revisiting the matching scenarios for matching between source and load, there can be different classes as follows:

- ***Real to Real impedance transformer:*** This type of topology include both source and load impedance to be real.
- ***Real to Complex impedance transformer:*** This type of topology include source as real and load impedance to be complex.
- ***Complex to Complex impedance transformer:*** This type of topology include both source and load impedance to be complex.

The above-discussed architecture literature will be extensively scrutinized in the next section.

Dual-Band Impedance Transformers

The conventional quarter-wave transmission line is the familiar solution for matching real load and source. However, its bandwidth is very narrow and is limited to only a single frequency. The $\lambda/4$ transformer matches only real loads. Most active devices, like PA, LNA, Active Filters etc., have a complex input/output impedance (which may or may not be frequency-dependent) that must be matched to another real/complex impedance. Thus, the $\lambda/4$ transformer fails to serve the purpose. Thus, there started the necessity for multi-band impedance transformers. As discussed, the literature on the matching network is replete with dual-band matching network architectures. This type of architecture includes both real and complex sources or loads, depending on the application. The real source and real load found rare applications in practical terms since impedance found at load (e.g. impedance at the output side of power amplifier) is complex in practical situations. So, subsequent subsections discuss dual-band impedance transformers with real and complex loads.

The original research in dual-band impedance matching networks started in 2002 with a paper authored by Chow [25] who proposed an impedance matching technique for the

first time which uses a two-section 1/3rd wavelength transmission line which could provide matching at a particular frequency of interest and its harmonics. Matching was obtained between a 50 Ω port impedance (Z_0) with a load equal to KZ_0, where K is a constant. The input impedance is forced to be real and equal to KZ_0, the simplification of which leads to transcendental equations of the 4^{th} order. This is followed by a CAD solution for a particular case of K=2. The major limitation of this design was that the analysis was not exact, and the design equations were not in closed form. In addition to it, only the harmonic match was another limitation.

An extension of Chow transformer [25] was presented by Monzon [26] which addresses the problem mentioned above. The Monzon transformer was a simple two-section circuit that could provide dual-band impedance matching at any two arbitrary frequencies of interest. The structure of this configuration is similar to that of Chow, except that θ_1 and θ_2 are not fixed to be 1/3-wavelength. After these two breakthroughs, a two-section dual-band Chebyshev transformer was proposed by Sophocles [27]. This transformer established that the Monzon transformer is a special case of it. Moreover, the Chebyshev transformer was more general in that it showed a trade-off between the out of band reflection coefficient and the achievable bandwidth. A multi-section dual-band Chebyshev transformer was proposed in [28]. Another architecture consisting of pi-structure operating at arbitrary dual-band frequency was proposed by Y. Wu et al. [29] for matching real load to real source. The exact design equations have been developed with infinite solutions. The horizontal length of this transformer is half of the Monzon transformer. M.J. Park et al. [30] proposes a new design method for a single stub matching network. This proposed architecture consists of a single transmission line and a shunt stub open or short at the load or source side. This gives the impedance transformer great flexibility as it can address many impedance environments. A coupled-line based impedance transformer with DC blocking capability was proposed in [31]. This architecture consists of a coupled line and a shunt stub at the load or source side. The

distinct feature of this design is the inherent DC blocking feature with easy design equations. A new type of dual-frequency impedance transformer is presented for ultra-high transforming ratio [32]. The proposed configuration consists of parallel coupled-line, series transmission lines and short-ended stubs. Since existing architectures are limited to a transforming ratio of 5, these transformers achieve a transforming ratio of 10, making them more practical and can be used in different environments. All the above-discussed architectures match real load to real source at two distinct frequencies. Nevertheless, a more practical scenario describes matching a real source to a complex load at two distinct arbitrary frequencies as in power amplifiers. Many researchers proposed different matching networks to consider this scenario. Few remarkable works have been discussed here.

A three-section transformer and later a generalized impedance transformer were reported in [33] and [34], respectively. Both of these have very complex design equations of the fourth degree. Neither of them reported any fabricated prototype. However, [33] derives an important equation for generating conjugate at two frequencies with a single transmission line which is utilized in many future architectures. Another shunt stub dual-band impedance transformer is proposed in [35]. This transformer has two sections: a two-section transmission line and two-section shunt stubs, either single-sided or double-sided resulting in complex non-linear equations. A simple T-section dual-band transformer was proposed in [36] that utilizes [33] conjugate property but had severe flaws in the sense that the solution was not physically fabricable in some cases and was not a generalized case. No prototype has been fabricated. A π-structure impedance transformer for frequency-dependent complex loads was proposed by [37]. This architecture is compact but based on non-linear equations to be solved simultaneously. Another π-structure based architecture along with L-network for dual-band matching has been reported in [38]. Closed-form design equations are derived along with their application in the dual-band power amplifier. Applications of coupled lines in matching complex load were reported in [28]-[30]. An inherent DC block coupled

line dual-band tuner was reported in [39]. Its application in dual-band T-junction power divider was also reported. The coupled lines used in [39] have to guarantee match both for real as well as for imaginary parts of Z_{in}, that too, at two different frequencies, which is often difficult with microstrip coupled line having unequal even/odd mode phase velocities. Another Coupled-line based architecture was reported in [40] and [41] along with L-network in cascade. Simple closed-form design equations have been discussed utilizing [39] conjugate property.

Different architectures by Maktoomi et.al were reported in [42] ,[43] . In [42] design, a dual-band quarter-wave line has been utilized along with another L-network. In [44], an important dual-band admittance property of a two-section transmission line was reported. This architecture consists of two-section transmission along with a dual-band stub. This paper also reported its application in power-divider. All architectures have fabricated prototypes along with closed-form design equations.

Tri-band Matching Networks

As evident from the numerous designs cited and discussed in the previous section, dual-band impedance matching is a well-lit research topic in the community. Contrary to this, tri- and quad-band impedance matching is not much dealt with. [45] proposed a tri-frequency impedance transformer, though specific to a Wilkinson Power Divider, with its limitation being the approximation and curve-fitting techniques used to establish the same. An LC resonator-based tri-band impedance matching circuit has been proposed in [46] whose limitation lies in the use of lumped components, thus proving incompetent at high frequencies. [47] , [48] proposes tri-band designs based on cascaded C-type coupled lines. This has a complicated layout and requires even and odd-mode velocity compensation when designed in microstrip technology. The multi-band impedance transformer discussed in [48] transforms real to real impedances, and that too not at any arbitrary frequency - this being a limitation.

Post-tri-band, designs have been proposed that accounts for generalized theorems that can be extended to match any number of frequency bands of interest. [49] discussed such a generalized impedance matching technique. Though the design equations are closed form, the design process becomes complicated as the number of bands exceeds 3 (owing to the fact that for implementing matching at each different band, an extra section gets added). This happens to be a major limitation of the design. A generic tri-band impedance matching network has been discussed in [50] that incorporates a dual to tri-band transformer stage. Though the design provides an advantage in selecting any dual-band impedance transformers, the drawback of this design lies in its complicated mathematics involved.

2.1.2 Power Dividers

Another important passive device in any RF front end is a power divider used to divide power between N ports, either equal or unequal, depending on the application. The most common power divider is the T-junction power divider, which has the drawback of isolation between two ports. This issue is readily addressed by Wilkinson Power Divider [19]. However, it suffers the disadvantage of narrow bandwidth because of quarter-wavelength transmission lines. The last decade has seen significant advancement in power dividers that provide solutions to multi-band or broadband designs. [52]-[105]. With the addition of several bands in emerging wireless technology to provide more and more functionality in a single device, the literature research on power dividers in the last decade mainly focuses on increasing the number of bands along with excellent performance in terms of return loss and isolation between the ports [52]-[68]. As discussed in case of matching networks, there is also plenty of research done in designing of dual-band power dividers [52] - [64], followed by multi-band power dividers [65] - [68].

A literature survey related to recent reports on WPD design reveals that the importance has been on increasing the number of bands and isolation bandwidth [52]-[68]. There are

number of design techniques to increase the number of bands in the operating frequency range. Originally, the dual-band WPDs [52]-[64] evolved, later followed by tri-/quad-band WPDs [65]-[68]. However, expanding the number of bands lead to increased circuit size along with circuit complexity. The dual-band WPDs in the literature includes WPD without reactive elements namely by attaching two central transmission line stubs in the conventional structure [52], unequal WPD operating at arbitrary dual-frequencies [53], WPD with composite left-/right-handed transmission lines [54], WPD with high power division operating at two bands by cascading dual-band T-section structures[55], with reactive elements including two-transmission lines and reactive lumped elements [56], WPD without stubs and additional lumped elements [57], WPD with common inductor with complex load [58], coupled-line based WPD and including four lumped elements [59], multi-band WPD utilizing multi-section LC-ladder circuits [60], with extended frequency ratios including two-section two resistor WPD with design able frequency ratio from 1 to ∞ [61], coupled lines and open stubs based to provide compensation [62], an enhanced frequency ratio coupled-line dual-band WPD with different ratios [63], speculation of different frequency ratio is presented by choosing different physical lengths ratio [64] and a lot more. Few tri-band WPDs includes, WPD operating at three frequencies utilizing $\lambda/4$ open stubs with less frequency bandwidth in the operating bands [66], WPD operating at three distinct bands with open and short circuit stubs at the input and output port [65],tri-band WPD utilizing coupled-lines [67], and quad-band WPD using generalized negative-refractive-index transmission-line unit cells [68] etc.

Another solution lies in developing WPD design schemes for wideband operations. There are several techniques to design wideband WPD by integrating dual-operation of filtering and frequency selectivity at single/multi-band simultaneously [70]-[78]. The distinct methods to design filtering WPDs include replacing the quarter-wave transmission line with the bandpass filter [70]-[71], merging the filtering and divider circuits to obtain the desired operation [72],

etc. A few examples for designing these WPDs include the use of resonators such as spiral resonators to realize the compact size and bandpass filtering response [73], filtering WPD based on four quarter-wave resonators to improve out-of-band rejection [74], substituting quarter-wave transmission line with resonators (multi-mode) capable of splitting the power and selecting the frequency simultaneously [75], filtering power divider with resonators to enhance the second harmonic suppression [76], a combination of Gysel PD and WPD to enhance out-of-band rejection [77], dual- wideband with filtering characteristics [78] and many more. These techniques provide dual-operation but suffer the disadvantage of narrow passband at the centre frequency, restricting their usage in ultra-wideband applications.

Hence, other techniques were proposed to increase the passband of WPDs to provide power splitting at a wider range of operations [79] - [105]. These approaches entail the increment of the operating bandwidth along with enhanced isolation between the output ports. A technique to extend the operating bandwidth is multi-layer microstrip- to - slot - line transition [79]-[85]. These techniques include design of WPD with multi-layer slot line with isolation resistor present between two layers [79], multi-layer balanced-to-unbalanced PD with three metallic layers and two substrate layers [80], WPD based on slot line resonators with two-layer substrate [81], WPD using stepped impedance three-line coupled structure [82], out-of-phase PDs using tightly coupled lines and slot line transitions [83], out-of-phase WPD based on slot line [84], out-of-phase PD based on double-sided parallel strip-lines [85], etc. However, these circuits are paradigmatic for applications that require heat sinks because of the two-layer substrate, such as power amplifiers. Other broadband WPD design techniques are designed using multi-mode resonators [86]-[88], parallel-coupled lines [89]-[91] or quasi-coupled line based design [92], three-line coupled lines [93]-[97], multi-section WPDs [98], stepped impedance lines with open-circuited stubs [99]-[100], DC isolated wideband WPD along with core WPD and coupled lines at the input and output port [101]. Although many of these techniques provide appropriate port matching and isolation between

output ports, they include complicated design procedures and a lack of appropriate analysis to design an isolation network. Moreover, the use of reactive lumped components in the isolation network restricts the usefulness of reported wideband WPDs in many advancing applications [102]-[105]. Another critical design aspect along with wideband operation is the DC blocking capability, which is extremely useful for Doherty and balanced power amplifiers etc. The WPD with DC-blocking capability utilizes resonators, coupling structures, and stepped-impedances, making the design either complicated or based on optimization algorithms.

2.1.3 Power Amplifiers

The history of amplifiers dates back to 1912 when Lee De Forest invented the triode vacuum tube-based amplifier [106]. Advancements in modern systems result in significant contributions in designing different amplifiers to achieve good performance. Based on biasing, different linear operations are defined; namely, Class-A, B, AB and C. Power amplifier classes are mainly based on the current conduction angle during which current passes through the device. Another class of amplifiers known as switched-mode amplifiers are Class-D and Class-E. Class-A, B, AB and C has a theoretical maximum efficiency of 50%, 78.5%, 65% and 90%. These amplifiers are used for linear designs; however, switched-mode power amplifiers, including Class-D and E, utilize the active device as a switch rather than the linear gain device. The first switched-mode power amplifiers are reported by Gerald D. Ewing [107] and first published in 1975 [108]. Another important classification of the power amplifier is based on the termination of harmonics and hence labelled as harmonic-tuned power amplifiers. Class-F and F^{-1} are two important harmonic-tuned amplifiers in which different harmonics at the drain of the transistor is tuned to achieve desired performance. The maximum theoretical efficiency achieved by Class-F and F^{-1} is 100%.In class-F PA, the even-harmonics are short-circuited, while odd-harmonics are open-circuited at the drain of

the transistor and vice-versa for Class-F^{-1}. It results in no overlapping between the current and voltage, resulting in zero internal dissipation power. It is well defined in a harmonic-tuned power amplifier; maximum efficiency can be achieved by altering the infinite harmonics. However, it is impossible to control infinite harmonics; the first few harmonics are altered to achieve optimum performance. To date, remarkable contributions have been made in this domain and are extensively explained briefly.

Different harmonic-tuned power amplifiers that are required to provide short/open-conditions at the drain of the transistor for increasing efficiency reported as Class-F PA by F. H. Raab with maximally flat waveforms [109] that derives the basic derivations among the various Fourier coefficients of waveform and proves the effect of addition of harmonics in maximizing the efficiency and study of different classes of amplifiers including Class-C, E and F based on finite harmonics [110]. Another research reported in [111] features a new class of switching amplifiers considering the features of both Class-E and F^{-1}. It incorporates the Class-E, F^{-1} features such as consideration of parasitic allowing zero-voltage switching and some harmonics are tuned to achieve more desirable voltage and current waveforms, respectively. The two early methods to design harmonic-tuned PA provide the theoretical foundation without simulation results. The harmonic tuning at the drain of the transistor improves the performance; different methods were proposed for examining the effect of harmonic tuning at the input of the transistor [112] - [113]. Alongwith the input harmonic terminations, optimization of biasing currents also affect the performance of the power amplifier [112]. The reported PA justifies the second harmonic input termination influence on the performance verified by the simulated waveforms. An early report of the second harmonic tuned power amplifier [114] demonstrates the effect of second harmonic variation on the performance; however the achieved measured results are not quite comparable. To study the behaviour of harmonic tuned PAs including Class F and F^{-1} [115]-[117], the research includes best harmonic tuning for highest efficiency with simulation results [115],

experimental operating conditions of Class F^{-1} with a non-linear output capacitor [115] and operational behaviour of Class F and F^{-1} [116]. [116]-[117] reports another class of amplifiers with waveform shaping defined as the saturated amplifier. In [115], saturated amplifiers elaborates the performance improvement over linear C_{out} amplifier.

Another method to design a harmonic tuned PA is based on composite right/left-handed transmission lines [118]-[121]. [118], [119] describes the harmonic tuner and trap method based on composite right/left-handed (CRLH) transmission line. In [118], two structures for Class-F power amplifier is designed; one uses open CRLH stub and the other two CRLH stubs to suppress second third and fourth harmonics, respectively, while maintaining the match at the fundamental frequency. Similarly, utilizing the same design approach, Class-F^{-1} PA is designed with series CRLH, and one open CRLH transmission line [119]. However, for both design methods, performance in terms of efficiency is not optimum. Another design approach utilizing a double CRLH transmission line is exploited to design the harmonic control network of high-efficiency Class-E^{-1} [120]. Likewise, utilizing dual-band CRLH transmission line input and output networks are designed for achieving high efficiency in Class-F PA [121]. However, design methods based on CRLH transmission lines are complicated, and performance is not optimum. Another methods for designing a Class-F^{-1} are proposed in [122]- [124]. The method proposed in [122] depicts tunable output matching network for achieving high performance, however suffers the disadvantage not considering the effect of parasitic. Another method to optimize the losses in distributed multi harmonic matching network to achieve high efficiency is defined in [123]. Similarly, [124] a optimized output matching network is designed and utilizes a bare-die transistor, hence not considering the effect of parasitic elements inside the transistor. Few recent research in the design of harmonic tuned PA includes high-frequency multi harmonic controlled Class-F PA [125], examining of an optimum third harmonic condition after the second-harmonic injection using a multi-harmonic load-pull simulation [126] and , a network known as Bowtie-Shaped

harmonic control circuit [127]. The method proposed in [125] is based on a three-stage low pass output matching network based on transmission lines with harmonic control of fourth order. The methodology defined in [126] includes harmonic injection of second harmonic while optimizing the third harmonic termination. The designed circuit requires two transistors i.e. one main and other is auxiliary transistor, hence increasing the form-factor and power dissipation. The method based on harmonic control circuit reported in [127] is based on harmonic control network in bowtie-shape along with output matching network. Although the defined networks provide good performance in terms of efficiency and gain, but there are no defined closed-form design equations and hence cannot be modified for other frequencies of operation.

Due to the increased demand of broadband RF front end, other continuous class of power amplifier for broadband operation is defined theoretical for the first time in [128]. This research reports a new design space for designing high efficiency broadband power amplifiers. It also includes the variation of fundamental and second harmonic variation while maintaining the performance over the wide range of operation. The research based on harmonic tuned continuous class power amplifier includes emphasizing the non-linear capacitance for wave shaping the continuous Class-F amplifier by reducing the dependence on second and third harmonics [129], extended version of continuous Class-F^{-1} by defining the new version of current waveform [130], another based on a modified elliptic low-pass filtering (LPF) matching network (MN) to design a single-mode continuous Class-F power amplifier [131], a broadband PA designed based on the series of inverse continuous modes (SICMs) [132] and few more. These defined methods are designed to provide optimum PA performance over a wideband range with or without harmonic variation.

Chapter 3

Impedance Matching Networks - Dual-Band with FDCL

3.1 Introduction

The impedance matching network is ubiquitous and crucial in any RF front end. The primary impedance matching network designed was a quarter-wave transformer that matches the resistive source and load at a single frequency of operation, as shown in Fig.3.1 [3]. The main disadvantage of using the quarter-wave transformer is the narrow bandwidth resulting from the utilization of quarter-wave transmission lines.

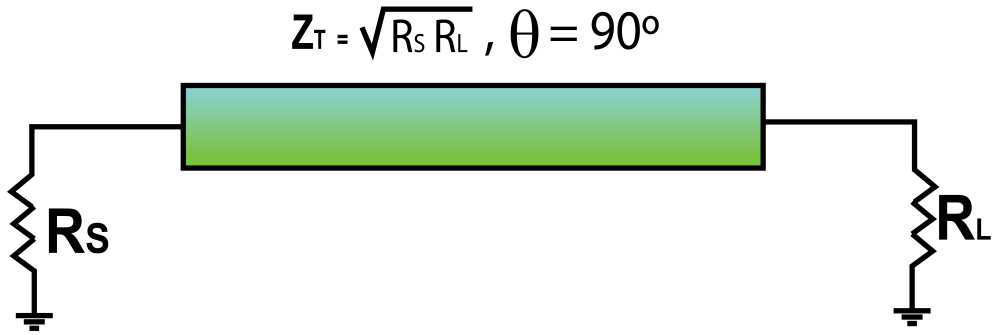

Fig. 3.1 Quarter-wave transformer

Another fundamental tool for impedance matching at a single frequency is Smith Chart, which allows the user to choose the load and source (resistive or reactive) impedance and helps to design the impedance matching network as shown in Fig. 3.2 [133]. With the help of the Smith Chart, the designer can arbitrarily choose source and impedance on the chart; then, depending upon the design methodology, either lumped or distributed elements can be selected. It is an important tool for designing the matching network but is limited to a single frequency of operation.

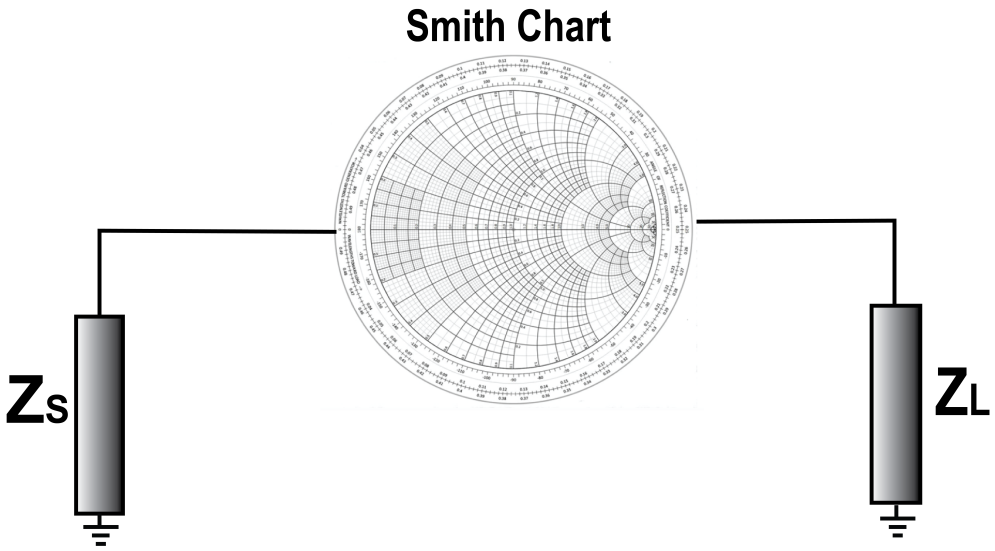

Fig. 3.2 Smith chart tool to match source impedance to load impedance

Wireless standards have transformed communication devices from single-function devices to multi-function ones. Multi-frequency impedance matching networks are crucial in the RF front end of such devices. For example, dual-band operations require dual-band matching networks. In this context, a couple of exciting early contributions include a dual-band two-section 1/3- wavelength transformer that operates at the fundamental, and its first harmonic [25], and a matching network that provides matching at two uncorrelated frequencies with closed design equations [26]. The subsequent dual-band impedance transformers providing important insights include π-structure [29], T-type architecture [36], and coupled-lines

based high impedance ratio transformer [32]. Other reports include dual-band matching for Frequency Dependent Complex Loads (FDCLs) using two-section shunt stub [35], and dual-band $\lambda/4$ lines [42].

In a pragmatic framework, the load impedance seen by the matching network is not resistive but reactive. Considering an RF front end, the impedance matching network residing between the power amplifier and antenna will see the complex impedance represented as $Z_S = R_S + jX_S$ and $Z_L = R_L + jX_L$ at the source and load side respectively as shown in Fig. 3.3. It can be

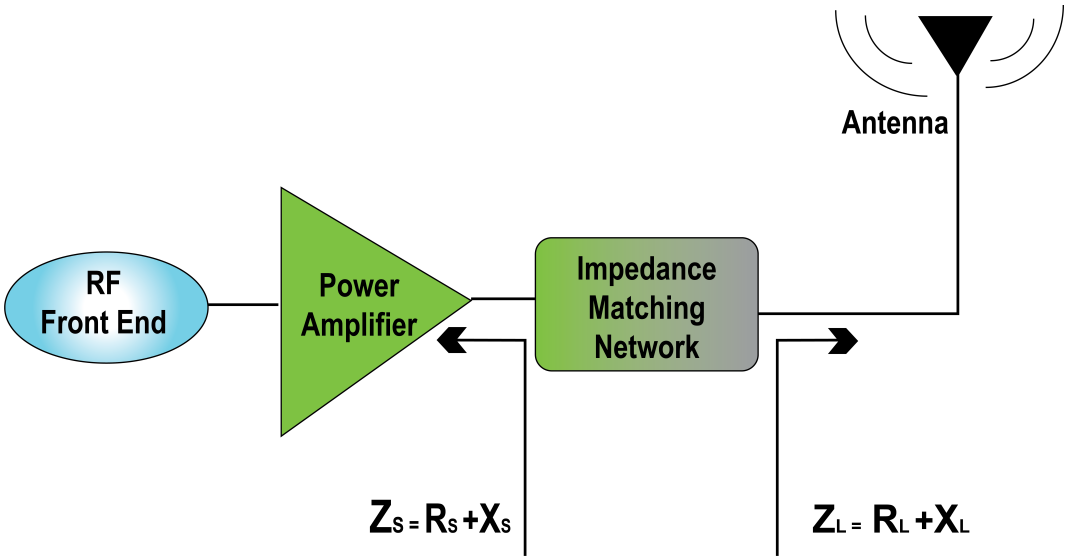

Fig. 3.3 Block diagram depicting different modules of RF front end with single matching network

seen that the there are two solutions for designing the impedance matching network in such scenario:

- Design a matching network that will match the complex impedance both at source and load as shown in Fig. 3.3
- Design two matching networks in cascade, one will transform the source impedance to resistive impedance R_X and the other will match the R_X to load impedance as shown in Fig. 3.4.

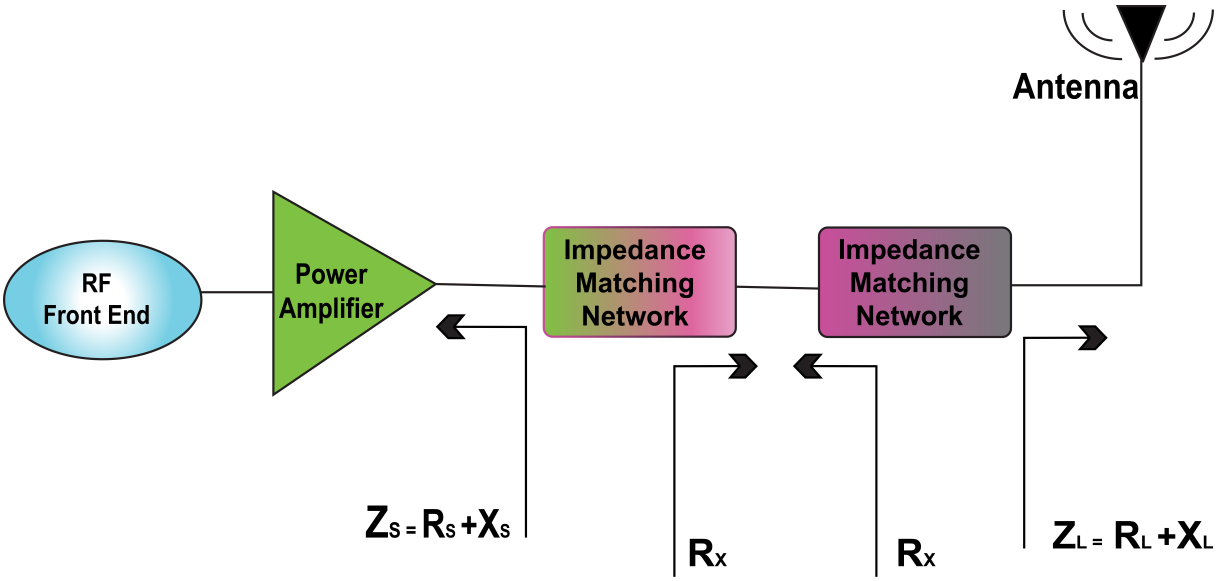

Fig. 3.4 Block diagram depicting different modules with cascaded matching networks

The other salient feature of designing the network is that it should operate at multiple frequencies simultaneously. In this thesis, the research focuses on developing the basic idea of designing impedance matching networks that will operate at two frequencies (Dual-band), considering both the former cases described.

3.2 Analysis of Dual-Band Impedance Matching Network - Design 1

The impedance matching network with resistive source and reactive load operating at two frequencies simultaneously is discussed. This study advances the dual-band matching state-of-the art by presenting a dual-frequency impedance transformer capable of matching a real source to Frequency Dependent Complex Load (FDCL) by cascading two transmission lines [35] in conjunction with just one stub that is defined as "unequal susceptance cancellation stub", able to provide the desired dual-band impedance matching.

3.2.1 Proposed Matching Network

We proposed the dual-band impedance transformer, presented in Fig. 3.5, which has two distinct sub-sections, namely Section-A and Section-B. Section-A is a two-section transmission line with distinct impedances and electrical lengths Z_1, Z_2, θ_1, θ_2 and transforms the load impedance into complex admittance whose real part, Re[Y_{in2}], equals the source admittance. Section-B is a dual-band open- or short-stub and is employed to cancel the unequal imaginary parts, Imag[Y_{in2}], of the admittance Y_{in2} at two uncorrelated frequencies. It is important to note that the term Imag[Y_{in2}] could be of the same or distinct sign at the two frequencies and therefore necessitates a slightly different design approach for the two scenarios.

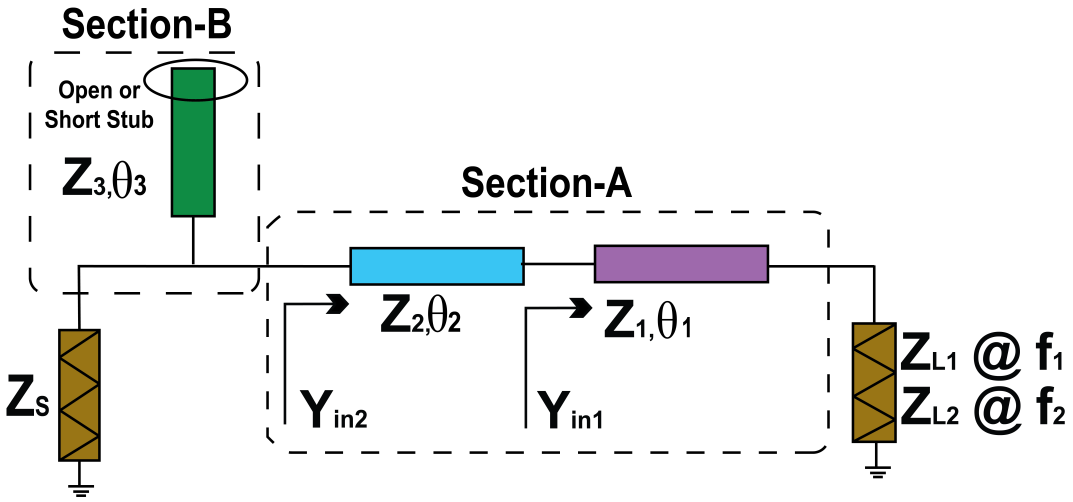

Fig. 3.5 Proposed dual-band impedance transformer

Design of Section - A

The load impedance can be either equal or different at two arbitrary frequencies i.e. Z_{L1} @ f_1 and Z_{L2} @ f_2. This section transforms the load into admittance Y_{in2} given in (3.1) [35].

$$Y_{in2} = G_{in2} + jB_{in2} \tag{3.1}$$

The real part of Y_{in2}, i.e. Z_{in2}, relates the transmission line parameters and the load impedance according to (3.2) and (3.3).

$$Z_{in2} = Z_2 \frac{Z_{in2} + jZ_2 tan\theta_2}{Z_2 + jZ_{in1} tan\theta_2} \tag{3.2}$$

$$Z_{in1} = Z_1 \frac{Z_L + jZ_1 tan\theta_1}{Z_1 + jZ_L tan\theta_1} \tag{3.3}$$

For matching, Re(Y_{in2}), i.e. G_{in2}, should equal the source admittance at two uncorrelated frequencies simultaneously i.e.

$$G_{in2} = Re[Y_{in2}] = \frac{1}{Z_s} = Y_s @ f_1; f_2 \tag{3.4}$$

Equations (3.2)-(3.4) can be solved to determine the values of electrical lengths θ_1 and θ_2. The resulting expressions in (3.5a)- (3.5b) assumes that the values of impedance's Z_1 and Z_2 should be within fabricable limits i.e. [20,150] Ω.

$$a_1 tan^2\theta_2 + b_1 tan\theta_2 + c_1 = 0 \tag{3.5a}$$

$$a_2 tan^2 r\theta_2 + b_2 tanr\theta_2 + c_2 = 0 \tag{3.5b}$$

Here, r is the frequency ratio (f_2/f_1) and the coefficients $a_{1,2}$, $b_{1,2}$ and $c_{1,2}$ are dependent on the transmission line parameters $Z_{1,2}$, $\theta_{1,2}$, and load impedance $Z_{L_{1,2}}$.

$$a = (Z_2^4 R_L^2 Y_s + Z_2^4 X_L^2 Ys - Z_1^2 Z_2^2 R_L) tan^2(r\theta_1) \quad -2Z_1 Z_2^4 Y_s X_L tan(\theta_1) + (Z_1^2 Z_2^4 Y_s - Z_1^2 Z_2^2 R_L) \tag{3.6a}$$

$$b = (-Z_1^2 Z_b^3 X_L Y_s) tan^2(r\theta_1) \quad +2(Z_1^3 Z_2^3 Y_s - Z_1 Z_2^3 R_L^2 Y_s) tan(r\theta_1) + 2Z_a^2 Z_b^3 X_L Y_s \tag{3.6b}$$

$$c = (Z_a^4 Z_b^2 Y_s - Z_a^2 Z_b^2 R_L) tan^2(r\theta_1) + 2Z_a^3 Z_b^2 X_L Y_s tan(r\theta_1) + (Z_a^2 Z_b^2 X_L^2 Y_s + Z_a^2 Z_b^2 R_L^2 Y_s - Z_a^2 Z_b^2 R_L) \tag{3.6c}$$

Now the loads can be equal / unequal at frequencies f_1 and f_2. Here, for example, a_1, b_1, c_1 corresponds to Z_{L1} @ f_1, while the coefficients a_2, b_2, c_2 corresponds to the situation Z_{L2} @ f_2. Under these conditions the design parameters of the transmission line segments can then be obtained using (3.5a)- (3.5b).

Design of Section B

For dual-band matching, the source impedance, Y_s, is matched to the $Re[Y_{in2}]$, i.e. G_{in2}, at both the frequencies. Therefore the section-B need to be designed in such way to cancel the $Imag[Y_{in2}]$, i.e. B_{in2} given by (3.7), at the two uncorrelated frequencies i.e. f_1 and f_2.

Required Susceptance B_1 and B_2 of same sign

When the signs of B_{in2} are of same sign then the required susceptances from section B will be of same sign. The section B could be either a short or open stub. For instance, the open stub need to fulfill (3.8a)-(3.8b) for dual-band impedance matching.

$$jB_1 = \frac{jtan(\theta_3)}{Z_3} \qquad @f_1 \tag{3.8a}$$

$$jB_2 = \frac{jtan(r\theta_3)}{Z_3} \qquad @f_2 \tag{3.8b}$$

$$B_{in2} = \frac{Z_2X_Ltan(r\theta_1) + (Z_1^2 - Z_2^2R_LY_s)tan(r\theta_2)tan(r\theta_1) + Z_1X_Ltan(\theta_2) + Z_1Z_2R_LY_s - Z_1Z_2}{Z_1^2Z_2tan(r\theta_1) + Z_2^2X_Ltan(r\theta_2)tan(r\theta_1) + Z_1Z_2^2tan(r\theta_2) + Z_1Z_2X_L} \tag{3.7}$$

Required Susceptance B_1 and B_2 of different sign

In this case, an open stub should fulfill (3.9a)-(3.9b) for achieving dual-band impedance matching.

$$jB_1 = \frac{jtan(k\pi - \theta_3)}{Z_3} \qquad @f_1,\ \ k \in 1,2...N \tag{3.9a}$$

$$jB_2 = \frac{jtan(r\theta_3)}{Z_3} \qquad @f_2 \tag{3.9b}$$

The stub parameters Z_3 and θ_3 can be determined by solving (3.8) and (3.9).

3.2.2 Design Example and Case studies

To validate the theory, we consider different case studies given in Table 3.1. Here the load impedance could be real, unequal or FDCL and is a distinct scenario when compared to [44]. Cases 1 and 3 in Table 3.1 specifically support the situations represented by (3.8) and (3.9), respectively. The simulation results in Fig. 3.6 demonstrate the effectiveness of the proposed technique.

Table 3.1 Design parameters for different loads at different frequencies

Case	**Frequencies (GHz)**	**Load** (Ω)	Z_1 (Ω), $\theta_1(^\circ)$	Z_2 (Ω), $\theta_2(^\circ)$	$Z_3(\Omega)$, $\theta_3(^\circ)$
1	f_1 = 2.4 f_2 = 5.8	R_{L1}=180 R_{L2}=280	90, 70.9	70, 48.5	60.03, 22.86, Open Stub
2	f_1 = 2.4 f_2 = 5.8	R_{L1}=200+j60 R_{L1}=250+j100	100, 89	70, 38.5	81.13, 25.95 Open Stub
3	f_1 = 1.0 f_2 = 3.0	R_{L1}=100 R_{L2}=120	80, 45	60, 47.61	150.75, 137.5, Open Stub

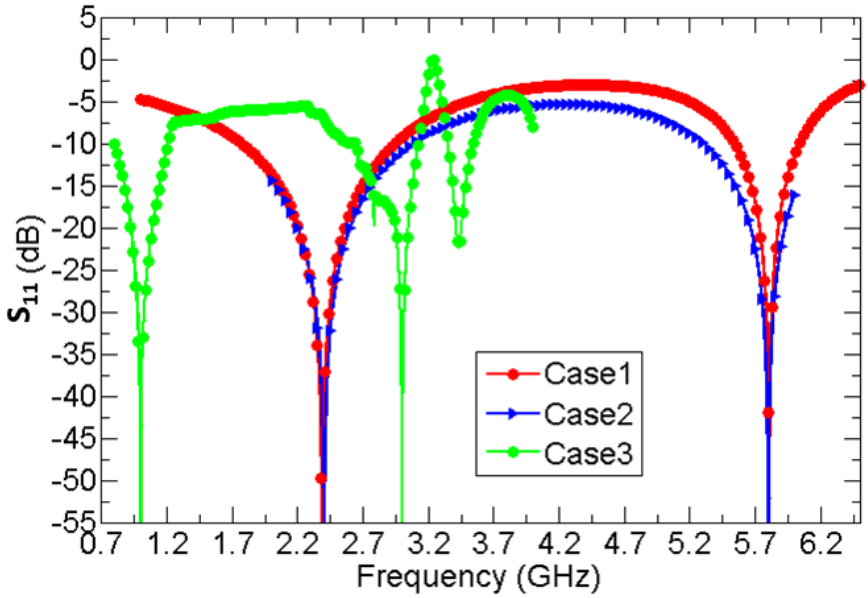

Fig. 3.6 S_{11}(dB) for different cases listed in table 3.1

For the evaluation of the proposed technique, the prototypes, in Fig. 3.7 and Fig. 3.8, have been developed on RO5880 substrate for cases in Table 3.2. The subsequent measured and simulated return loss, depicted in Figs. 3.9, 3.10, 3.11 and Table 3.3 show very good agreement and thus validate the proposed concept.

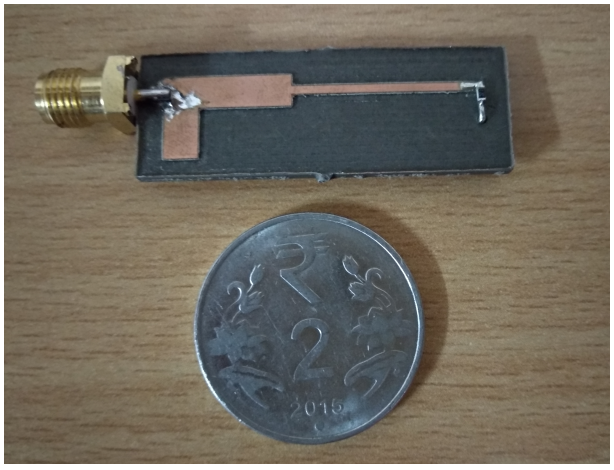

Fig. 3.7 Fabricated prototype for real load of 250Ω

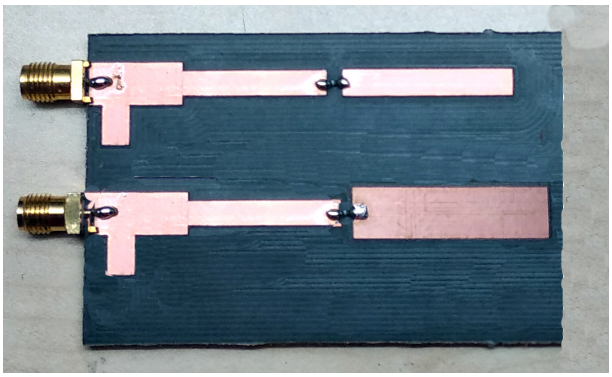

Fig. 3.8 Fabricated prototype for FDCL of 100-j35.4Ω and 150-j6.4Ω

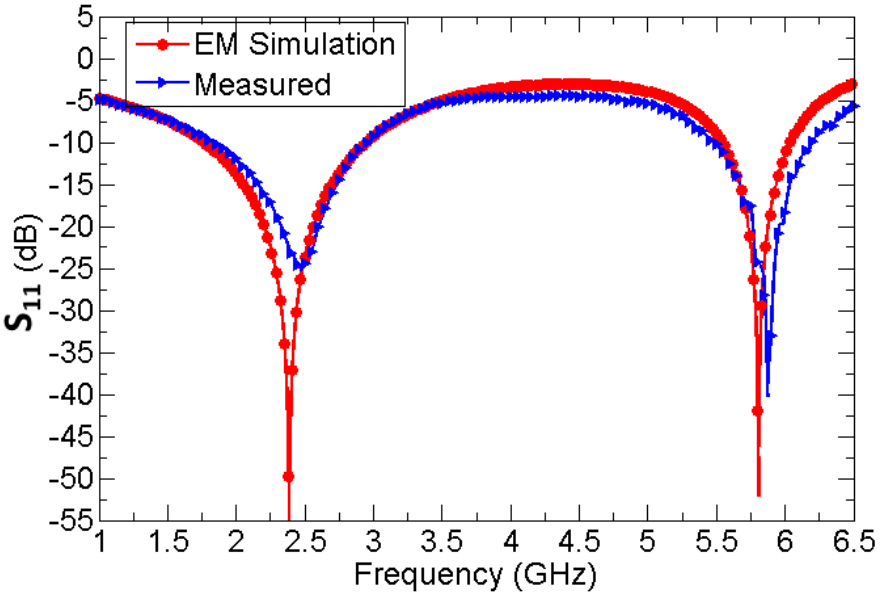

Fig. 3.9 EM simulation vs measured results for real load of 250 Ω

Table 3.2 Design parameters for fabricated prototypes

Case	**Frequencies (GHz)**	**Load (Ω)**	Z_1 (Ω), $\theta_1(^\circ)$	Z_2 (Ω), $\theta_2(^\circ)$	Z_3(Ω), $\theta_3(^\circ)$
Real	f_1 = 2.4 f_2 = 5.8	Z_{L1}=250 Z_{L2}=250	100, 84	60, 41.9	65.43, 24.5, Open Stub
FDCL	f_1 = 0.9 f_2 = 2.4	Z_{L1}=100-j35.4 Z_{L2}=150-j6.4	60, 87	40, 34.2	56.11, 18.6, Open Stub

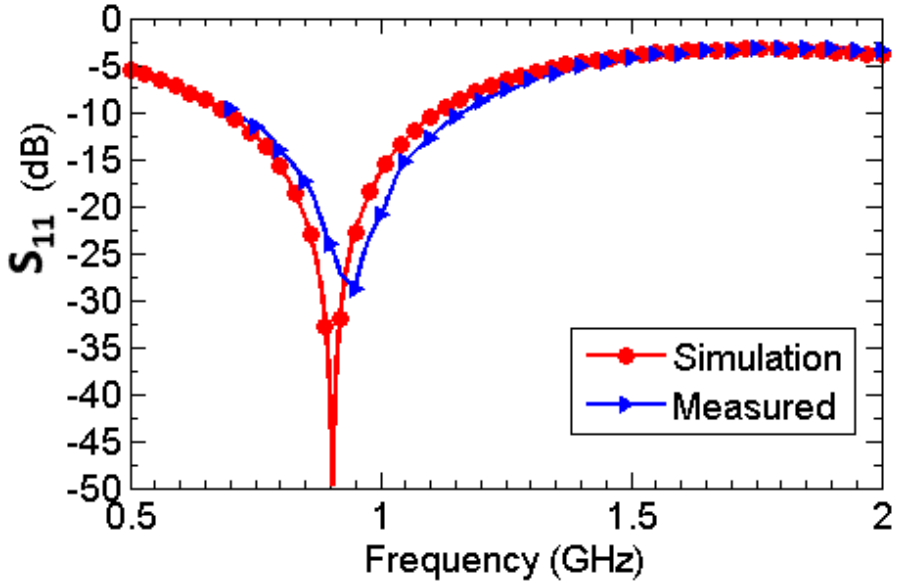

Fig. 3.10 EM simulation vs measured results for load=100-j35.4 @0.9GHz

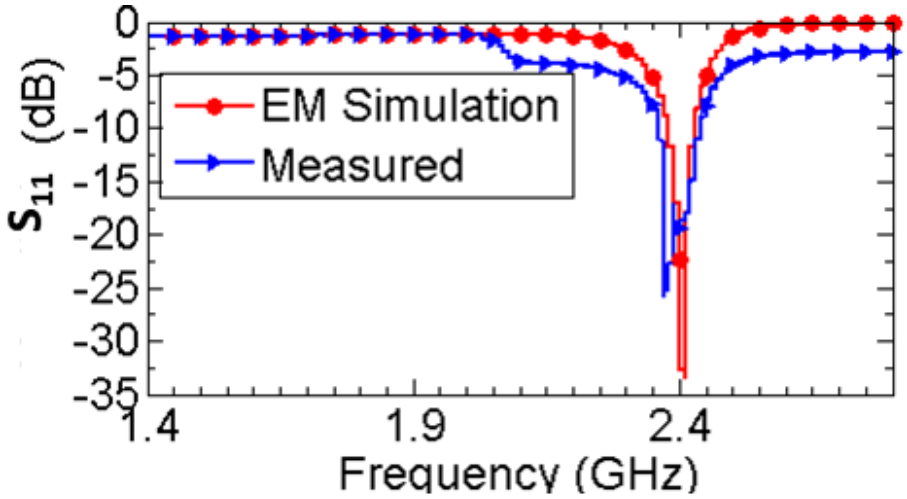

Fig. 3.11 EM simulation vs measured results for load=150-j6.4 @2.4GHz

Table 3.3 Simulation & measured results for FDCL load

Parameter	**Simulated Results**		**Measured Results**	
Frequencies (GHz)	0.9	2.4	0.95	2.36
S_{11}**(dB)**	-52.2	-33.8	-28.6	-25.2

Table 3.4 compares the designed matching network with the other state-of-the-art dual-band design methodologies.

Table 3.4 Comparison with the other state-of-the-art

References	Venue	Method used	Load type	Design equations
(2016),[45]	MWSCAS	admittance property of two-section transmission line	Real	simple
(2008), [29]	JPIER	pi-structure	Real	complex
(2010),[35]	TMTT	two-section transmission line along with two-section stubs	FDCL	complex
This work (2018)	APMC	**single stub for cancellation unequal susceptance**	**FDCL**	simple

3.3 Analysis of Dual-Band Impedance Matching Network - Design 2

In this design, we used two unequal susceptance cancellation stubs and a transmission line to form a π-structure dual-band impedance transformation network. The main idea is to cancel the unequal susceptance of the load using a single open/short stub, then match the remaining unequal real impedance to the source at two arbitrary frequencies of interest. Since the single stub is to cancel the unequal susceptance at two uncorrelated frequencies, non-linear equations need systematic evaluation either using a graphical approach or numerical method techniques. The proposed design procedure is supported through design equations and several case studies. A prototype has been fabricated on RO5880, providing measurement verification with theoretical and simulation results.

3.3.1 Proposed Matching Network

The design structure of proposed dual-band matching network is shown in fig. 3.12. This π-structure impedance transformer matches FDCL load to a real source at two uncorrelated frequencies of interest. This architecture consists of two sections, namely sections A and B. Section-A consists of a single stub having characteristic impedance Z_1 and electrical

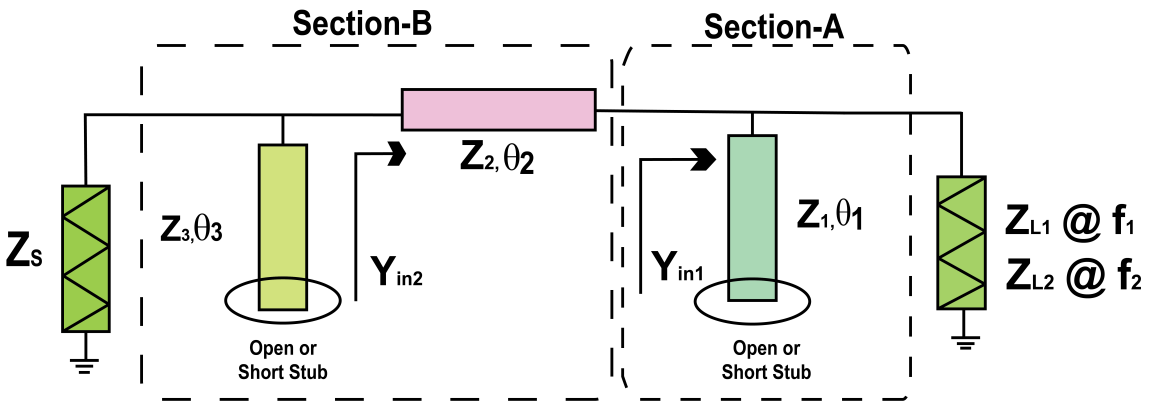

Fig. 3.12 Proposed dual-band impedance transformer

length θ_1, that cancels the imaginary part of load at two frequencies. A single stub cancels the imaginary value leaving only an unequal real part of the load. Section-B consists of a transmission line along with a stub having different impedance's and electrical lengths Z_2, Z_3, θ_2, and θ_3 respectively. The admittance Y_{in1} at the input of Section-B contains the only real part but of distinct values at two arbitrary frequencies. The role of a transmission line is to match the unequal real impedance at two frequencies to the source impedance i.e Re $[Y_{in2}]$ = G_s @ f_1 and f_2. After matching the unequal real part to the source impedance, the remaining susceptance will again be cancelled by stub, i.e.Imag$[Y_{in2}]$=0. The mathematical design equations and analysis of the proposed design are discussed in the subsequent sections.

Design of Section A

The section-A shown in Fig. 3.13 consists of single stub that will cancel the imaginary part of the load. The load can be either equal or different at two arbitrary frequencies i.e. Z_{L1} @ f_1 and Z_{L2} @ f_2, given by:

$$Z_{L1} = R_{L1} + jX_{L1} \qquad @f_1 \tag{3.10a}$$

$$Z_{L2} = R_{L2} + jX_{L2} \qquad @f_2 \tag{3.10b}$$

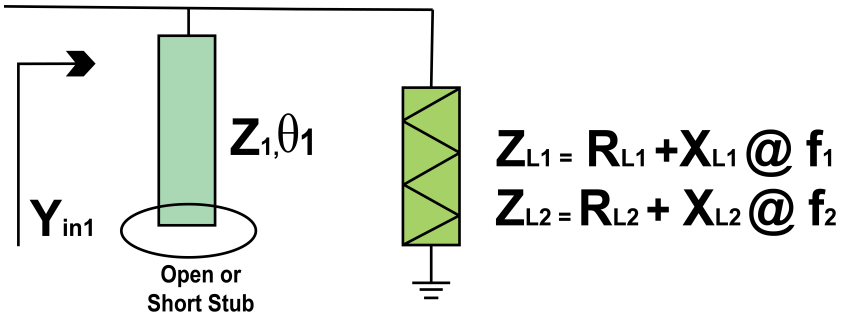

Fig. 3.13 Section-A cancelling the imaginary value of load

The imaginary part of the load i.e. X_{L1} @ f_1 and X_{L2} @ f_2 need to be cancelled using a single stub that can be open or short depending on the load. For open stub to cancel imaginary part of the load, the following equations need to be satisfied:

$$jB_{in1} = \frac{jtan(\theta_1)}{Z_1} \qquad @f_1 \tag{3.11a}$$

$$jB_{in2} = \frac{jtan(r\theta_1)}{Z_1} \qquad @f_2 \tag{3.11b}$$

Here, r is the frequency ratio i.e. f_2/f_1 The values of characteristic impedance Z_1, and electrical length θ_1 can be found out using equations (3.11a) and (3.11b). The admittance looking into the stub i.e. Y_{in1} has imaginary part equal to zero at two arbitrary frequencies of interest i.e. Imag[Y_{in1}]=0 and is given by:

$$Y_{in1} = G_{in1} = 1/R_{L1} \qquad @f_1 \tag{3.12a}$$

$$Y_{in1} = G_{in1} = 1/R_{L2} \qquad @f_2 \tag{3.12b}$$

The role of section-B is to match the two unequal real impedance to source impedance at two frequencies.

Design of Section B

The mathematical analysis of this section is as follows: The input admittance looking into a transmission line with characteristic impedance Z_2, and electrical length θ_2 as shown in Fig.3.14 can be defined as follows:

$$Y_{in2} = \frac{Z_2 + jZ_L tan\theta_2}{Z_2[Z_L + jZ_2 tan\theta_2]} \tag{3.13}$$

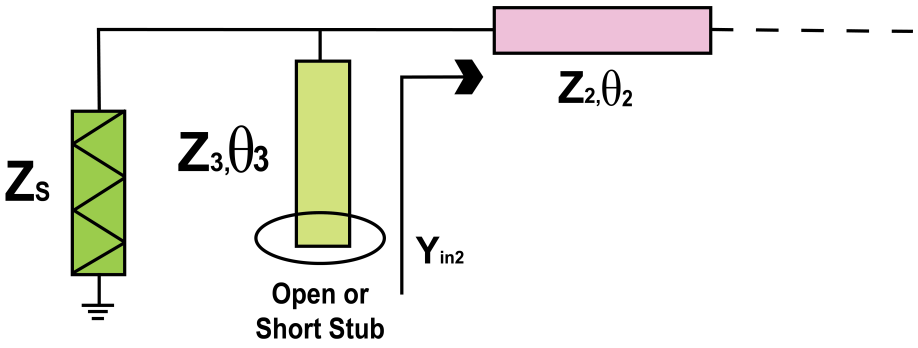

Fig. 3.14 Section-B matching the unequal real value to source

Here, Z_L is defined as the remaining unequal real load at two frequencies. Since, real part of the transmission line has to be equal to source impedance Z_s, the real and imaginary part of Y_{in2} i.e. G_{in2} and B_{in2} respectively is given by equation (3.14a) and (3.14b).

$$G_{in2} = \frac{R_1 + R_1 tan^2\theta_2}{R_1^2 + Z_1^2 tan^2\theta_2} \tag{3.14a}$$

$$B_{in2} = \frac{R_1^2 tan\theta_2 - Z_1 tan\theta_2}{Z_1[R_1^2 + Z_1^2 tan^2\theta_2]} \tag{3.14b}$$

As can be seen from Fig. 3.14, the real part of Y_{in2} i.e G_{in2} should be equal to source admittance i.e. $1/Z_s$, the resulting equations are as follows:

$$(Z_2^2 - Z_s R_{L1})tan^2\theta_2 + (R_{L1}^2 - Z_s R_{L1}) = 0 \qquad @f_1 \tag{3.15a}$$

$$(Z_2^2 - Z_s R_{L2})tan^2(r\theta_2) + (R_{L2}^2 - Z_s R_{L2}) = 0 \qquad @f_2 \tag{3.15b}$$

Solving equations (3.15a) and (3.15b), the value of Z_2 and θ_2 can be calculated.
The remaining part is the resulting susceptance at the input of the transmission line, i.e. B_{in2} which can be easily cancelled by a single stub at two frequencies of interest using equations (3.11a) and (3.11b). The susceptance generated can be of the same or distinct sign at two frequencies, which necessitates a slightly different approach for the second scenario. If both unequal susceptances generated will be of distinct sign, for the open stub to cancel susceptance at two frequencies, the following equations need to be satisfied:

$$jB_1 = \frac{jtan(k\pi - \theta_3)}{Z_3} \quad @f_1, \;\; k \in 1,2...N \tag{3.16a}$$

$$jB_2 = \frac{jtan(r\theta_3)}{Z_3} \qquad @f_2 \tag{3.16b}$$

Similarly, the value of Z_3 and θ_3 can be found out solving (3.16).

Here, one interesting feature of this architecture is that, for matching of two unequal real loads at two uncorrelated frequencies, only section-B is required as shown in Fig. 3.15. All designs equations remain valid for section-B alone.

3.3.2 Design Example and Case studies

In this section, to validate the theory, different case studies has been considered. Different FDCL loads at different frequencies are considered. Fig 3.16 demonstrate the effectiveness

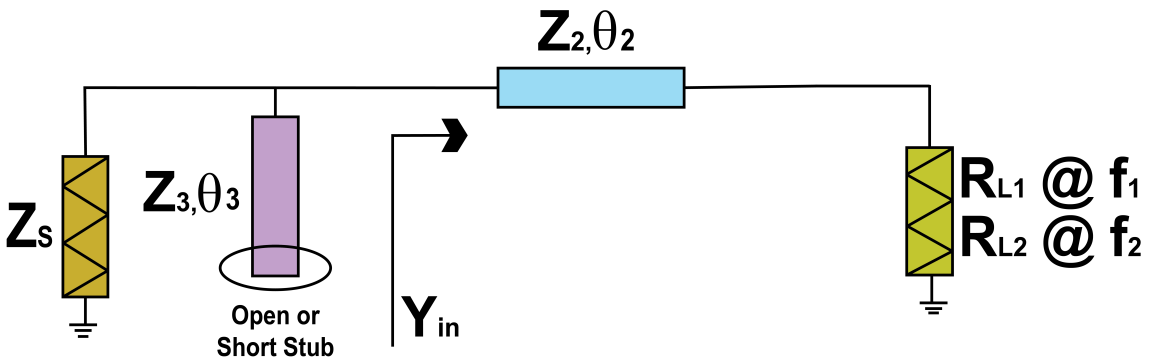

Fig. 3.15 Architecture for matching of unequal real loads

Table 3.5 Design parameters for different loads at different frequencies

Case	**Frequencies** (GHz)	**Load** (Ω)	Z_1 (Ω), $\theta_1(^\circ)$	Z_2 (Ω), $\theta_2(^\circ)$	$Z_3(\Omega)$, $\theta_3(^\circ)$
1	f_1 = 1.0 f_2 = 1.8	R_{L1}=100+j*80 R_{L2}=150+j*100	120.28, 210.84	74.92, 67.48	107.3, 128.8, Open Stub
2	f_1 = 1.8 f_2 = 2.4	R_{L1}=60+j*10 R_{L2}=40+j*20	141, 15.72	41.82, 149.9	198, 201.3, Open Stub
3	f_1 = 1.0 f_2 = 1.8	R_{L1}=50+j*80 R_{L1}=60+j*120	109.9, 212.98	55.64, 74.024	51.35, 129 Open Stub

of the proposed impedance matching scheme.

A prototypes given in Fig. 3.17 and 3.18, has been developed on RO5880 substrate for case 3 in Table 3.5. The chosen frequencies are $f_1 = 1.0GHz$ and $f_2 = 1.8GHz$. The measured and simulated return loss, depicted in Fig. 3.19, 3.20 and Table 3.6, shows good agreement and hence validated the proposed dual-band matching network. Table 3.7 compares the proposed network with other existing networks.

The above-discussed methods are defined for matching the FDCL to a resistive source. Practically, there can be scenarios where there is a need for a network that has frequency-dependent complex source and load, as discussed in the next section.

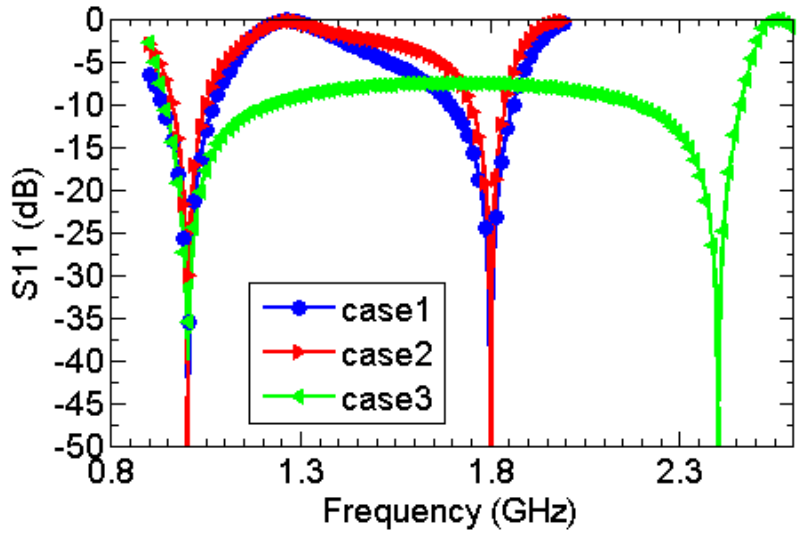

Fig. 3.16 S_{11}(dB) for different cases listed in table 3.5

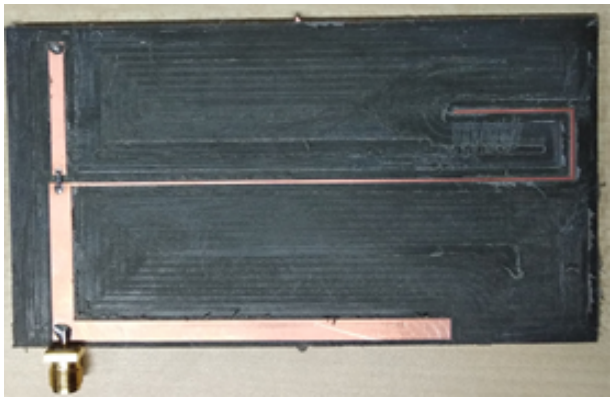

Fig. 3.17 Fabricated prototype with load-A @ 1 GHz: Load A-50+j80

Table 3.6 Simulation & measured results

Parameter	**Simulated Results**		**Measured Results**	
Frequencies (GHz)	1.0	1.80	1.1	1.78
S_{11}**(dB)**	-48.6	-43.2	-25.292	-40.210

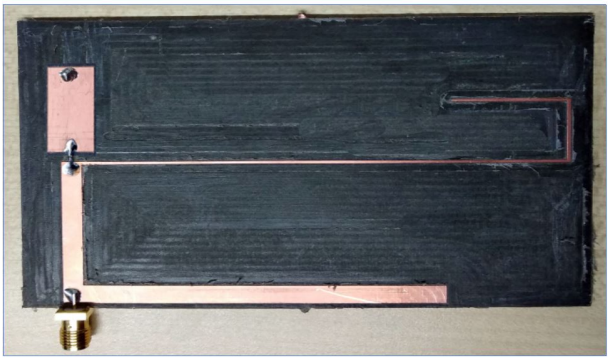

Fig. 3.18 Fabricated prototype with load-B @ 1 GHz: Load B-60+j120

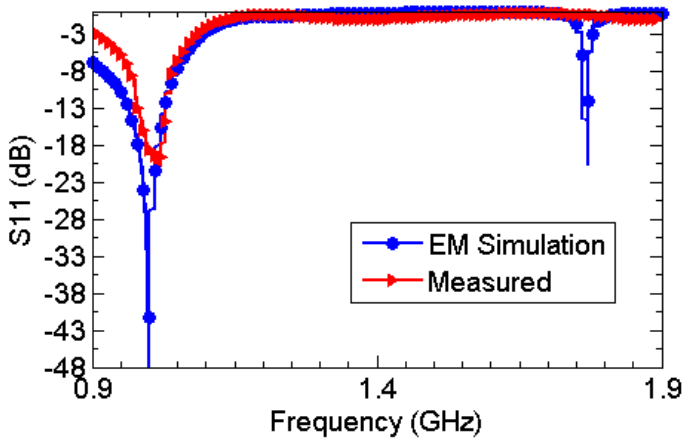

Fig. 3.19 EM simulation vs measured results

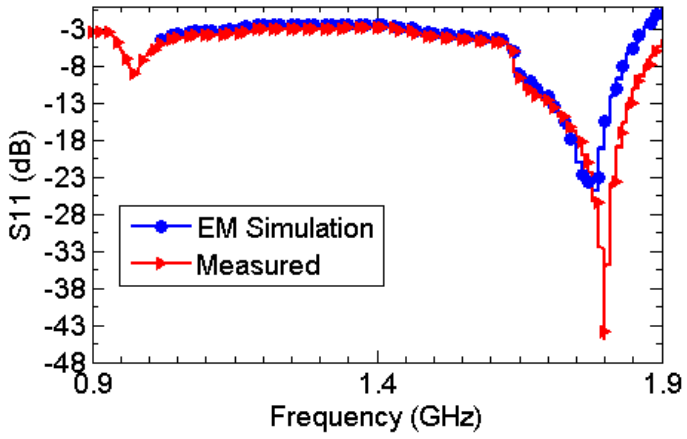

Fig. 3.20 EM simulation vs measured results

Table 3.7 Comparison with the current state-of-the-art

References	Venue	Method used	Load type	Design Equations
(2008), [29]	JPIER	pi-structure	real	complex
(2016), [45]	MWSCAS	admittance property of two-section transmission line	real	simple
(2012), [38]	JPIER	pi-architecture along with L-network	FDCL	complex
(2015),[42]	JPIER	conjugate generation and cancellation by single stub	FDCL	simple
***This work*, (2018)**	IMaRC	**single stub for cancellation unequal susceptance**	**FDCL**	simple

3.4 Analysis of Dual-Band Impedance Matching Network - Design 3

In this method, we propose a dual-band matching network capable of providing impedance matching between two arbitrary frequency-dependent complex source and load impedances. The proposed topology consists of three sections, namely two L-network and a π-network and possesses closed-form design equations. Many case studies are incorporated to demonstrate the validity of the proposed technique for different source and load impedances at two uncorrelated frequencies of interest. A prototype fabricated on RO5880, working at two uncorrelated frequencies of f_1 = 1 GHz and f_2 = 1.8 GHz, shows a perfect agreement between the measured and simulated results. Several techniques have been reported subsequently to address dual-band impedance matching issues. For the specific scenario of both the source and load impedance being complex and frequency-dependent as depicted in Fig. 3.21, often encountered in dual-band RF front-ends, there are a couple of reports, but they involve either require a large number of transmission line segments or complex mathematical equation.

Usually, at two different bands, in power amplifiers, the optimum load impedance is complex and needs to be matched with the complex impedance of either the next stage or

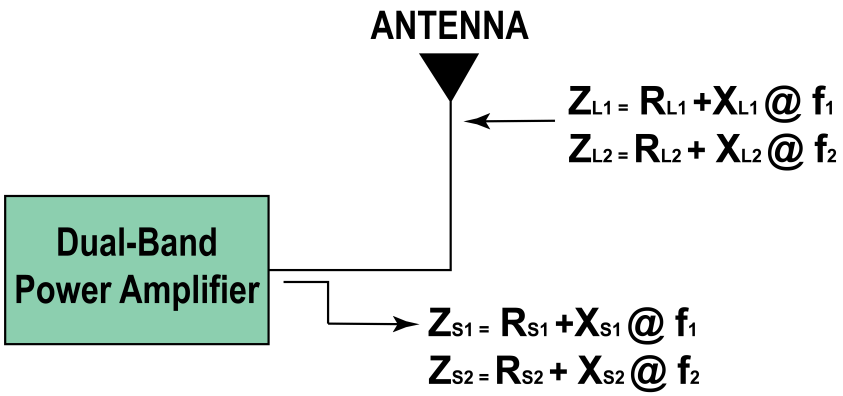

Fig. 3.21 Block diagram of a typical dual-band front-end

the antenna. Therefore, a compact matching network with simplified closed-form design equations is proposed to address this critical scenario of both the source and load being frequency-dependent complex.

3.4.1 Proposed Matching Network

It consists of three sections, namely section-A, Section-B and section-C, as shown in Fig. 3.22. Sections A and B are L-network, whereas section C is a π-network. The corresponding characteristic impedances and electrical lengths are marked.

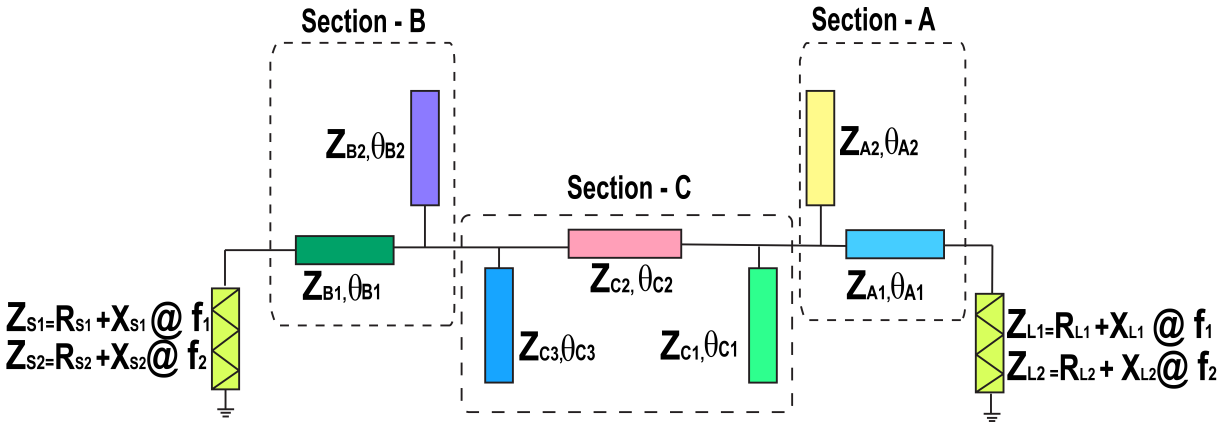

Fig. 3.22 Proposed dual-band matching network

3.4.2 Design Equations

The role of Section-A is to transform the frequency dependent complex load (FDCL), assumed as Z_{L1} @ f_1 and Z_{L2} @ f_2, at two arbitrary uncorrelated frequencies of f_1 and f_2 into real values R_A and cancelling its imaginary part as depicted in Fig. 3.23. For section-A, the respective frequency dependent complex load at two arbitrary frequencies of interest is considered as Z_{L1} @ f_1 and Z_{L2} @ f_2. The transmission line with characteristic impedance Z_{A1} and electrical length θ_{A1} given by (3.17a) and (3.17b) transforms the load impedance to an admittance of Y_{in1} which is a complex conjugate of each other at two uncorrelated frequencies as depicted in Fig. 3.23 and expressed by (3.18a) and (3.18b) [33]

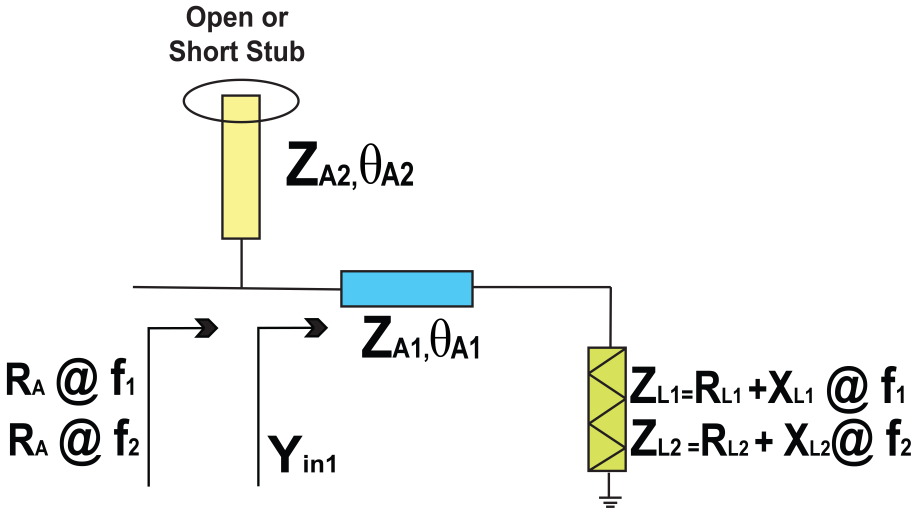

Fig. 3.23 Design of section-A

$$Z_{A1} = \sqrt{R_1R_2 + X_1X_2 + \frac{X_1 + X_2}{R_1 + R_2}(R_1X_2 - R_2X_1)} \tag{3.17a}$$

$$\theta_{A1} = \frac{n\pi + arctan\frac{Z_A(R_1 - R_2)}{R_1X_2 - R_2X_1}}{1 + r} \tag{3.17b}$$

where, 'r' is the frequency ratio i.e. f_2/f_1.

$$Y_{in1} = G_{in1} + jB_{in1} \quad @f_1 \tag{3.18a}$$

$$Y_{in1} = G_{in1} - jB_{in1} \quad @f_2 \tag{3.18b}$$

Subsequently, the cancellation of the imaginary part of Y_{in1} requires a stub, open or short, with characteristic impedance of Z_{A2} and electrical length θ_{A2}. For an open stub, mathematical analysis give expressions (3.19a) and (3.19b) to cancel the susceptances at two frequencies of interest.

$$B_{in1} = j\frac{tan\theta_{A2}}{Z_{A2}} \tag{3.19a}$$

where,

$$\theta_{A2} = \frac{n\pi}{1+r} \quad n = 1,2.....N \tag{3.19b}$$

Similarly, section-B transforms arbitrary complex source in real values R_B. The mathematical expressions regulating this design are also similar to (3.17) - (3.19) with appropriate changes in the characteristic impedances and electrical lengths. Finally, section-C, a dual-band real-to-real π-type impedance transformer [29], matches the two real values R_A and R_B at the chosen frequencies of f_1 and f_2. The design equations to achieve matching between R_A and R_B are given in (3.20a) - (3.20c).

$$z_{c1} = \frac{k\alpha^2}{1+\sqrt{k}} \tag{3.20a}$$

$$z_{c2} = \sqrt{k} \tag{3.20b}$$

$$z_{c3} = \frac{\sqrt{k}\alpha^2}{1+\sqrt{k}} \tag{3.20c}$$

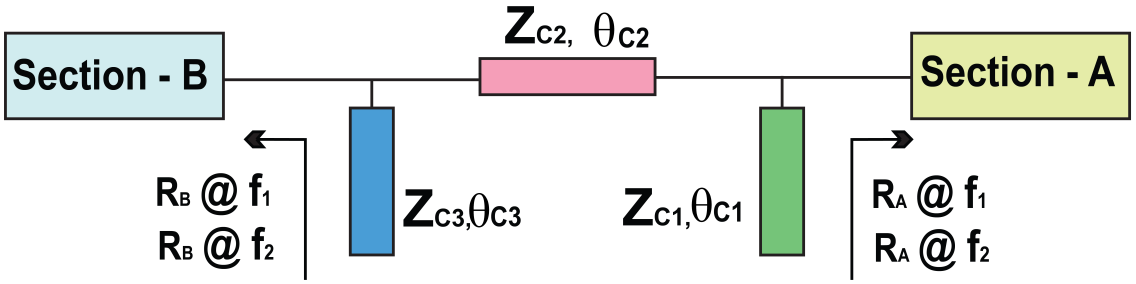

Fig. 3.24 Design of section-C

where, k = R_A/R_B and the parameters are related to the characteristic impedances as Z_{C1} = z_{c1}*R_B, Z_{C2} = z_{c2}*R_B, Z_{C3} = z_{c3}*R_B. The electrical lengths of section-C follows the expression (3.20). This completes the design process.

3.4.3 Design Examples, Prototype, and Results

Table 3.8 includes design parameters for several case studies, and it can be noted that all the characteristic impedances are within 20Ω - 150Ω of the microstrip fabrication limits. The substrate chosen for these case studies is Rogers RO5880. The simulation results (S_{11}) in Fig. 3.25 demonstrate the effectiveness of the proposed design.The chosen frequencies for case study are f_1 = 1.0 GHz and f_2 = 1.8 GHz (GSM), 2.4 GHz (Wi-fi) and for 3.5 GHz (WiMax) applications.

For experimental evaluation, case 1 in Table 3.8 has been prototyped and shown in Fig. 3.26. It can be observed in the prototype that an impedance transforming network[40] has been provided to synthesize a complex source impedance from the standard 50Ω impedance of the SMA connector. The complex load impedance is realized using an SMD resistor in series with a transmission line. It is apparent from Figs. 3.27 and 3.28 that the measured and EM simulated results are in consonance and therefore validate the proposed design of a dual-band impedance transformer.

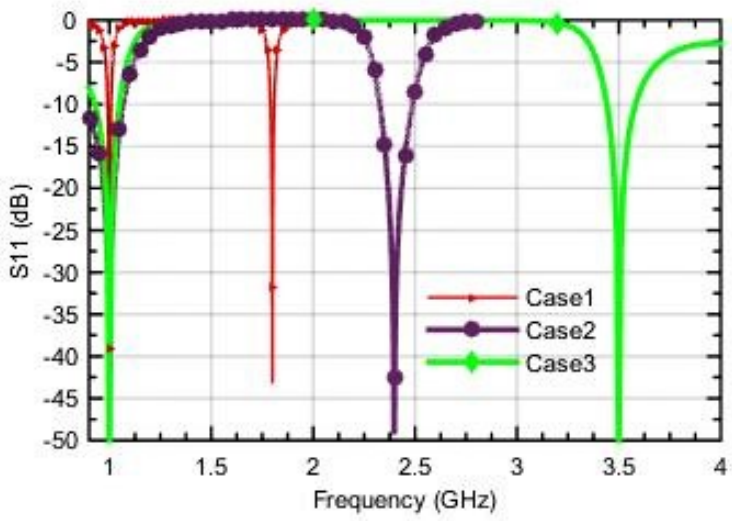

Fig. 3.25 S11(dB) for different cases listed in table 3.8

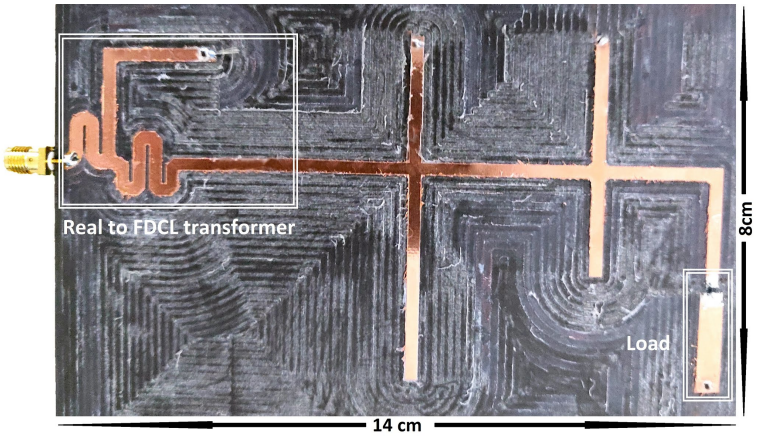

Fig. 3.26 Prototype of dual-band matching network

Table 3.8 Comparison with the other architectures

References	Venue	Method used	Load	Source	Design equations
(2009), [34]	MWCL	Different length transmission line	complex	complex	tedious
(2015), [51]	APMC	Coupled-Lines	complex	complex	tedious
(2018), [134]	MWSCAS	All-pass coupled lines	complex	real	simple
***This work* (2019)**	PRIME	**L-network and pi-network**	**complex**	**complex**	simple

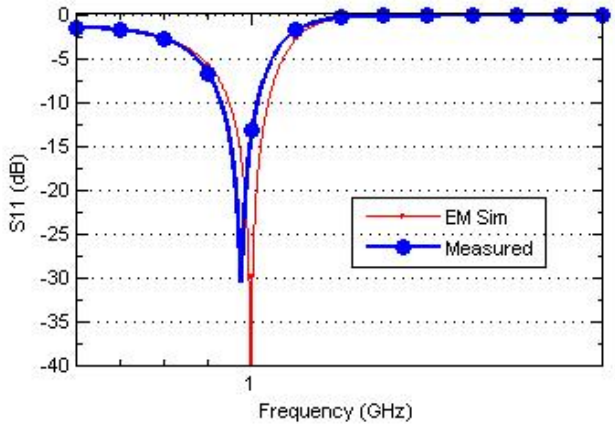

Fig. 3.27 Result for load = 30+j*100 and source = 60-j*130 at freq=1 GHz (Case 1)

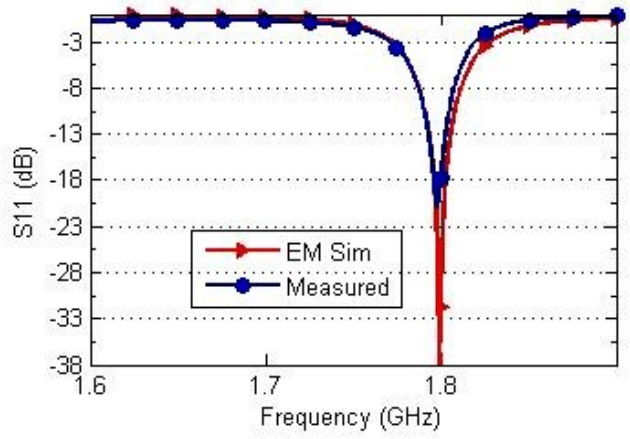

Fig. 3.28 Result for load = 40+j*120 and source = 80+j*150 at freq=1.8 GHz (Case 1)

Table 3.9 Design parameters for different loads at different frequencies

Case	Frequencies (GHz)	Load (Ohm)	Source (Ohm)	Z_{A1}, θ_{A1}	Z_{A2}, θ_{A2}	Z_{B1}, θ_{B1}	Z_{B2}, θ_{B2}	Z_{C2}, θ_{c2}	Z_{C3}, θ_{C3}	Z_{C1}, θ_{C1}
1	f_1 = 1.0 f_2 = 1.8	Z_{L1} = 30+j100 Z_{L1} = 40+j120	Z_{S1} = 60-j130 Z_{S2} = 80+j150	66.33, 85.32	25.35, 64.28 S.S	68.55, 62.84	20.07, 64.28 S.S	46.96, 64.28	42.62, 64.28 O.S	155.78, 64.28 O.S
2	f_1 = 1.0 f_2 = 2.4	Z_{L1} = 100+j80 Z_{L2} = 20-j10	Z_{S1} = 50-j60 Z_{S1} = 30-j40	58.94, 34.96	151.03, 52.94 S.S	53.85, 29.56	34.32, 52.94 S.S	93.45, 52.94	59.27, 52.94 O.S	104.61, 52.94 O.S.
3	f_1 = 1.0 f_2 = 3.5	Z_{L1} = 40+j50, Z_{L2} = 50+j80	Z_{S2} = 70-j40 Z_{S2} = 80-j50	122.8, 26.59	139.84, 40 O.S	101.48, 56.34	139.84, 40 O.S	146.82, 40	35.54, 40 O. S	67.82, 40 O.S

*O.S - Open Stub and S.S - Short Stub

3.5 Summary

This chapter presents the different methods for designing dual-band impedance matching networks. Design-1 and design-2 represent the methods for matching frequency-dependent complex load to the real source. At the same time, design-3 illustrates the design methodology for matching frequency-dependent complex source and load, addressing a critical scenario encountered in emerging wireless applications. A thorough analysis backed by closed-form equations is developed to generalize the design procedure for all the discussed design strategies. Several case studies catering to distinct frequency ratios and impedances are presented to show the versatile nature of the proposed techniques. The prototypes have been designed, and measurement results show the proposed techniques' effectiveness. A comparison with the other state-of-the-art designs has been made to show the effectiveness of the designed procedures. The proposed methods were simple, and the closed-form equations helped the designers to mathematical represent analysis and results.

Chapter 4

Power Dividers - Broadband Frequency Response

4.1 Introduction

The advancements in communication standards and protocols have led to several innovations in both active and passive circuits, components, and devices [135]-[139]. Within the passive components regime, there have been abundant designs for power dividers, impedance transformers, baluns, and couplers used in ultra-modern configurations. In the case of the power dividers, the T-junction configuration can be considered the most preliminary design, but it is restricted by poor isolation between the output ports. Wilkinson Power Divider readily addresses the isolation issues (WPD) [19]. The Wilkinson Power Divider achieves good matching at the ports with excellent isolation between the output ports. However, the WPD uses a quarter-wavelength transmission line that limits the intrinsic bandwidth at a single frequency. Nonetheless, there have been extensive advancements in the WPD design techniques to meet the requirements of multi-standard communication systems. A majority of the research focus in the last decade has largely been on multi-band [52]-[68] and broadband

WPDs [70]-[105]. This chapter will discuss different methodologies for designing broadband power dividers.

4.2 Broadband Power Divider - Design 1

This design proposes a two-stage quarter-wave transmission line WPD, including DC blocking capability. The distinguishing characteristics of the proposed WPD are listed below:

1. Simple and generalized mathematical analysis.
2. Fully Resistive isolation network.
3. Closed-form equations for determining the value of isolation resistor without involving optimization.
4. Flexible transmission bandwidth.
5. Good isolation between two ports along with excellent port matching.
6. Ready scalability for DC blocking application.

Several case studies are also included to show the versatility of the proposed technique. Two prototypes are developed using the proposed approach, which provides an excellent agreement between the simulated and measured results.

4.2.1 Design and Analysis

Fig. 4.1 is a depiction of the proposed wideband WPD. It consists of two transmission lines, short-circuits stubs, and two isolation resistors. The main advantage of short-circuit stubs is a simple structure with excellent ultra-wideband performance and reduced complexity in circuit fabrication. It is a symmetrical network and hence can be split into two halves along

the line of symmetry. Consequently, the proposed WPD can be analyzed using the standard odd- and even-mode techniques. The overall S-parameters can then be obtained from the respective even- and odd-mode S-parameters considering that they are related as $S_{11} = S_{11e}$, $S_{22} = S_{33} = (S_{22e}+S_{22o})/2$ and $S_{23} = (S_{22e}-S_{22o})/2$, where, S_{11e}, S_{22e} and S_{22o} are parameters of even and odd-mode circuits respectively [3]. Here, subscripts "o" and "e" refers to the odd- and even-mode parameters.

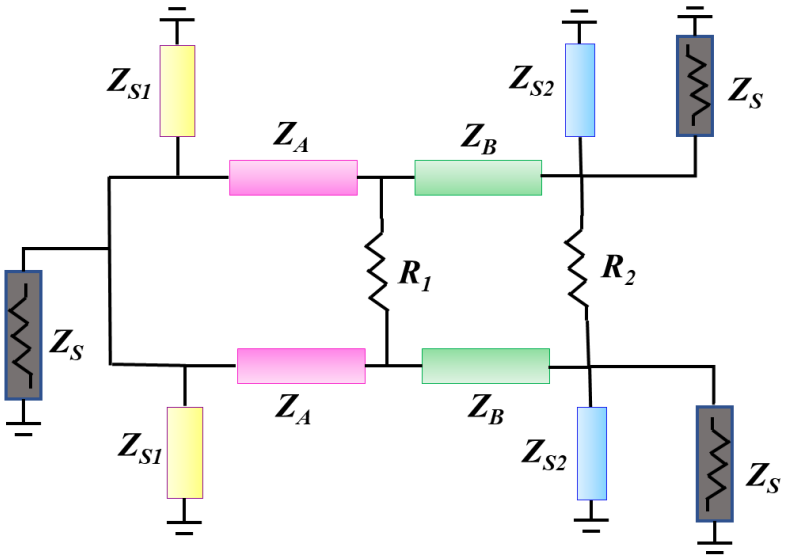

Fig. 4.1 Schematic of the proposed wideband WPD

Even-Mode Analysis

Fig. 4.2 represents the even-mode half circuit of the proposed wideband WPD. It is well known that a two-port asymmetrical network with load Z_L (here Z_S) and source Z_S (here $2Z_S$) is characterized in terms of ABCD parameters and its associated scattering matrix in (4.1a)-(4.1b).

$$S_{11} = \frac{AZ_L + B - CZ_SZ_L - DZ_S}{AZ_L + B + CZ_SZ_L + DZ_S} \tag{4.1a}$$

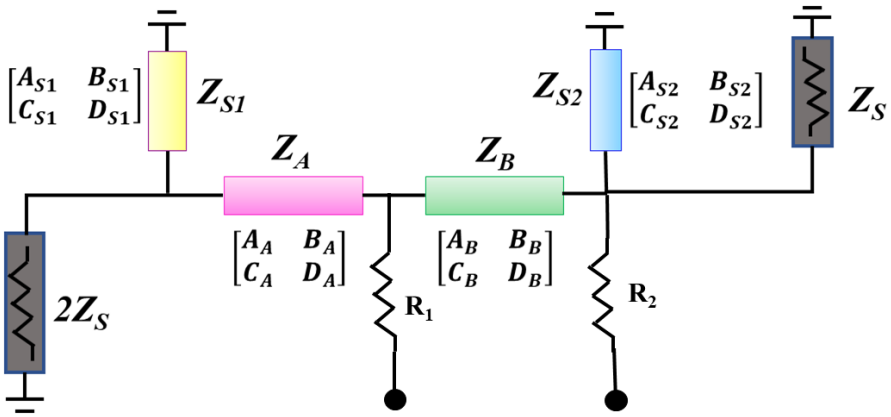

Fig. 4.2 Even-mode half-circuit

$$S_{21} = \frac{2\sqrt{Z_S Z_L}}{AZ_L + B + CZ_S Z_L + DZ_S} \tag{4.1b}$$

The comprehensive ABCD matrix of the even-mode circuit shown in Fig. 4.2 can be calculated by augmenting the individual ABCD parameters of the stubs and the transmission lines. Here A_A, B_A, C_A, D_A and A_B, B_B, C_B, D_B are the elements of the ABCD matrices of lines Z_A and Z_B respectively while $A_{S1}, B_{S1}, C_{S1}, D_{S1}$ and $A_{S2}, B_{S2}, C_{S2}, D_{S2}$ are that of the short circuit stubs as expressed in (4.2a) and (4.2b) respectively. This can be interpreted to deduce the ABCD parameters, using (4.3) and (4.4), for the even-mode circuit.

$$\begin{bmatrix} A_a & B_a \\ C_a & D_a \end{bmatrix} = \begin{bmatrix} \cos\theta & jZ_a \sin\theta \\ j\sin\theta / Z_a & \cos\theta \end{bmatrix} \tag{4.2a}$$

where a = A, B

$$\begin{bmatrix} A_{Sx} & B_{Sx} \\ C_{Sx} & D_{Sx} \end{bmatrix} = \begin{bmatrix} 1 & 0 \\ -j\cos\theta / Z_{Sx} & 1 \end{bmatrix} \tag{4.2b}$$

where x = 1, 2

$$\begin{bmatrix} A_{cas} & B_{cas} \\ C_{cas} & D_{cas} \end{bmatrix} = \begin{bmatrix} A_{S1} & B_{S1} \\ C_{S1} & D_{S1} \end{bmatrix} \times \begin{bmatrix} A_A & B_A \\ C_A & D_A \end{bmatrix} \times \begin{bmatrix} A_B & B_B \\ C_B & D_B \end{bmatrix} \times \begin{bmatrix} A_{S2} & B_{S2} \\ C_{S2} & D_{S2} \end{bmatrix} \quad (4.3)$$

$$A_{cas} = \cos^2\theta + \frac{Z_A \cos^2\theta \sin\theta}{Z_{S2}} + \frac{Z_B \cos^2\theta \sin\theta}{Z_{S2}} - \frac{Z_A \sin^2\theta}{Z_B} \quad (4.4a)$$

$$B_{cas} = jZ_A \cos\theta \sin\theta + jZ_B \cos\theta \sin\theta \quad (4.4b)$$

$$C_{cas} = j\frac{\sin\theta\cos\theta}{Z_A} - j\frac{\cos^3\theta}{Z_{S1}} - j\frac{\cos^3\theta}{Z_{S2}} - j\frac{Z_A \sin\theta \cos^3\theta}{Z_{S1}Z_{S2}} + j\frac{Z_B \sin^2\theta \cos\theta}{Z_A Z_{S1}} - j\frac{Z_B \cos^3\theta \sin\theta}{Z_{S1}Z_{S2}} + j\frac{\sin\theta cos\theta}{Z_B} + j\frac{Z_A \cos\theta \sin^2\theta}{Z_{S1}Z_B} \quad (4.4c)$$

$$D_{cas} = \cos^2\theta + \frac{Z_A \cos^2\theta \sin\theta}{Z_{S1}} - \frac{Z_B \sin^2\theta \cos\theta}{Z_A} + \frac{Z_B \cos^2\theta \sin\theta}{Z_{S1}} \quad (4.4d)$$

where $A_{cas}, B_{cas}, C_{cas}, D_{cas}$ are the elements of the overall cascaded ABCD matrix. The filtering characteristics of the circuit can be obtained by amplitude squared transfer function, S_{21} given in (4.5). Here, impedance transformation ratio is $p = Z_L/Z_S$ with $p \leq 1$ (with, load impedance Z_S and source impedance $2Z_S$). From (4.1a)-(4.1b), F_{WPD} is given by (4.6). Based on (4.4) and (4.6), the F_{WPD} can be calculated in terms of design parameters expressed in (4.7) and simplified in (4.8). The transfer characteristics of the proposed network is plotted as function of electrical length in Fig.4.3 with different values of impedances within the

fabricable range of 20Ω-150Ω. The transfer characteristic as a function of S_{21} and electrical length θ is plotted to illustrate its filtering response which can be compared to other filters.

$$|S_{21}^{WPD}|^2 = \frac{1}{1+|F_{WPD}|^2} \tag{4.5}$$

where $F_{WPD} = S_{11}/S_{21}$

$$F_{WPD} = \frac{A_{cas} + B_{cas} - pC_{cas} - pD_{cas}}{2\sqrt{p}} \tag{4.6}$$

$$F_{network} = (A_2 cos^2\theta + A_1 + B_1 cos\theta - pC_3 cos^3\theta - pC_1 cos\theta - kD_2 cos^2\theta - kD_1)/2\sqrt{p} \tag{4.7}$$

$$F_{network} = (-pC_3 cos^3\theta + (A_2 - pD_2)cos^2\theta + (B_1 - pC_1)cos\theta + (A_1 - pD_1)/2\sqrt{p} \tag{4.8}$$

From Fig. 4.3, it can be noted that the characteristics is similar to a band pass filter and hence it can be compared with any theoretical band pass filter namely Chebyshev or Butterworth filter to determine the characteristic impedances of transmission lines and stubs. The Chebyshev bandpass filter transfer function is chosen here due to its fast roll-off speed compared to other filter functions. The impedances of transmission line and stubs are determined by comparing the transfer function of the proposed network with the theoretical Chebyshev transfer function F_{CH}, where ε is the equal ripple factor, given in (4.9). Here, the transfer function F_{CH} is represented by (4.10) [69] where T_{n+1} is Chebyshev polynomial of degree n, $x = cos\theta$, $x_c = cos\theta_c$. The term θ_c is defined as the electrical length at lower cut-off frequency [69]. For n = 2, Chebyshev polynomial T_{n+1} are $T_3 = 4x^3$-$3x$ and $T_1 = x$. Representing (4.10) in terms of x, x_c, T_3 and T_1, the expression in (4.10) results in (4.11).

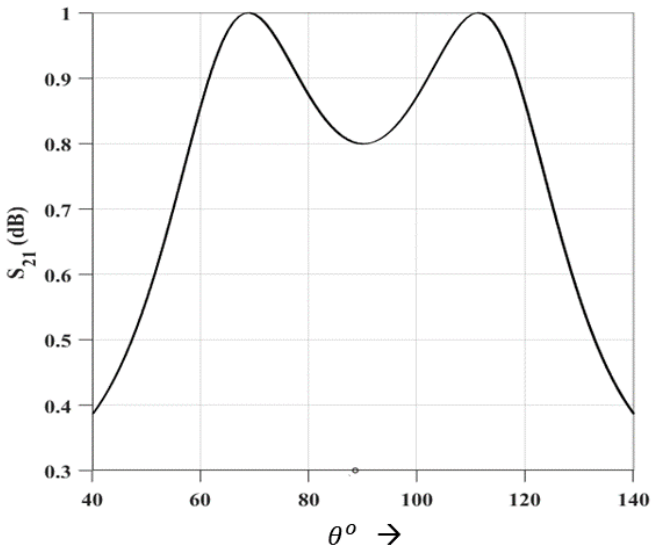

Fig. 4.3 Transfer characteristics of the proposed network

$$|S_{21}(CH)|^2 = \frac{1}{1+\varepsilon^2|F_{CH}|^2} \tag{4.9}$$

$$F_{CH} = \frac{(1+\sqrt{1-x_c^2})T_{n+1}(\frac{x}{x_c}) - (1-\sqrt{1-x_c^2})T_{n-1}(\frac{x}{x_c})}{2\sqrt{1-x^2}} \tag{4.10}$$

$$F_{CH} = \frac{\frac{4(1+\sin^2\theta_c)\cos^3\theta}{\cos^3\theta_c} - \frac{(4-2\sin\theta_c)\cos\theta}{\cos\theta_c}}{2\sin\theta} \tag{4.11}$$

The transmission characteristic parameter S_{21} of the Chebyshev function in (4.11) is plotted as function of θ and θ_c in Fig. 4.4. It is noted that at $\theta = 90\,^\circ$, the filter has band-pass characteristics with a change in bandwidth for different values of θ_c.

To calculate the design parameters of the network, $|S_{21}^{WPD}|^2 = |S_{21(CH)}|^2$ should be maintained and this entails that $|F_{WPD}| = \varepsilon\,|F_{CH}|$. The resultant design equations are presented in (4.12) below.

$$\frac{pC_3}{2\sqrt{p}} = \varepsilon\frac{4(1+\sin^2\theta_c)}{2\sin\theta\cos^3\theta_c} \tag{4.12a}$$

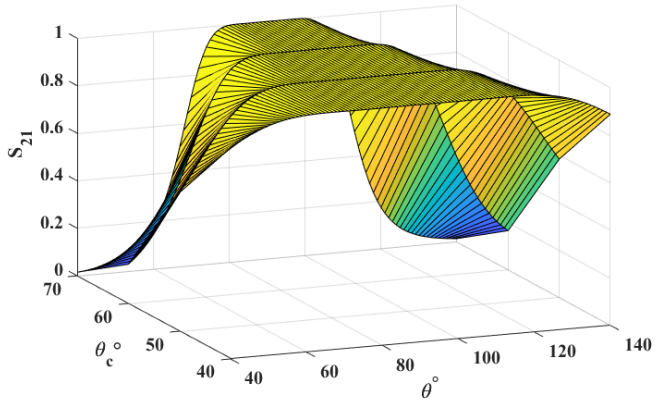

Fig. 4.4 Transfer characteristics of Chebyshev band pass filter

$$A_2 - pD_2 = 0 \tag{4.12b}$$

$$\frac{B_1 - pC_1}{2\sqrt{p}} = \varepsilon \frac{4 - 2\sin\theta_c}{2\sin\theta\cos\theta_c} \tag{4.12c}$$

$$A_1 - pD_1 = 0 \tag{4.12d}$$

Here, the electrical length θ of each element is 90°. The value of Z_A, Z_B, Z_{S1} and Z_{S2} can be calculated from (4.12) using MATLAB, for different values of transformation ratio p, ripple factor ε and θ_c.

The values of the isolation resistors are also a critical design parameter. These are obtained in the next section from the odd-mode half-circuit analysis.

Odd-Mode Analysis

The odd-mode circuit half-circuit is depicted in Fig. 4.5. It simplify the conditions for calculating the design values of resistors R_1 and R_2. It is noticeable that the electrical length of the transmission line and stubs are 90°, hence impedance at node X remains at short-circuit resulting in the modified odd-mode circuit shown in Fig. 4.6. For preserving the conditions of perfect matching, the odd-mode half-circuit impedance Z_{out} should be perfectly matched with output port impedance Z_S. It should be noted that the line with characteristic impedance Z_B is a quarter-wave transmission line with load $R_1/2$. Here, Z_Z is the impedance at node Z.

Solving (4.13b), the relation between resistors R_1 and R_2 is obtained and provided in (4.14). The impedance parameters and isolation resistor values for wideband WPD with different θ_c are tabulated in Table 4.1.

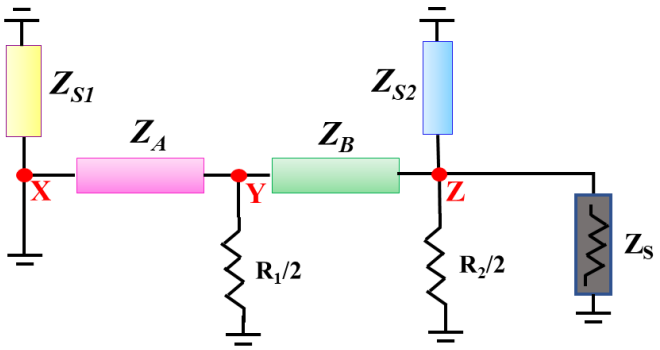

Fig. 4.5 Odd-mode half-circuit

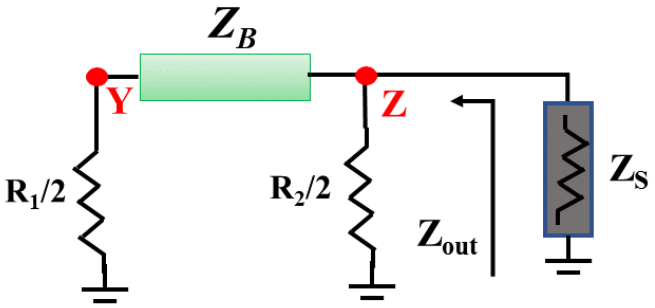

Fig. 4.6 Transformed odd-mode half-circuit

$$Z_Z = \frac{(Z_B)^2}{R_1/2} \tag{4.13a}$$

$$Z_{out} = Z_Z \parallel R_2/2 = Z_S \tag{4.13b}$$

$$R_1 = \frac{1}{Z_S}(2Z_B^2 - \frac{(4Z_S Z_B^2)}{R_2}) \tag{4.14}$$

For different values of Z_B, (4.14) results in distinct sets of isolation resistor combinations. Fig. 4.7 represents the variation of resistors for different values of Z_B (for different values of θ_c) listed in Table 4.1.

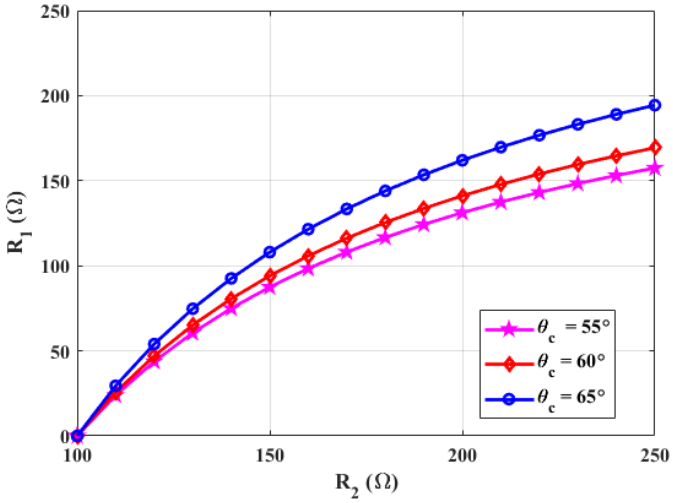

Fig. 4.7 Relation between isolation resistor values

Table 4.1 Design parameters of wideband WPD

Parameters	**Cases**		
$\theta_c(^\circ)$	**55**	**60**	**65**
Z_A (Ω)	115	127	120
Z_B (Ω)	81	90	94
Z_{S1} (Ω)	110	55	35
Z_{S2} (Ω)	40	31	24
R_1 (Ω)	131	94	162
R_2 (Ω)	200	150	200

Design Steps

The procedure for designing wideband power divider is discussed below:

- Choose the center frequency f_c.
- Divide the network designed using transmission lines and short-circuit stubs into half-circuit because of the symmetrical structure.
- Perform the even-mode analysis to determine the impedance values, Z_A, Z_B, Z_{S1} and Z_{S2} according to (4.12) at centre frequency for distinct θ_c.

- Perform the odd-mode analysis to determine the values of the isolation resistors from (4.14).
- For EM simulation and eventually layout, model the junction discontinuities properly using tapers and bends.

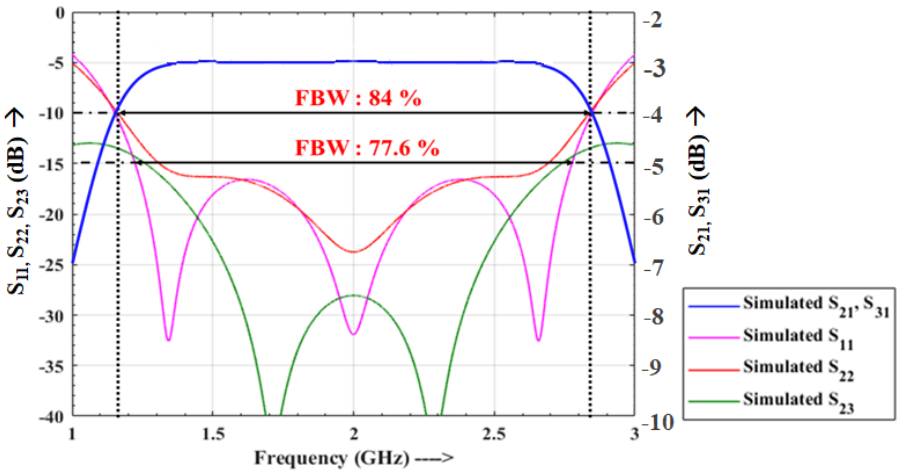

Fig. 4.8 Simulated S-parameter for $\theta_c = 55°$

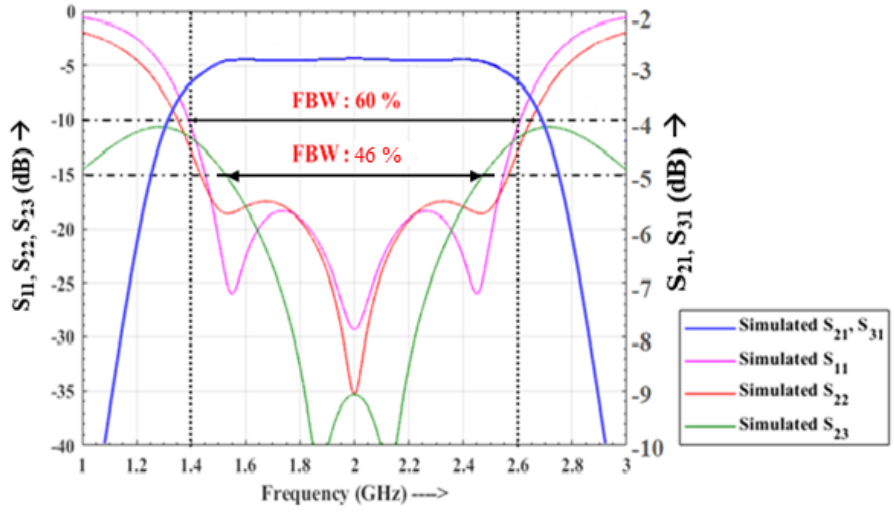

Fig. 4.9 Simulated S-parameters for $\theta_c = 60°$

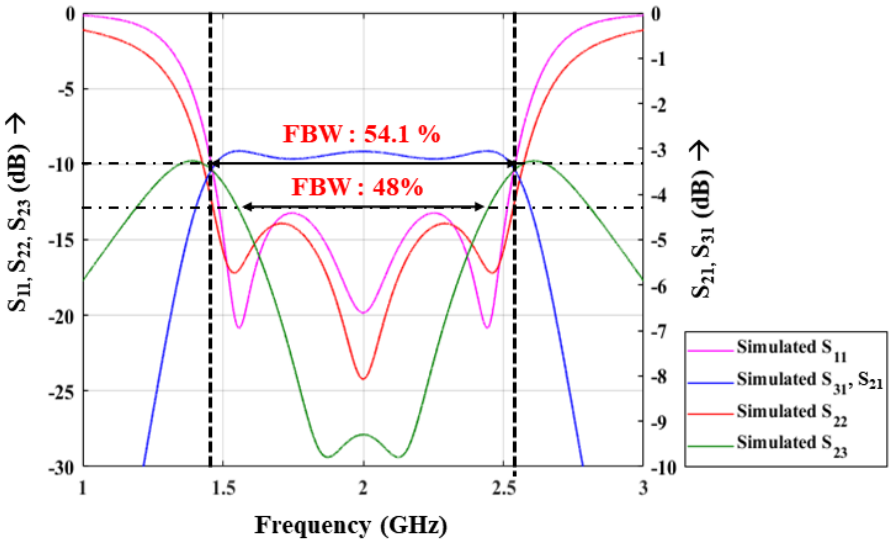

Fig. 4.10 Simulated S-parameters for $\theta_c = 65°$

4.2.2 Case-studies, Results and Analysis

Based on the above design procedure and calculated design parameters listed in Table 4.1, simulation results of different case studies are presented in Figs. 4.8 - 4.10 illustrating S-parameters for varying θ_c. It can be noted from the simulation results that, with an increasing value of θ_c, the bandwidth of the power divider decreases. The prototype shown in Fig 4.11 has been fabricated on RO5880 substrate with dielectric constant ($\varepsilon_r = 2.2$), dissipation factor = 0.0009 and substrate thickness of 1.52 mm. The measurement setup is depicted in Fig. 4.12 along with the EM simulation and measured results in Fig. 4.13 - 4.15. It can be observed that there is a slight discrepancy in EM simulation and measurement results which can be attributed to the cables and connector losses that tend to degrade over time.

The measured return loss S_{11} (dB) and isolation S_{23} (dB) is better than -10 dB and -12 dB respectively within the frequency range of 1.0 - 3.0 GHz. The measured insertion losses at output ports, S_{21} (dB) and S_{31} (dB) are -3.0±0.4 dB which are comparable to the simulated results of -3 dB.

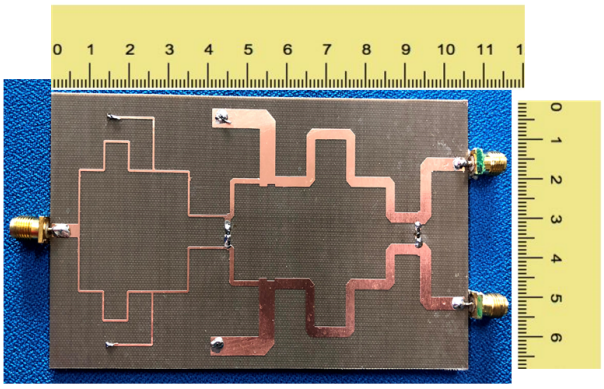

Fig. 4.11 Fabricated prototype of the proposed WPD

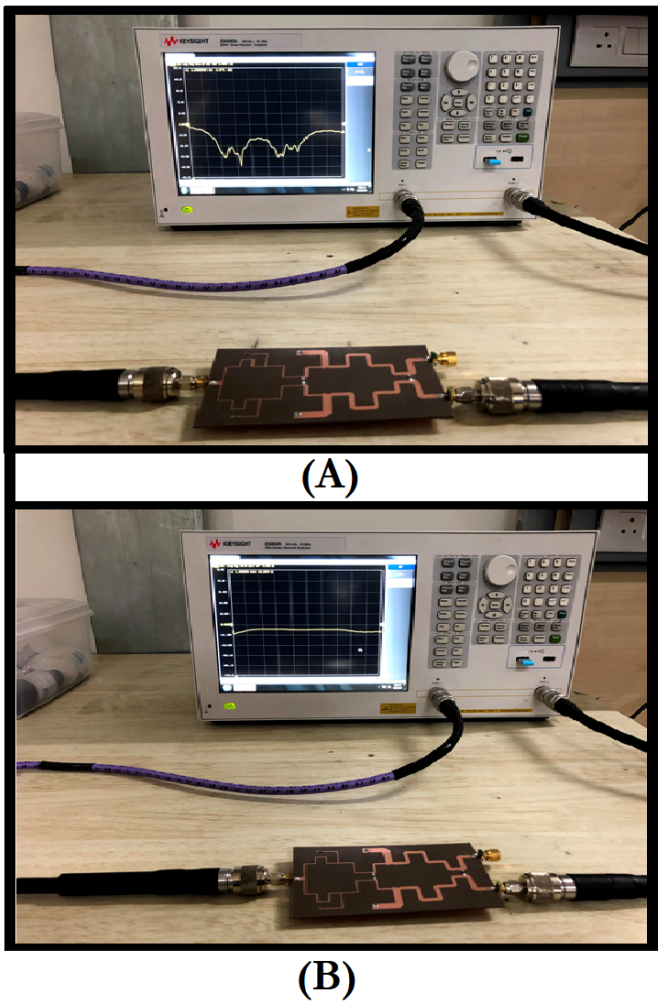

Fig. 4.12 Measurement setup for (A): S_{11} (B): S_{21} for $\theta_c = 55^\circ$

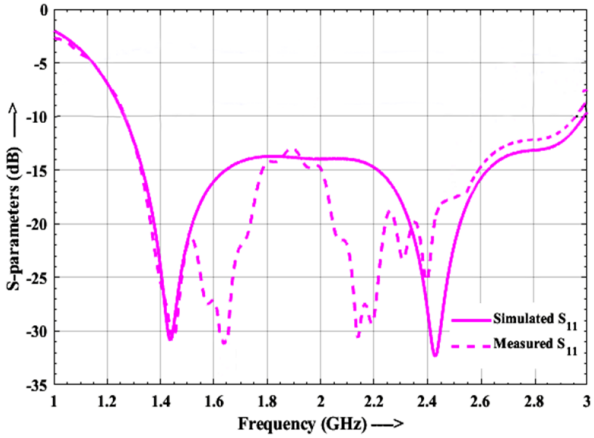

Fig. 4.13 EM vs measured S-parameters for S_{11} for $\theta_c = 55°$

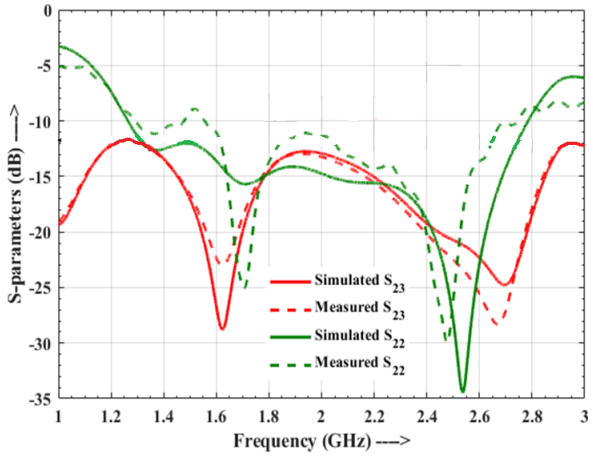

Fig. 4.14 EM vs measured S-parameters for S_{23}, S_{22} for $\theta_c = 55°$

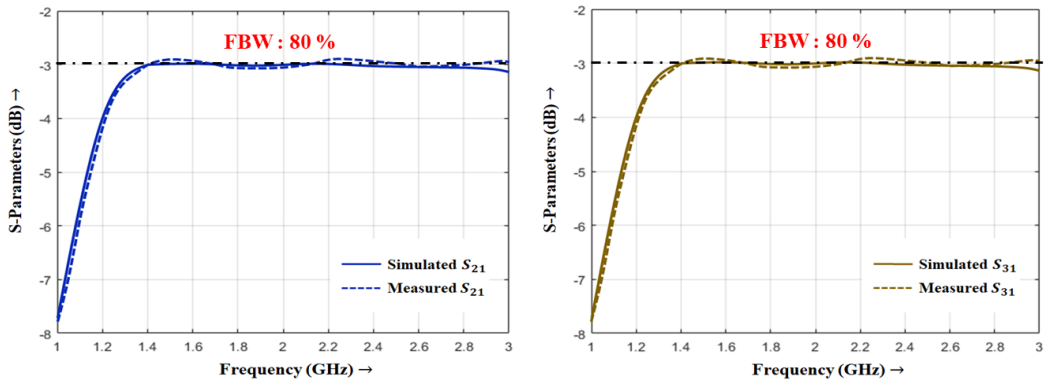

(a) A (b) B

Fig. 4.15 EM vs measured S-parameters for (A) S_{21} (B) S_{31} for $\theta_c = 55°$

4.2.3 Wideband DC Isolated WPD

The schematic of the proposed wideband DC isolated WPD is presented in Fig. 4.16. For DC isolation, it consists of core wideband WPD with coupled lines with electrical length θ = 90° and Z_e, Z_o as the even- and odd-mode characteristic impedance at the input side. The Z_S are port terminations at the input and output sides.

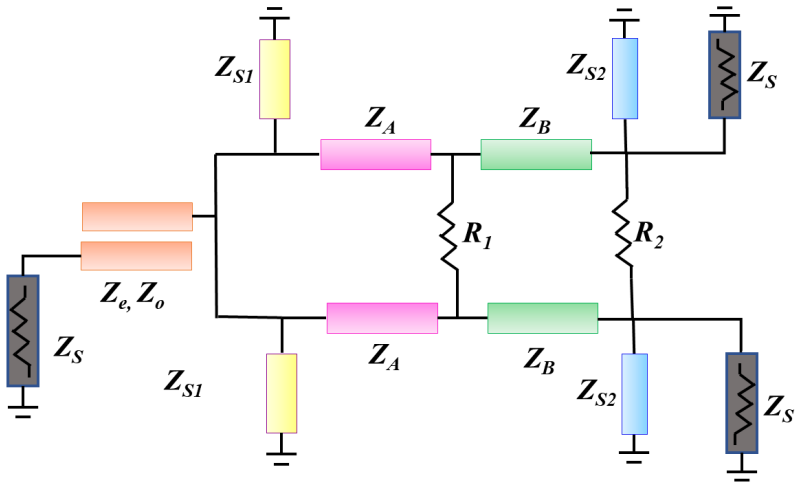

Fig. 4.16 Schematic of the proposed DC isolated wideband WPD

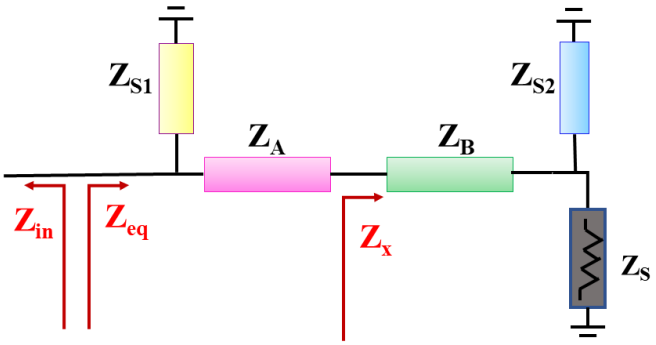

Fig. 4.17 Even-mode analysis of half-network

Even-Mode Analysis:

The even-mode half-network is presented in Fig. 4.17. It is to be noted that the even-mode half-network is lossless and reciprocal; thus, matching at port-1 and port-2 remains the same.

As mentioned earlier, the port matching requirement at port one, i.e., S_{11}, is related in terms of even-mode half-circuit port matching, S_{11e}. This conveys that Z_{in} should be equal to Z_{eq} in Fig. 4.17. For fulfilling the port matching requirement, the resulting equations are as follows (assuming that Z_{S1} and Z_{S2} result in open-circuit because of 90° electrical length):

$$Z_x = \frac{Z_B^2}{Z_S} \tag{4.15a}$$

$$Z_{eq} = \frac{Z_A^2}{Z_x} = \frac{Z_A^2 Z_S}{Z_B^2} \tag{4.15b}$$

The value of impedance looking into coupled line, Z_{in} can be calculated using (4.16) [3], where Z_x = (Z_e + Z_o)/2 and Z_y = (Z_e - Z_o)/2.

$$Z_{in} = -j(Z_x \cot\theta) + \frac{Z_y^2 \csc^2\theta}{Z_S - jZ_a \cot\theta} \tag{4.16}$$

For θ = 90°, (4.16) results in (4.17) and for matching conditions, $Z_{in} = Z_{eq}^*$ which results in equations (4.18a)-(4.18b).

$$Z_{in} = \frac{(Z_e - Z_o)^2}{4Z_S} \tag{4.17}$$

$$Z_{eq} = \frac{Z_A^2}{Z_x} = \frac{Z_A^2 Z_S}{Z_B^2} \tag{4.18a}$$

$$(Z_e - Z_o) = 2\frac{Z_S Z_A}{Z_B} \tag{4.18b}$$

Equation (4.18b) is the design equation for the coupled line and it gives the difference between even and odd-mode characteristic impedance of the coupled line.

Odd-Mode Analysis:

The odd-mode analysis for the DC isolated WPD is the same as discussed in section-2. Table 4.2 provides the impedance parameters for wideband WPD with different θ_c. The relationship between R_1 and R_2 according to (4.14) is plotted in Fig. 4.18 for different θ_c. To better illustrate the isolation between two ports of WPD, considering the case-1 in Table-II, S_{23} (dB) is plotted for different values of isolation resistors calculated from Fig. 4.18.

Table 4.2 Design parameters of DC isolated wideband WPD

Parameters	**Cases**		
$\theta_c(^\circ)$	**55**	**60**	**65**
Z_1 (Ω)	110	50.82	35
Z_2 (Ω)	88.63	127	92
Z_3 (Ω)	56.5	90	68
Z_4 (Ω)	70	47.4	48
Z_e (Ω)	131	160	129
Z_o (Ω)	30	69	42
R_1 (Ω)	38	100	62
R_2 (Ω)	150	150	150

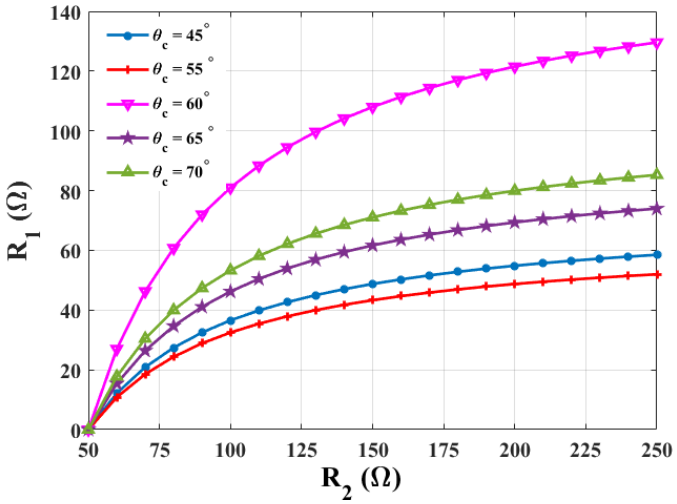

Fig. 4.18 Relation between R_1 and R_2 for different θ_c

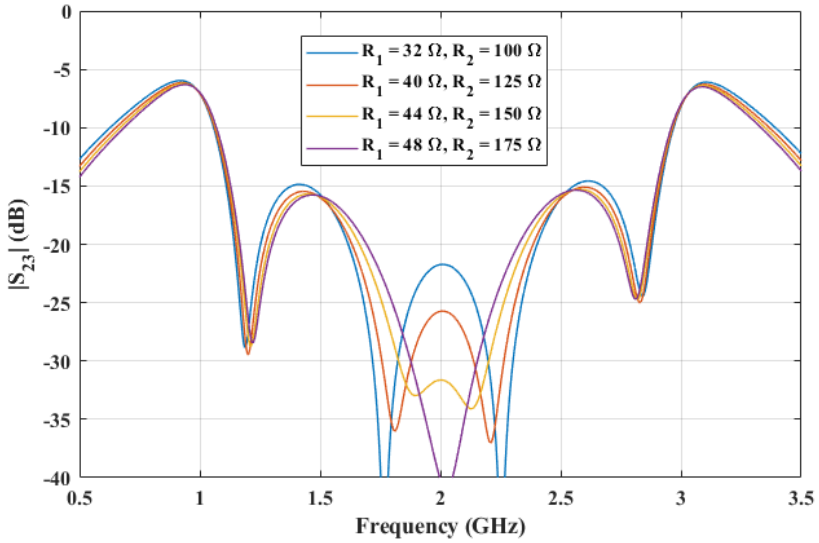

Fig. 4.19 Variation of S_{23}(dB) for $\theta_c = 55^\circ$ with different isolation resistors

It can be observed from Fig. 4.19 that the value of S_{23} (dB) varies with different values of R_1 and R_2 . Fig. 4.20 - 4.21 presented the $S-parameters$ (dB) for different cases with varying θ_c and all parameters are within realizable range of 20 - 160 Ω.

The approach described above has been utilized to design a wideband DC isolated WPD with a centre frequency of 2 GHz and $\theta_c = 55^\circ$. The prototype depicted in Fig.4.22 has been fabricated on RO4350B substrate with dielectric constant ($\varepsilon_r = 3.66$), dissipation factor = 0.0037 with substrate thickness of 1.52 mm. The prototype, along with the measurement setup, is presented in Fig. 4.23. The EM simulation and measured results are depicted in Figs. 4.24, 4.25. It can be noted that there is a slight discrepancy in EM simulation and measurement results as a result of the utilization of bends and tapers post-processing to avoid junction discontinuities and substrate parameter variation.

The measured return loss S_{11} (dB) and isolation S_{23} (dB) is better than -10 dB and -10 dB respectively within the frequency range of 1.0 - 3.0 GHz. The measured insertion losses at output ports, S_{21} (dB) and S_{31} (dB) are -3.0±0.4 dB which is quite comparable to the simulated results of -3 dB. Table - 4.3 presents the comparison of the proposed wideband WPD with the previous designed WPDs.

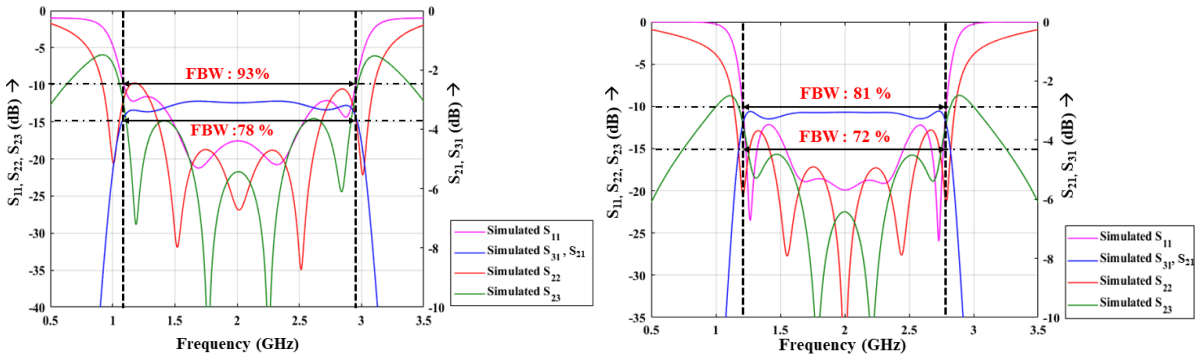

(a) A (b) B

Fig. 4.20 EM vs measured S-parameters for (A) S_{21} (B) S_{31} for $\theta_c = 55°$

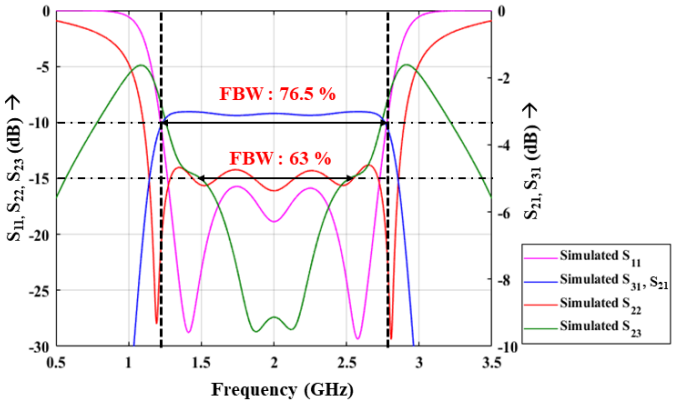

Fig. 4.21 Simulated S-parameters for $\theta_c = 65°$

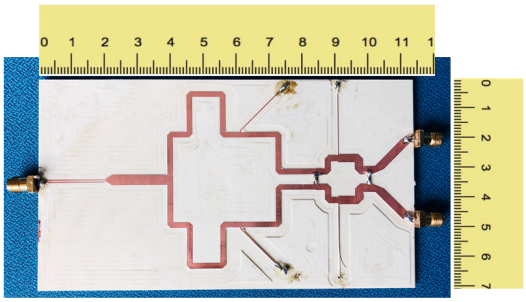

Fig. 4.22 Fabricated prototype of the proposed DC isolated WPD

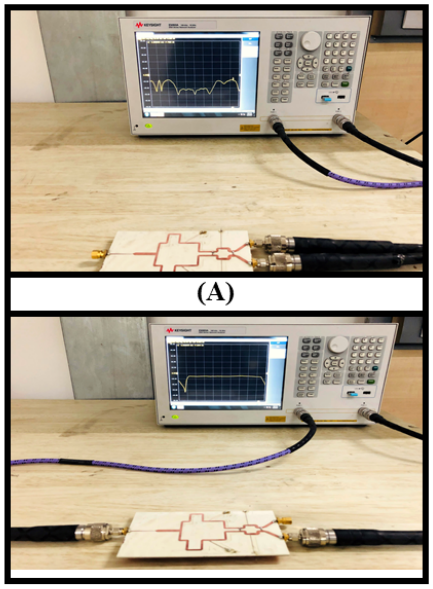

Fig. 4.23 Measurement setup for (A): S_{23} (B): S_{21} for $\theta_c = 55°$

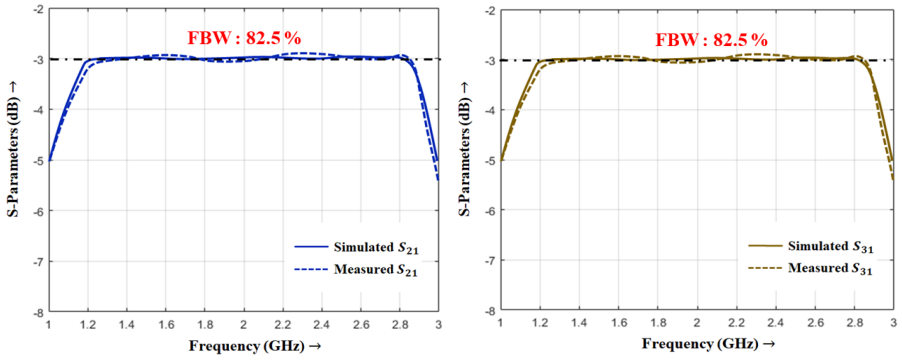

(a) A (b) B

Fig. 4.24 EM vs measured S-parameters for (A) S_{21} (B) S_{31} for $\theta_c = 55°$

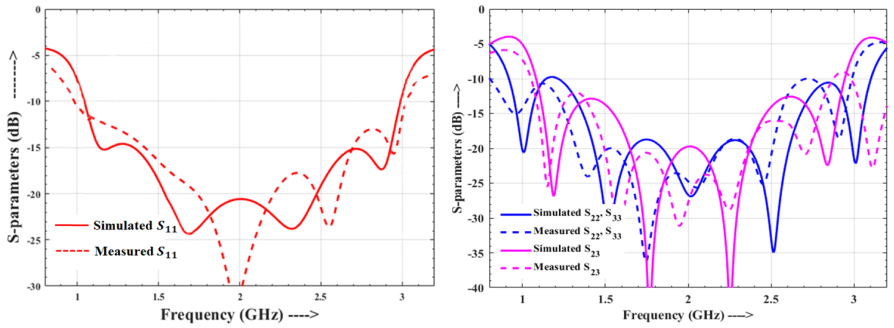

(a) A (b) B

Fig. 4.25 EM vs measured S-parameters for (A) S_{21} (B) S_{31} for $\theta_c = 55°$

Table 4.3 Comparison with previous wideband WPDs

References	**Frequency Range (GHz)**	**Topology**	**FBW*** ($\|S_{21}= S_{31}\|$)	**DC Isolation**	**Isolation Network**	**Size** ($\lambda_g * \lambda_g$)
MWCL [87]	2.7 - 4.7	Dual Resonant Modes in single resonator	53.5 % (3 dB)	No	1 Resistor	1.06*0.89
MWCL [101]	1.25 - 2.5	Coupled-lines at Input / Output port	51 % (3 dB)	Yes	1 Resistor	0.89*0.57
TMTT [92]	1.45 - 4.6	Quasi-coupled Lines	77 % (3 dB)	No	1 Resistor 1 Capacitor	0.2*0.15
MWCL [90]	1.55 - 4.24	Embedded Transversal Signal Interference	84 % (3 dB)	No	1 Resistor 1 Inductor 1 Capacitor	0.8*0.5
Access [97]	1.42 -3.42	Three Line coupled structure	58 % (3 dB)	Yes	1 Resistor	0.62*0.5
TCPMT [94]	1.5 -3.55	Three Line Coupled structure	64 % (3 dB)	No	1 Resistor	0.05*0.32
This Work (2020)	**1.3 - 2.9**	**Two-stage Configuration**	**80 % (3dB)**	**No**	**2 Resistors**	**1.03*0.62**
	1.01 - 3.02	**Two-stage with Coupled Lines**	**82.5 % (3dB)**	**Yes**	**2 Resistors**	**1.2 *0.86**

*FBW- Fractional Bandwidth

4.3 DC Isolated Broadband Power Divider - Design 2

We proposed another topology for designing a broadband power divider with inherent DC blocking capability because of the utilization of coupled lines. In a conventional WPD [19], the core of the design includes quarter-wave transmission lines, which make such a design suitable for operation at one frequency. This strategy shows that this design exhibits wide band behaviour with inherent DC isolation and achieves good in-band return loss and excellent port-to-port isolation.

4.3.1 Circuit Topology and Analysis

The circuit is presented in Fig. 4.26 comprising two coupled lines in cascade with two isolation resistors envisaged to enhance the bandwidth.

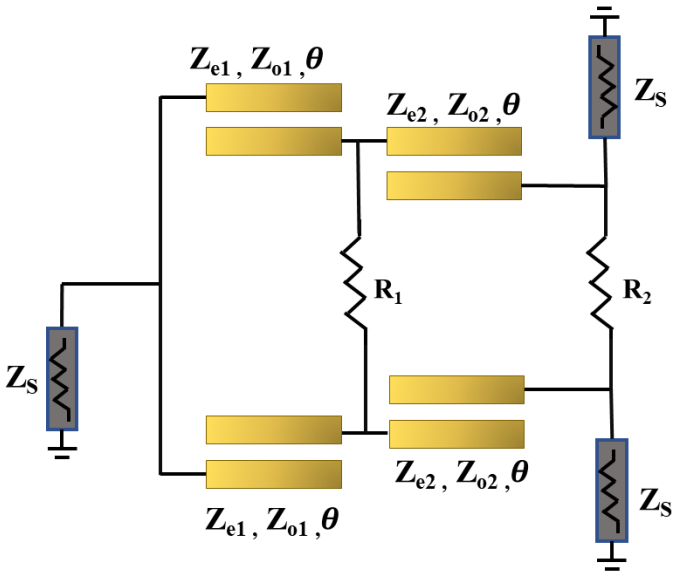

Fig. 4.26 Schematic representation of proposed WPD

The frequency response of this proposed WPD investigates its S-parameters obtained using even/odd-analysis. The S-parameters of this WPD in terms of even/odd-mode are S_{11} = $S_{11,e}$, S_{22} = ($S_{22,e}$+$S_{22,o}$)/2, S_{23} = ($S_{22,e}$-$S_{22,o}$)/2 [3]. Here, subscript 'e' and 'o' stands for even-/odd-mode circuit respectively. In the even mode circuit, shown in Fig. 4.27, because of

virtual open-circuit at the plane of symmetry, the isolation resistors are eliminated. It consists of two distinct coupled-line sections of equal electrical lengths θ, namely sections-A and B, with Z_{e1}, Z_{o1}, Z_{e2}, Z_{o2} being the even/odd-impedances. The analysis of this even-mode circuit, for the determination of its transfer function, involves cascading of their ABCD parameters expressed by (4.19)-(4.20).

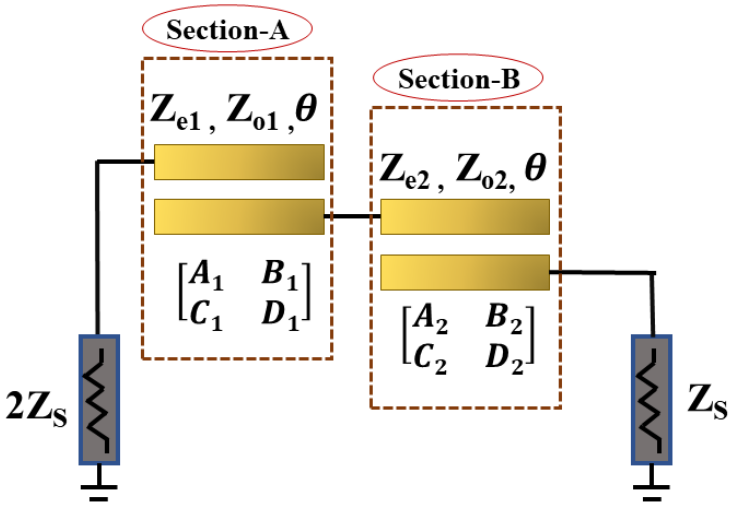

Fig. 4.27 Even-mode representation of proposed WPD

$$\begin{bmatrix} A_a & B_a \\ C_a & D_a \end{bmatrix} = \begin{bmatrix} A_x & B_x \\ C_x & D_x \end{bmatrix} \tag{4.19}$$

where x = 1, 2

$$A_x = \frac{(Z_{ex}+Z_{ox})\cot\theta}{(Z_{ex}-Z_{ox})\csc\theta} \tag{4.20a}$$

$$B_x = (-j/2)^2(Z_{ex}+Z_{ox})^2\cot^2\theta - (-j/2)^2(Z_{ex}-Z_{ox})^2\csc^2\theta/(-j/2)(Z_{ex}-Z_{ox})\csc\theta \tag{4.20b}$$

$$C_x = \frac{1}{(-j/2)(Z_{ex}-Z_{ox})\csc\theta} \tag{4.20c}$$

$$D_x = \frac{(Z_{ex}+Z_{ox})\cot\theta}{(Z_{ex}-Z_{ox})\csc\theta} \tag{4.20d}$$

The overall ABCD parameters A_{WPD}, B_{WPD}, C_{WPD} and D_{WPD}, outlined in (4.21) - (4.22), of the even-mode circuit in Fig.4.27 are utilized for deducing the performance behavior of the proposed WPD.

$$\begin{bmatrix} A_{WPD} & B_{WPD} \\ C_{WPD} & D_{WPD} \end{bmatrix} = \begin{bmatrix} A_1 & B_1 \\ C_1 & D_1 \end{bmatrix} \begin{bmatrix} A_2 & B_2 \\ C_2 & D_2 \end{bmatrix} \tag{4.21}$$

$$A_{WPD} = \frac{\cot^2\theta\sin^2\theta(Z_{e1}+Z_{o1})(Z_{e2}+Z_{o2})}{(Z_{e1}-Z_{o1})(Z_{e2}-Z_{o2})} - \frac{\sin^2\theta\sigma_4}{\sigma_1\sigma_2} \tag{4.22a}$$

$$B_{WPD} = \frac{\cot\theta\sin^2\theta(Z_{e2}+Z_{o2})\sigma_4}{(Z_{e2}-Z_{o2})\sigma_1} - \frac{\cot\theta\sin^2\theta(Z_{e1}+Z_{o1})\sigma_3}{(Z_{e1}-Z_{o1})\sigma_2} \tag{4.22b}$$

$$C_{WPD} = \frac{-\cot\theta\sin^2\theta(Z_{e1}+Z_{o1})}{(Z_{e1}-Z_{o1})\sigma_2} - \frac{\cot\theta\sin^2\theta(Z_{e2}+Z_{o2})}{(Z_{e2}-Z_{o2})\sigma_1} \tag{4.22c}$$

$$D_{WPD} = \frac{\cot^2\theta\sin^2\theta(Z_{e1}+Z_{o1})(Z_{e2}+Z_{o2}}{(Z_{e1}-Z_{o1})(Z_{e2}-Z_{o2}} - \frac{\sin^2\theta\sigma_3}{\sigma_1\sigma_2} \tag{4.22d}$$

where,

$$\sigma_1 = j\frac{(Z_{e1}-Z_{o1})}{2} \tag{4.22e}$$

$$\sigma_2 = j\frac{(Z_{e2}-Z_{o2})}{2} \tag{4.22f}$$

$$\sigma_3 = j\frac{\cot^2(\theta)(Z_{e2}+Z_{o2})^2}{4} - \frac{(Z_{e2}-Z_{o2})^2}{\sigma_5} \tag{4.22g}$$

$$\sigma_4 = j\frac{\cot^2(\theta)(Z_{e1}+Z_{o1})^2}{4} - \frac{(Z_{e1}-Z_{o1})^2}{\sigma_5} \tag{4.22h}$$

$$\sigma_5 = 4\sin^2\theta \tag{4.22i}$$

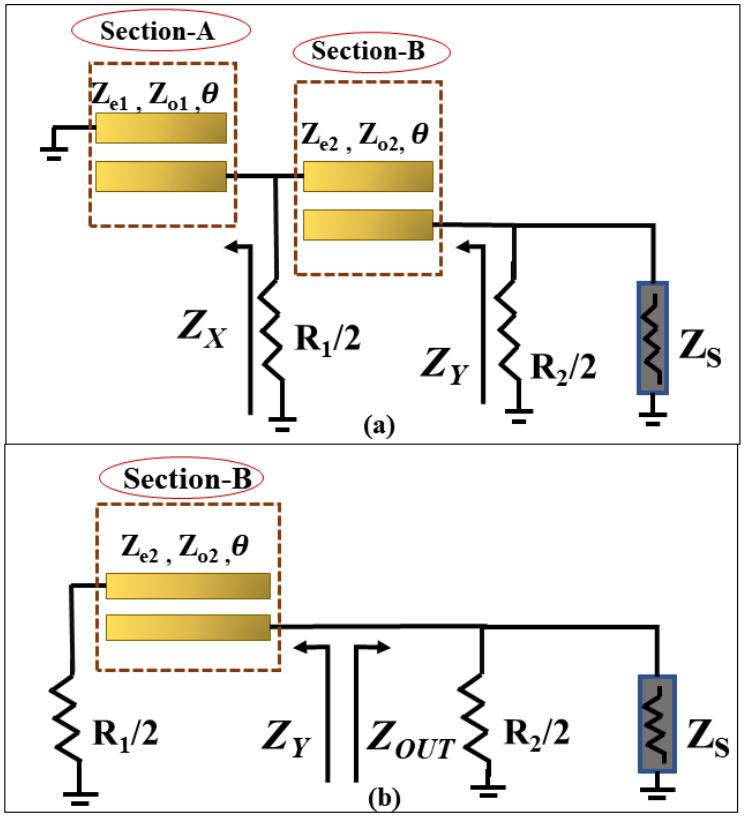

Fig. 4.28 (a) Odd-mode circuit of proposed WPD (b) revised equivalent circuit

The odd-mode circuit, in Fig. 4.28(a), has been arrived at by considering a virtual short-circuit at the plane of the symmetry of WPD. Now, the impedance looking into section-A, Z_X, in terms of impedances Z_{e1} and Z_{o1} can be given by (4.23). Here, Z_a = (Z_{e1} + Z_{o1})/2 and Z_b = (Z_{e1} - Z_{o1})/2. It should be noted that Z_S is grounded and electrical length θ = 90° at the design frequency, the impedance looking into it will be an open-circuit resulting in a modified equivalent circuit presented in Fig. 4.28(b). It can be inferred that for a perfect output matching condition, Z_{out} should be equal to Z_Y, the impedance looking into Section-B. These simplifications, carried out using (4.24) and (4.25), eventually result in a

very simplified closed-form expression for the isolation resistor.

$$Z_X = -j(Z_a \cot\theta) + \frac{Z_b^2 \csc^2\theta}{Z_S - jZ_a \cot\theta} \tag{4.23}$$

$$Z_Y = \frac{Z_b^2}{R_1/2} \tag{4.24a}$$

$$Z_{OUT} = Z_S||(R_1/2) = \frac{Z_S R_2}{2Z_S + R_2} \tag{4.24b}$$

$$Z_{OUT} = Z_Y \tag{4.25a}$$

$$R_1 = \frac{(Z_{e2} - Z_{o2})^2(2Z_S + R_2)}{2Z_S R_2} \tag{4.25b}$$

4.3.2 Frequency Response Analysis

The even- and odd-mode analysis leads to simplified expressions for the frequency response analysis with an eventual determination of the design parameters of the proposed WPD. First, the ABCD parameters in (4.20) have been studied to understand the behavior of the proposed WPD. Apparently, the ABCD-parameters can be utilized to develop the transfer characteristics of the proposed WPD [69], where k is the impedance transformation ratio i.e. Z_L/Z_S, with Z_L and Z_S being the load and source impedances respectively.

$$F_{WPD} = \frac{A_{WPD} + B_{WPD} - kC_{WPD} - kD_{WPD}}{2\sqrt{k}} \tag{4.26}$$

The equations (4.20) and (4.26) can be simplified together to achieve the transfer function of the proposed WPD circuit in terms of even/odd-mode impedances of the coupled lines as outlined in (4.27). The transfer function can then be used to find the insertion loss character-

istics of the proposed WPD according to the well-known expression given in (4.28) [69]. The transfer function in (4.27) and the insertion loss characteristics in (4.28) are apparently dependent on the design parameters, the electrical length θ and characteristic impedances Z_{e1}, Z_{o1}, Z_{e2} and Z_{o2}. In order to assess the parameter's dependence on performance characteristics, these are investigated as functions of θ for different values of Z_{e1}, Z_{o1}, Z_{e2} and Z_{o2} within the range of 50Ω to 250 Ω and plotted in Figs. 4.29 and 4.30. It can be noticed that around $\theta = 90^{\circ}$, the bandwidth varies as a function of even/odd-mode impedances, exhibiting bandpass behaviour. This allows the generalized form of any filter with bandpass response, such as Chebyshev filter, Butterworth, and maximally flat, to calculate the unknown variables in the proposed circuit. Considering the merit of sharp transition between passband and stopband with low order filter, the insertion loss S_{21} (TH) in (4.29) for the Chebyshev transfer function has been examined to find out the unknown variables of the proposed WPD.

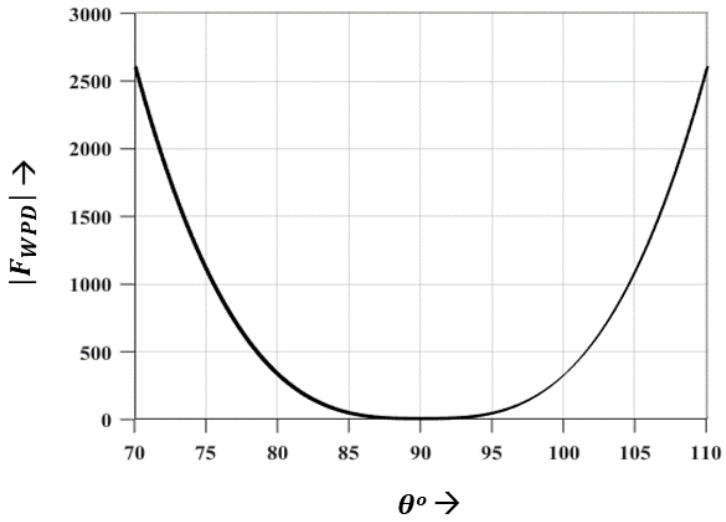

Fig. 4.29 Transfer characteristics of proposed WPD

$$|S_{21}^{WPD}|^2 = \frac{1}{1+|F_{WPD}|^2} \tag{4.28}$$

$$|S_{21}(TH)|^2 = \frac{1}{1+\varepsilon^2|F_{TH}|^2} \tag{4.29}$$

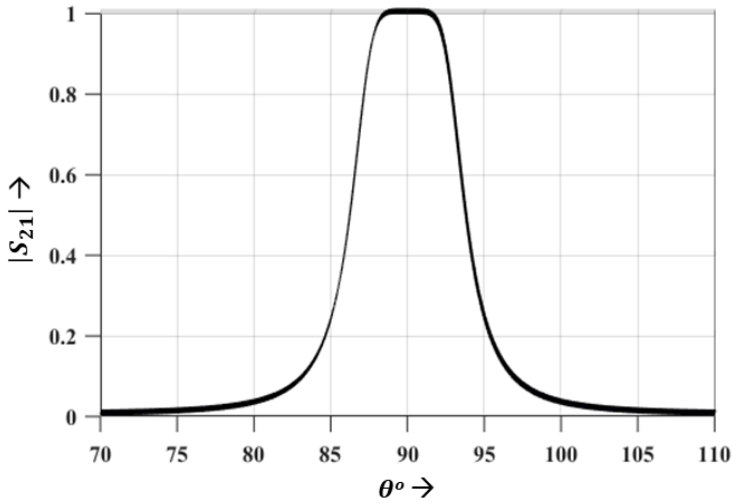

Fig. 4.30 Insertion loss characteristics of proposed WPD

$$F_{WPD} = (-j\cos^3\theta(\frac{a^2b}{2cd\sin\theta} - \frac{ab^2}{2cd\sin\theta}) + \cos^2\theta(\frac{ab+a^2+kab-ka^2}{cd}) + j\cos\theta(\frac{bc^2+ad^2}{2cd\sin\theta} - \frac{2ka\sin\theta+2kb\sin\theta}{cd}) + \frac{c^2(1-k)}{cd})/2\sqrt{k} \tag{4.27}$$

where, a = Z_{e1} + Z_{o1}, b = Z_{e2} + Z_{o2}, c = Z_{e1} - Z_{o1}, d = Z_{e2} - Z_{o2}

$$F_{TH} = \frac{(1+\sqrt{1-x_c^2})T_{n+1}(\frac{x}{x_c}) - (1-\sqrt{1-x_c^2})T_{n-1}(\frac{x}{x_c})}{2\sqrt{1-x^2}} \tag{4.30}$$

$$F_{TH} = \frac{\frac{4(1+\sin^2\theta_c)\cos^3\theta}{\cos^3\theta_c} - \frac{(4-2\sin\theta_c)\cos\theta}{\cos\theta_c}}{2\sin\theta} \tag{4.31}$$

In (4.29), ε is the equal ripple factor and F_{TH} is the theoretical Chebyshev transfer function given in (4.30). The term T_{n+1} is Chebyshev polynomial of degree n, $x = cos\theta$, and $x_c = cos\theta_c$. It is imperative to mention that θ and θ_c is defined as the electrical length at the centre and lower cut-off frequency respectively. For ready comprehension, let us consider a second order filter with $n = 2$, then the Chebyshev polynomial T_{n+1} are T_3 = $4x^3$-3x and $T_1 = x$. Therefore the simplified expression for F_{TH} in terms of x, x_c, T_3 and T_1 is

given in (4.31). The filtering characteristics of the theoretical Chebyshev function plotted for varying θ and θ_c in Fig. 4.31 clearly demonstrate a wideband behavior. It can be inferred that the proposed design's filtering feature represented by (4.29) has the possibility to provide wideband behavior if the coupled line parameters are chosen correctly.

To determine the unknown impedances of coupled lines of the proposed WPD, the magnitude of the transfer function in (4.27) are equated to the transfer function of chebyshev band-pass filter in (4.31). Apparently, the expressions (4.27) and (4.31) has equivalent form in terms of cosine function. Now, for impedance ratio k < 1, and electrical length $\theta = 90°$, the equations (4.32)-(4.35) can be obtained for different θ_c.

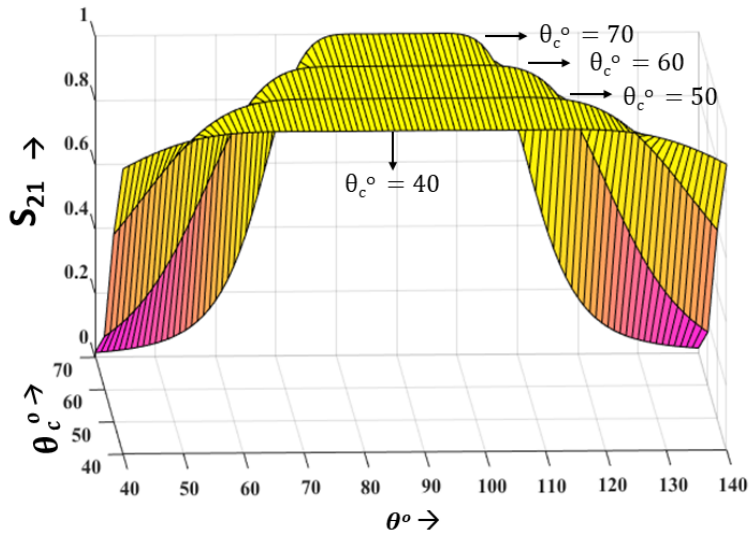

Fig. 4.31 Filtering characteristics of theoretical bandpass filter

$$\frac{(a^2b-ab^2)}{4cd\sqrt{(k)}} = \frac{4(1+\sin^2\theta_c)}{2\cos^3\theta_c} \tag{4.32}$$

$$\frac{(ab+a^2-kab-ka^2)}{2cd\sqrt{(k)}} = 0 \tag{4.33}$$

$$\frac{(bc^2+ad^2-2ka-2kb)}{4cd\sqrt{(k)}} = \frac{4-2\sin\theta_c)}{2\cos\theta_c} \tag{4.34}$$

$$\frac{(c^2(1-k))}{2cd\sqrt{(k)}} = 0 \tag{4.35}$$

The equations (4.32)-(4.35) can be solved using mathematical solvers, such as MATLAB, to compute the value of unknown impedances of the coupled line. Subsequently, the equations (4.24)-(4.25) can be used to determine the isolation resistors' value to maintain the good in-band isolation. A plot signifying the variation of R_1 and R_2 according to (4.25b) for excellent port matching is presented in Fig. 4.32. It can be noted that the isolation resistors depend on the characteristic impedance of Section-B only. There are plenty of choices available to select isolation resistors from the plot presented in Fig. 4.32.

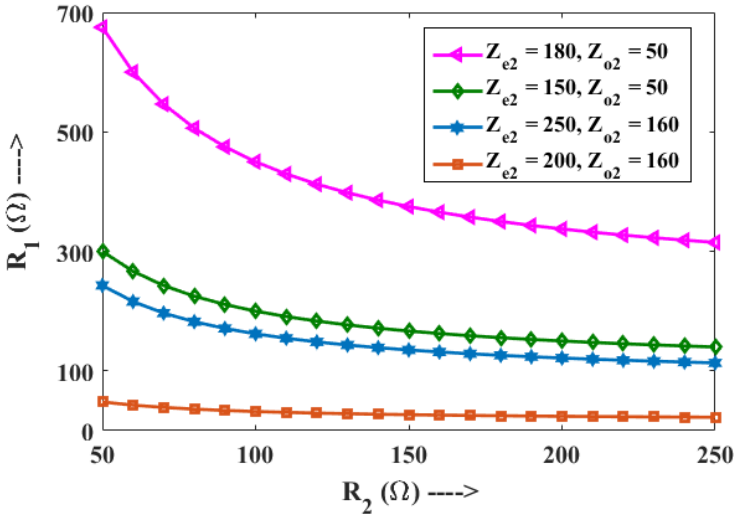

Fig. 4.32 Isolation resistor variation

4.3.3 Case Studies, Simulation and Measurement

Based on the above design procedure and calculated design parameters listed in Table - 4.4, simulation results of different case studies are presented in Fig. (4.33) - (4.36) illustrating S-parameters for varying θ_c. Fig. 4.33 represents the simulated S_{11} (dB) for different θ_c over a wide frequency range from 3GHz to 12 GHz. Similarly, Figs. (4.34), (4.35) and (4.36) illustrates the S_{21} (dB), S_{22} (dB) and S_{23} (dB) respectively. It can be noted from the

simulation results that, with increasing value of θ_c, bandwidth of power divider decreases.

Table 4.4 Parameters of the different case studies with varying θ_c

θ_c (°)	Z_{e1} (Ω)	Z_{o1} (Ω)	Z_{e2} (Ω)	Z_{e2} (Ω)
40	320	80	180	20
50	360	100	200	30
60	400	180	220	60
70	580	320	280	100

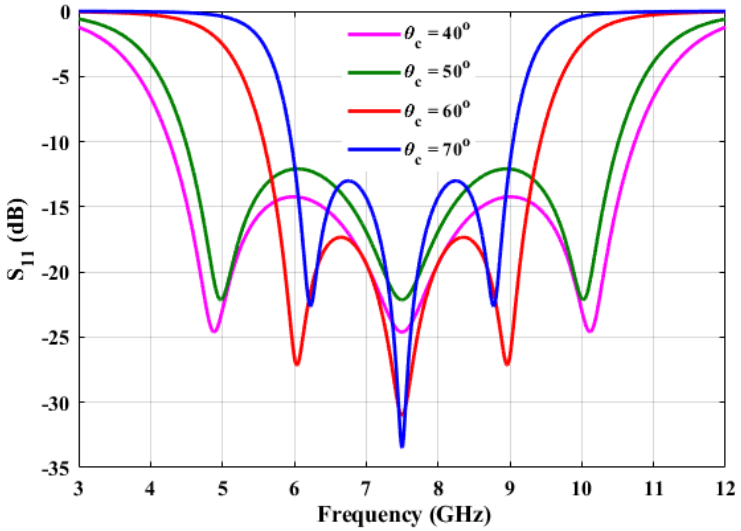

Fig. 4.33 $S_{11}(dB)$ vs frequency (GHz) with varying θ_c

From Table - 4.4, it can be inferred that techniques like a slotted ground, slot-coupled microstrip line, defected ground structures etc. should be employed to maintain the impedance values of the coupled lines within fabricable limits.

The proposed wideband WPD is fabricated on a Rogers RO4003C substrate with 1.52mm thickness and dielectric constant ε_r = 3.55. The parameters of the proposed WPD at the chosen center frequency of 7.5 GHz are Z_{e1} = 250 Ω, Z_{o1} = 60 Ω, Z_{e2} = 180 Ω, Z_{o1} = 60 Ω, R_1 = 450 Ω and R_2 = 100 Ω. The photograph of the fabricated prototype is shown in Fig. 4.37. Defected Ground Structure (DGS) has been employed at the bottom plane because

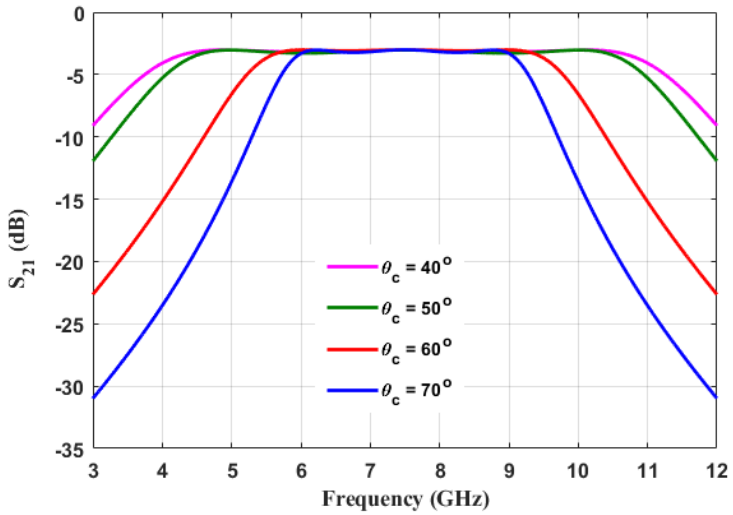

Fig. 4.34 $S_{21}(dB)$ vs frequency (GHz) with varying θ_c

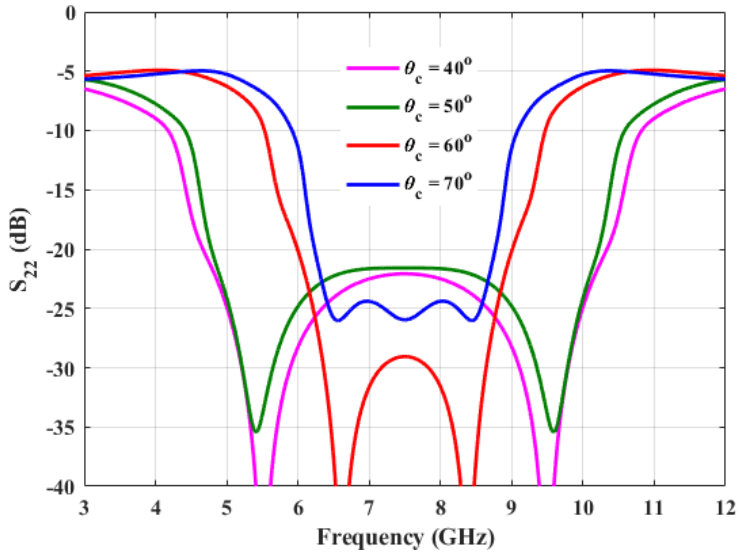

Fig. 4.35 $S_{22}(dB)$ vs frequency (GHz) with varying θ_c

of its advantage, including lowering the characteristic impedance of the coupled-line section and improving the overall bandwidth [140]. Tight coupling between the coupled line sections is used to lower the characteristic impedance. However, it is challenging to realize the coupled-line structures in microstrip because of fabrication limitations. The defected ground structure technique results in broader fabrication tolerance, including realizable coupled-line width and separation. The etching of the DGS on the ground plane of WPD can be realized

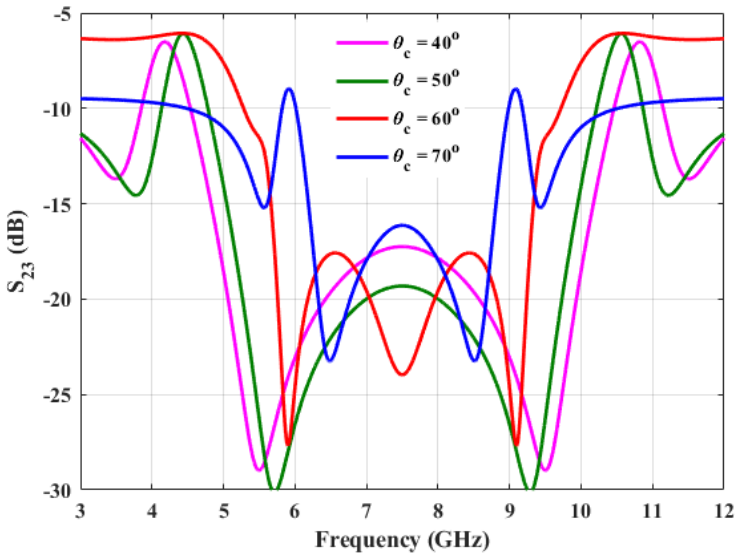

Fig. 4.36 $S_{23}(dB)$ vs frequency (GHz) with varying θ_c

by different geometric shapes, including rectangles, triangles, circles, hexagons, spirals etc. [141]. Initially, the slots in the ground plane were chosen with random dimensions and then subsequently optimized to make the planar circuit dimensions realizable, and compact [142].

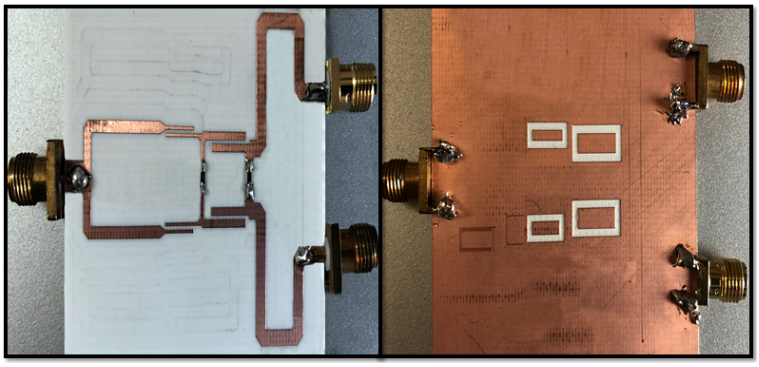

Fig. 4.37 Fabricated prototype (top and bottom view)

It can be observed in Fig. 4.38 that the measured bandwidth of 82% with minimum insertion loss S_{21} of -3.08 dB can be achieved at a return loss S_{11} of less than -15 dB for the proposed design. Apparently, the measured results align with the EM simulated results obtained in the ADS environment. Furthermore, Fig. 4.39 provides the measured isolation S_{23} of more than -15 dB over the entire frequency range of 4.0 - 11.0 GHz resulting in the bandwidth greater than 100%, with an excellent port matching bandwidth S_{22} of 89%. Once

Table 4.5 Comparison with the previous wide-band WPDs

References	Frequency Range (GHz)	Technique Used	Isolation Network	FBW/ (Return loss)	FBW(%) (Isolation)	DC Isolation
TMTT (2016) [145]	1.45 - 4.6	Quasi-coupled Lines	1 Resistor 1 Capacitor	104 (%)/ (15 dB)	100 (%)/ (17dB)	No
MWCL (2016) [143]	1.25 - 2.5	Coupled-lines at Input / Output port	1 Resistor	62 (%)/ (15dB)	71 (%)/ (18 dB)	Yes
Access (2018), [144]	1.42 -3.42	Three Line coupled structure	1 Resistor	62 % / 16 dB	16 % / 16 dB	Yes
TCPMT (2019), [146]	1.5 -3.55	Three Line Coupled structure	1 Resistor	82.6 % / 10 dB	-	No
TMTT (2020), [147]	1.44 - 4.61	Quasi Coupled Lines	1 Resistor	104.5 % (-15 dB)	-	No
This Work, (2021)	**4.2 - 10.5**	**Coupled -Lines as Core**	**2 Resistors**	**82.6 (%)/ (10 dB)**	**>100 (%) / (15dB)**	**Yes**

again, these results are in excellent agreement with the EM simulated results. Overall, the slight discrepancy in the measured and simulated results can be attributed to the cables and connectors losses, slight port mismatch etc., which are critical at higher frequencies. Finally, the performance of the proposed WPD is compared with the recently reported wideband WPDs in Table - 4.5. It is worth noting that the proposed work provides good in-band performance with DC isolation.

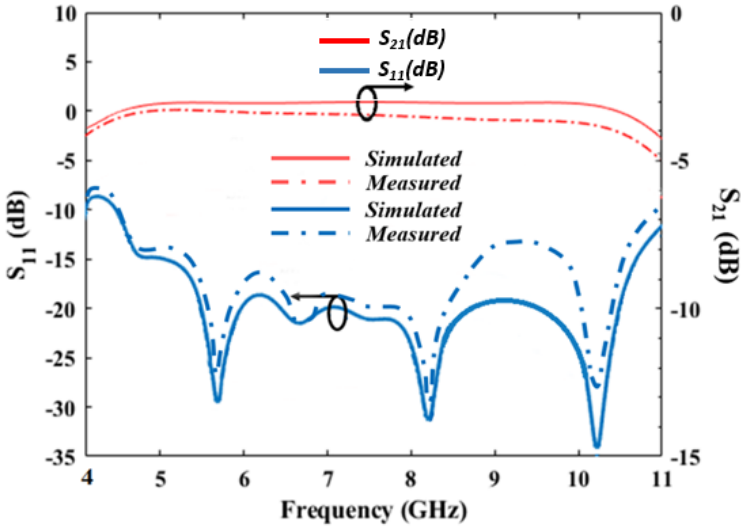

Fig. 4.38 Simulated vs measured S_{11}(dB) and S_{21} (dB)

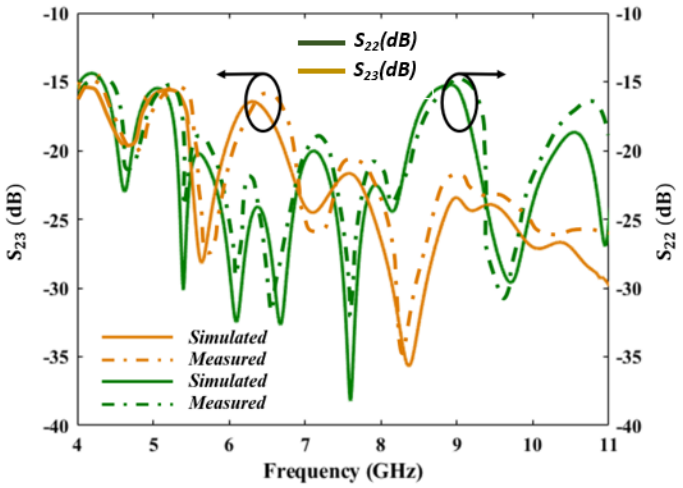

Fig. 4.39 Simulated vs measured S_{22}(dB) and S_{23} (dB)

4.4 Summary

This chapter discusses the different types of power dividers, including multi-band or broadband WPD utilizing different design techniques. Two different methods for designing broadband power dividers are proposed. Design 1 utilizes the transmission lines, short-circuit stubs and isolation resistors to provide broadband dividing operation with excellent isolation between ports. A modified DC isolated WPD is also illustrated with practical applications in devices such as Doherty Power Amplifier. Design 2 uses coupled lines in cascade to make inherent DC isolated WPD, with excellent port isolation and return loss. Design equations are developed along with their mathematical formulations, and equations for calculating the value of isolation resistors are presented. The transfer characteristics are plotted to calculate the design parameters for both designs. Different case studies have been discussed to validate the theoretical formulations. Also, prototypes are developed with simulated and measured results in good agreement.

Chapter 5

Harmonic Tuned Power Amplifier - Application of Matching Networks

5.1 Introduction

The power amplifier is an essential component required to convert a low-power radio-frequency signal into a higher power signal in any microwave device. The overall performance of a wireless transmitter is highly reliant on the features, namely Power Added Efficiency (PAE), output power, gain, etc., of RF Power Amplifiers (PAs). Different classes are defined to enhance the efficiency of a power amplifier. The PAs operating as Class-A, B, AB, and C are defined by controlling the current conduction angle. Theoretically, the class-A amplifier can achieve maximum 50% drain efficiency with both current and voltage waveforms as sinusoidal. However, to increase the efficiency, the current and voltage waveforms need to be reshaped. For reshaping the waveforms, drain voltage may contain a number of harmonics while maintaining the current waveform as sinusoidal or vice versa, as shown in Fig 5.1. This technique reduces the overlapping area between waveforms resulting in a new class of PAs, namely switched-mode (Class-D, Class-E) and harmonic-tuned PAs (Class-F or Class-F^{-1}) [148]-[152]. In the defined classes, the drain current and voltage waveforms are altered

by terminating the harmonic load impedances such that they contain an infinite number of harmonics. It is imperative to note that power dissipation can be minimised by avoiding overlap between voltage and current waveforms, and theoretically, drain efficiency can reach 100%. However, practically, it is impossible to alter infinite harmonics, but it is possible to achieve efficiency greater than 75 % by controlling the first few (two or three) harmonics. Also, it is traditional to drive the transistors in a nonlinear region of operation to achieve

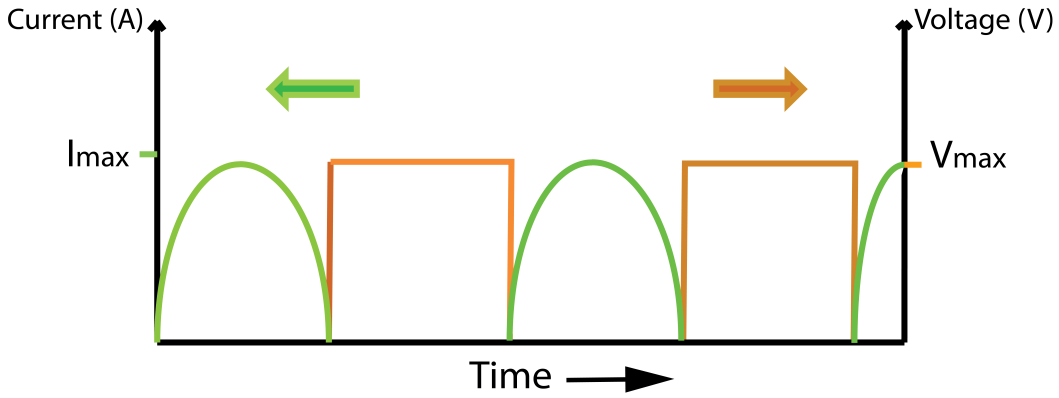

Fig. 5.1 Current and voltage waveform with zero overlapping area

high PAE and output power. A critical point in highly efficient RFPA configurations such as switched-mode PAs is a restriction in the frequency of operation. At higher frequencies, parasitic capacitance and inductance at the drain of the transistors play an essential role, which prevents operation as ideal switch [153]. Several design techniques have been reported in the past decade to circumvent this issue, and some of them can be considered seminal [154]-[164]. In general, designs utilizing input harmonic terminations [154], broadband harmonic tuned approach [155], external harmonic injection [156], independent harmonic tuned output network [159], harmonic treatment up to fourth order [160], concurrent dual-band harmonic-tuned [162], second harmonic tuned [163], harmonic tuned inverse Class-F using bare-die device [164], etc. have found wide approval because of their performance in practical applications and commercial products.

In the past, different multi-band passive networks have been proposed operating at different

frequencies concurrently, including tri-band branch-line coupler with open/short-circuit stubs [166], quad-band branch-line coupler based on optimization compensation technique [167], tri-band impedance transformer based on virtual impedance [168], etc. We proposes an idea to utilize the multi-band matching network to control the harmonics at the drain impedance of the transistor so that maximum efficiency can be achieved by considering the parasitic inside the transistor. The following sections will discuss the design methodologies for the harmonically tuned power amplifier by tuning either two or three harmonics and providing mathematical equations to utilize the multi-band matching networks as the output network for maximum efficiency.

5.2 Design of Harmonic Tuned Power Amplifier - Design 1

We proposed a design technique that makes use of a tri-band design methodology [166] as a two-port output network to match the optimal fundamental, second, and third harmonic impedances concurrently at the output of the transistor. This technique provides a method for designing an output matching network using closed-form equations. The proposed design is augmented by analytical formulations for obtaining the requisite design parameters for the two-port output network. It is demonstrated that the incorporation of a two-port output network enhances the performance of harmonically tuned PAs with a mathematical framework, apart from a reduction in the circuit complexity and form factor.

5.2.1 Circuit Design and Analysis

The Proposed Configuration

In harmonic tuned PAs, perfect terminations are required at the fundamental as well as the second and third harmonics [154] - [160]. For example, the design of the conventional $Class-F/F^{-1}$ power amplifiers requires proper short/open harmonic terminations at the

current generator plane, followed by the fundamental match. Usually, the matching at harmonic frequencies requires intense optimization and can be quite tedious [158] - [160]. The proposed design scheme depicted in Fig. 5.2 envisages addressing this concern. It incorporates a tri-band impedance transformer at the output to match the fundamental and harmonic impedances with the load R_L.

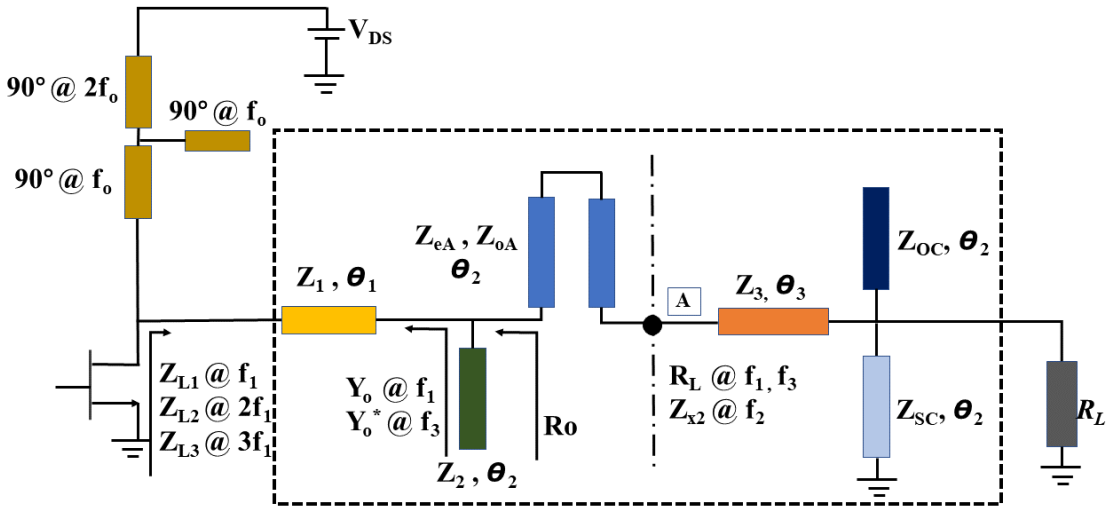

Fig. 5.2 Schematic of the proposed two-port output network

The two-port output network identified by the dashed box in Fig.5.2 primarily serves to match the fundamental and harmonic impedances at the transistor's drain terminal to a resistive load R_L. Here, the output impedance is represented by Z_{L1}, Z_{L2}, and Z_{L3} at the fundamental f_1, second f_2, and third f_3 harmonics, respectively.

Drain Network

For matching the drain impedance at a fundamental, second and third harmonic frequency to load resistance R_L, the drain biasing network should provide high impedance at all three harmonics. The designed drain network shown in Fig 5.3 is capable of providing infinite impedances at the designed fundamental frequency, its second and third harmonic as

discussed.

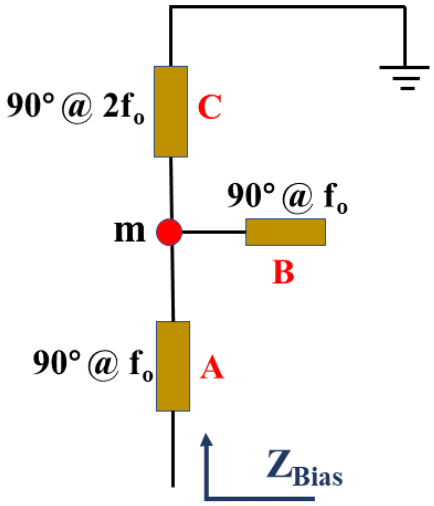

Fig. 5.3 Drain bias network

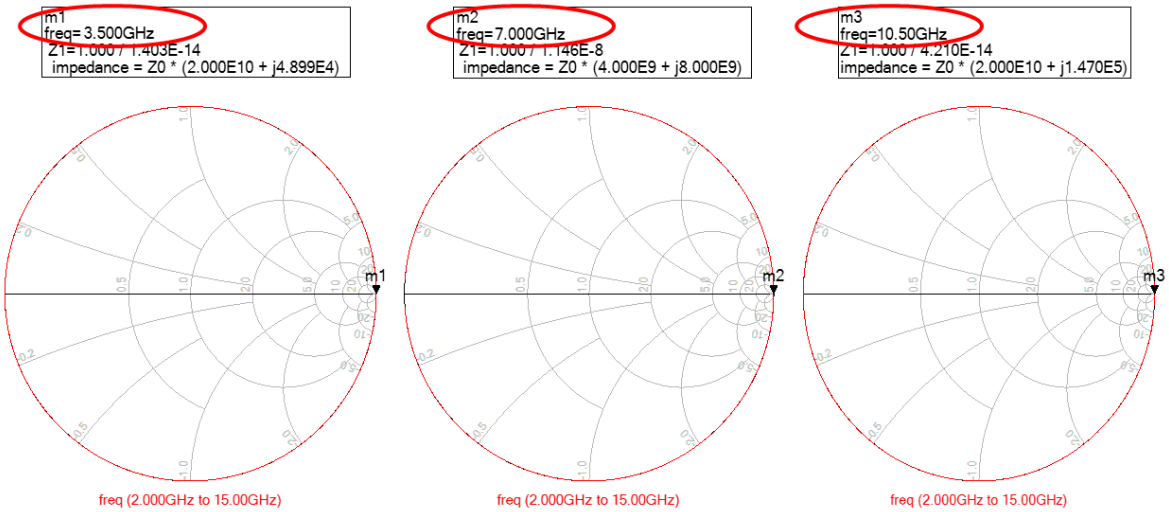

Fig. 5.4 Impedance looking at the drain bias network at fundamental frequency, second and third harmonic

At the fundamental frequency and third harmonic, Z_{Bias} in Fig.5.3 will be open-circuit because of quarter-wave transmission lines, and node 'm' is at short-circuit because of

transmission line 'B'. Hence, the transmission line will transfer short-circuit to open-circuit. Similarly, for the second harmonic, node 'm' will be at an open circuit due to the presence of transmission line C, and then transmission line A will see an open circuit as shown in Fig. 5.4.

Output Matching Network

In Fig. 5.2, the output network is a tri-band impedance transformer designed using the concept discussed in [166]. It comprises of a coupled-line dual-band impedance transformer [169] denoted by Z_{eA}, Z_{oA}, θ_2 and a dual-band transmission line-based L-network [40] indicated by Z_1, θ_1, and Z_2, θ_2. It eases the matching of the device's fundamental/harmonic impedances, $Z_{L1} = R_1 + jX_1$ at f_1, $Z_{L2} = R_2 + jX_2$ at f_2, and $Z_{L3} = R_3 + jX_3$ at $f_3 = 3f_1$, achieved using load-pull for optimal efficiency [165] and the load impedance R_L.
First, the impedances Z_{L1} and Z_{L3} are transformed into complex conjugate, i.e. $Y_O|_{f_1} = Y_O^*|_{f_3}$, by the segment $[Z_1, \theta_1]$ of the L-network. Here, $Y_O = 1/Z_O = G_O + jB_O$ @ f_1 and $G_O - jB_O$ @ f_3. Subsequently, the susceptance B_O is cancelled by the dual-band stub $[Z_2, \theta_2]$ of the L-network. The parameters $[Z_1, \theta_1]$ and $[Z_2, \theta_2]$ are calculated using (5.1) and (5.2) respectively [168]. The term $r_{31} = f_3/f_1$ is the frequency ratio.

$$Z_1 = \sqrt{R_1R_3 + X_1X_3 + \frac{X_1 + X_3}{R_1 + R_3}(R_1X_3 - R_3X_1)} \tag{5.1a}$$

$$\theta_1 = \frac{n\pi + arctan\frac{Z_1(R_1 - R_3)}{R_1X_3 - R_3X_1}}{1 + r_{31}} \tag{5.1b}$$

$$\theta_2 = \frac{n\pi}{1 + r_{31}} = \frac{n\pi}{4} \tag{5.2a}$$

$$Z_2 = \frac{-j\cot\theta_2}{B_O}\ (Short), \quad Z_2 = \frac{j\tan\theta_2}{B_O}\ (Open) \tag{5.2b}$$

The real part $R_O = 1/G_O$ is then matched with the load impedance, R_L, at f_1 and f_3 by the dual-band $\lambda/4$ coupled-line impedance transformer. The coupled line transformer's image impedance, $Z_A = \sqrt{R_O R_L}$ [169], is analogous to its corresponding even- and odd-mode characteristic impedances Z_{eA} and Z_{oA} are given in (5.3). Furthermore, in the process of matching at f_3 and f_1, second harmonic impedance Z_{L2} gets transformed to a new value Z_{X2} = G_{X2} + jB_{X2} @ f_2, expressed in (5.4), at the node A in Fig. 5.2.

$$Z_{eA} = Z_A \tan\theta_2 \tag{5.3a}$$

$$Z_{oA} = Z_A / \tan\theta_2 \tag{5.3b}$$

$$Z_{X2} = Z_A^2 [\frac{(Z_1 + jZ_{L2} tan\theta_1)}{(Z_1 Z_{L2} + jZ_1^2 tan\theta_1)}] + j * \frac{tan\theta_2}{Z_2} \tag{5.4}$$

At node A, as shown in Fig.5.2, the value of impedances present at three different frequencies are as follows: R_L @ f_1 and f_3, while Z_{x2} @ f_2. At the fundamental and third harmonic, the drain impedance previously matched to load impedance R_L, but Z_{x2} @ f_2 needs to be matched without disturbing the match at f_1 and f_3. Thus, a transmission line with characteristic impedance $Z_3 = R_L$ with electrical length θ_3 is used [166]. Here, the impedance Z_3 is equal to the load resistance R_L and accordingly matching at the fundamental and third harmonic will remain the same, while transforming the Z_{x2} @ f_2 to a new value, which can be controlled by its electrical length θ_3.

$$G_{X2} = \frac{1}{(\frac{R_L^3}{R_L^2 tan^2\theta_3 + R_L^3}) + (\frac{R_L^3 tan^2\theta_3}{R_L^2 tan^2\theta_3 + R_L^3})} \tag{5.5a}$$

$$B_{X2} = \frac{1}{(\frac{R_L^3 tan\theta_3}{R_L^2 tan^2\theta_3 + R_L^3}) - (\frac{R_L^2 Z_3 tan2\theta_3}{R_L^2 tan^2\theta_3 + R_L^3})} \tag{5.5b}$$

It can be seen from (5.5a) and (5.5b), by calculating the value of θ_3 the real part G_{X2} can be set equal to $1/R_L$. Thus, in a second harmonic, the real part matches the load perfectly. However, the generated susceptance by this transmission line needs to be cancelled without disturbing the matching at the fundamental and third harmonic. Therefore, a combination of open and short circuit stub with characteristic impedance Z_{OC} and Z_{SC} respectively is utilized. This network should be capable of cancelling the susceptance generated at the second harmonic while providing infinite admittance at the fundamental and third harmonic. For maintaining the infinite admittance seen by fundamental and third harmonic, the relation $Z_{OC} = Z_{SC} tan^2\theta_2$ should remain valid. However, the impedance generated by the stub network should cancel the susceptance B_{X2} @ f_2. The expression used to calculate the impedance of the stub network is given in (5.6):

$$B_{X2} = -jY_{OC}cot(X\theta_2) + jY_{SC}tan(X\theta_2) \tag{5.6}$$

Here, X is defined as f_2/f_1, while θ_2 is defined at the fundamental frequency. Substituting the value of $Y_{OC} = Y_{SC}\cot^2\theta_2$ in (5.6), the characteristic impedance of short-circuit stub Z_{SC} and hence open-circuit Z_{OC} is given in (5.7a) and (5.7b) respectively.

$$Z_{SC} = \frac{cot^2\theta_2 cot(x\theta_2) + tan(x\theta_2)}{B_{X2}} \tag{5.7a}$$

$$Z_{OC} = Z_{SC} tan^2\theta_2 \tag{5.7b}$$

The above discussion completes the mathematical derivation of the tri-band impedance transformer.

5.2.2 Case Study and Experimental Evaluation

For validating the theoretical proposition, first, the standard 10W GaN HEMT was biased at a gate voltage of $V_{GS} = -2.7V$ and drain voltage of $V_{DS} = 28V$ for the drain current of $I_D = 63mA$. After that, load-pull simulation was carried out for maximized efficiency by tuning the first three harmonics and the achieved fundamental and harmonic impedances as listed in Table - 5.1. After that, an output two-port network is designed using the concept presented. All the parameters are chosen to remain within the realizable limits of 20-150 Ω, inferred from the parameters listed in Table - 5.2.

Table 5.1 Optimum impedances at the drain of the transistor

Frequency	**Output Impedances (Ω)**
$f_1 = 3.5$ GHz	$10.27 + j1.245$
$f_2 = 7.0$ GHz	$1.1 + j1.5$
$f_3 = 10.5$ GHz	$7.75 + j14.35$

Table 5.2 Design parameters of matching network

L-Network	**Coupled-Line Transformer**	**Transformation Network**
Z_1= 26.44 Ω	Z_e= 55 Ω	Z_3= 50 Ω
Z_2 = 148 Ω	Z_o= 50 Ω	θ_3= 60.53 °
θ_1= 75 °	θ_2= 45°	Z_{OC} = 133 Ω
——	—-	Z_{SC} = 82 Ω

It is interesting to investigate the impedance trajectories. Fig. 5.5 illustrates the co-simulated trajectories of the fundamental, second, and third harmonic impedances for a frequency range of 3.4 - 3.7 GHz. The impedances lying on these trajectories correspond to drain efficiency of more than 50 %. Furthermore, the impact of the transmission line parameters on the overall design is also significant. The relationship of the optimal efficiency related to the electrical length of θ_1, is given in Fig. 5.6. The drain efficiency is maximum when θ_1 falls within the shaded region. At the design frequency of 3.5 GHz, it is evident

that θ_1 should be approximately 75°, which is close to the value obtained for the designed network given in the Table - 5.2. The impact of θ_2 is also significant on the achievable drain efficiency, as can be inferred from Fig. 5.7. The shaded region is earmarked for optimal efficiency, and it is in perfect agreement with the data in Table - 5.2. Furthermore, the

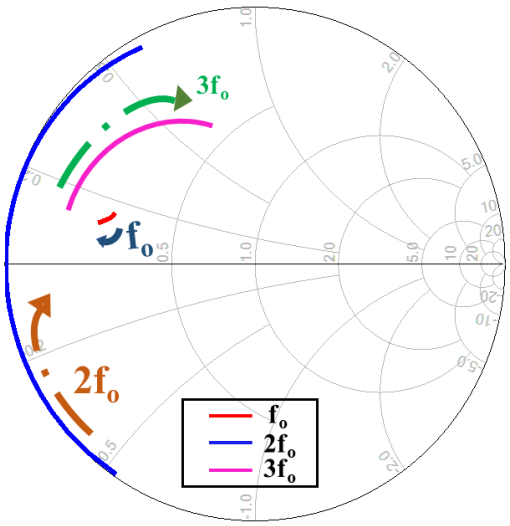

Fig. 5.5 Impedance trajectories at the drain of the transistor

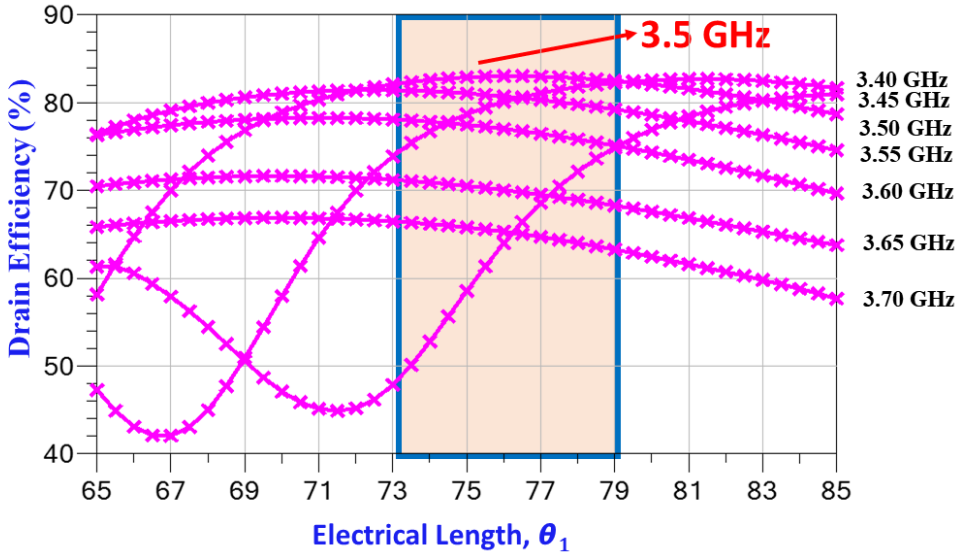

Fig. 5.6 Dependence of drain efficiency on θ_1 for different frequency

variation of drain efficiency with the drain impedance at the fundamental frequency is also

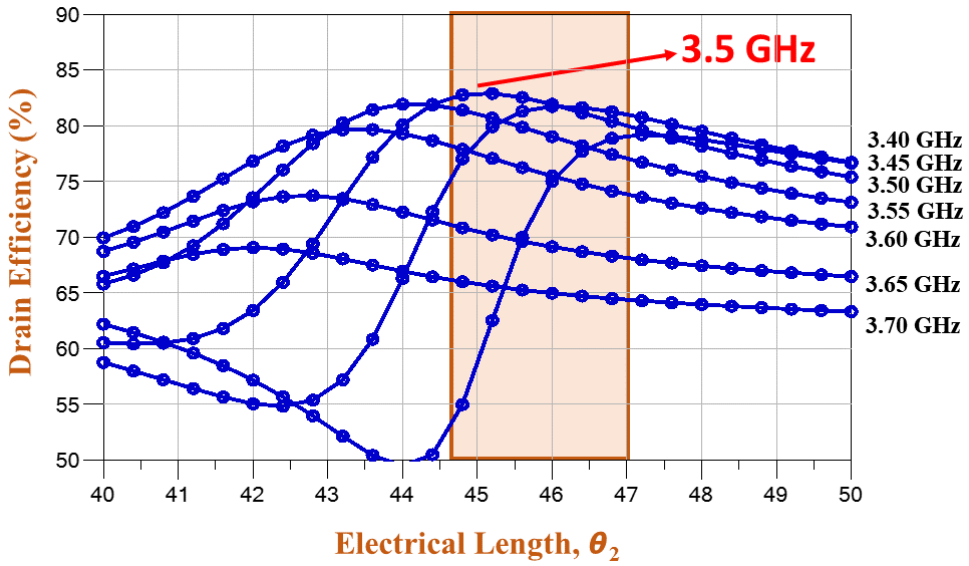

Fig. 5.7 Dependence of drain efficiency on θ_2 for different frequency

an important aspect. In this context, the variation of drain efficiency with load is depicted in Fig. 5.8. The boundary of impedance ratio at the fundamental frequency (i.e., Z_L/Z_S) for maintaining efficiency above 60% is between 0.1 to 0.5. It can also be inferred from Fig. 5.8 that, in this case, the maximum efficiency is achievable for the fundamental impedance, i.e., Z_{L1}, of 10.27+j*1.2 Ω obtained from load-pull.

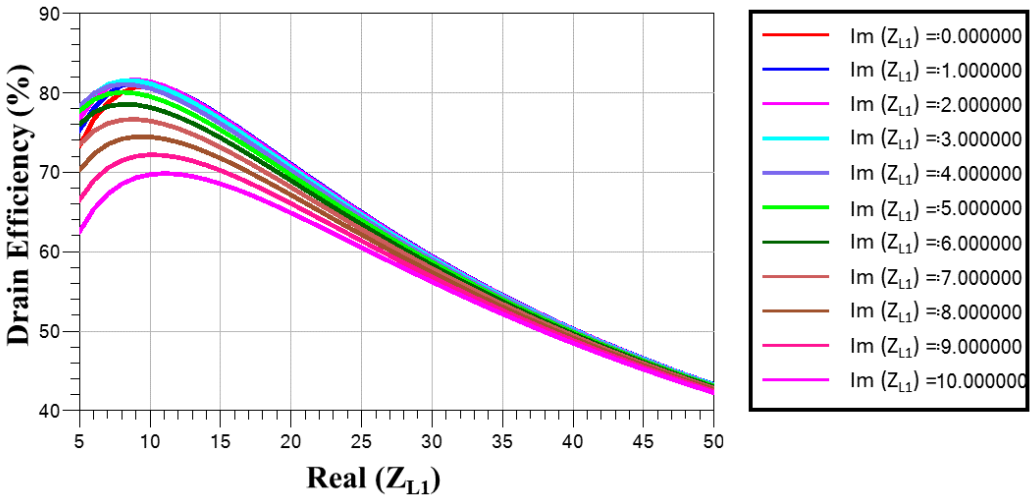

Fig. 5.8 Drain efficiency vs fundamental load
*Real - Real part of impedance (Z_{L1}) @ fundamental frequency, *Im - Imaginary part of impedance (Z_{L1}) @ fundamental frequency

The schematic of the measurement setup is shown in Fig. 5.9. Keysight's (MXG N5182B) and Vector Network Analyzer (PXA N9030B) are used for generating and receiving the signal, respectively. The developed PA prototype on RO5880 substrate (ε_r= 2.2, thickness 1.575mm, 1oz Cu) using 10W GaN Wolfspeed GaN HEMT, shown in Fig. 5.11, is measured at the design frequency of 3.5 GHz. The drive power is swept from 22-31 dBm, and then PAE, DE, and Gain are measured, plotted in Figs. 5.10 and 5.11. For an input power of 30 dBm, the maximum measured PAE and DE are 73.8 % and 77.3 %, respectively, while the gain is 10.4 dB. Also, current and voltage waveforms at the transistor's intrinsic plane are presented in Fig.5.12. These are in good agreement with the corresponding simulation results. Finally, the achieved results for the proposed design are compared with the previously reported design at 3.5 GHz in Table - 5.3. It demonstrates that the proposed design technique could be a potential alternative as the achieved results compare favourably to the reported designs.

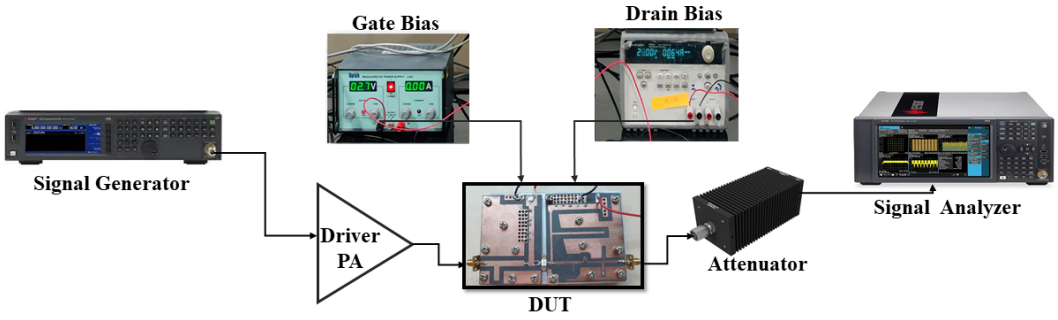

Fig. 5.9 Schematic of the measurement setup

Table 5.3 Comparison with the previous 3.5 GHz PA design

References	Transistor Used	Frequency (GHz)	Pout (dBm)	PAE (%)	DE (%)
EuMC $^{+}$ [170]	GaN HEMT	3.5	40.5	72	79
EuMC [163]	GaN HEMT	3.5	35.3	57.7	69
TMTT $^{+}$ [157]	GaN HEMT	3.5	40.2	70	75.8
TMTT [149]	GaN HEMT	3.54	55	63	70
This Work	**GaN HEMT**	**3.5**	**40.4**	**73.8**	**77.3**

$^{+}$ Class-E PA

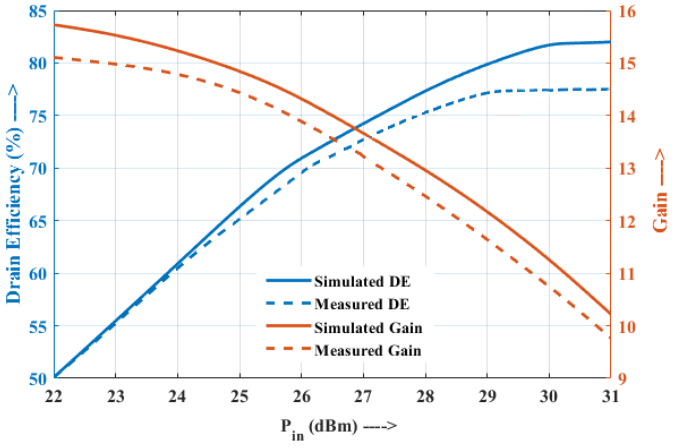

Fig. 5.10 Drain efficiency and gain for input power sweep

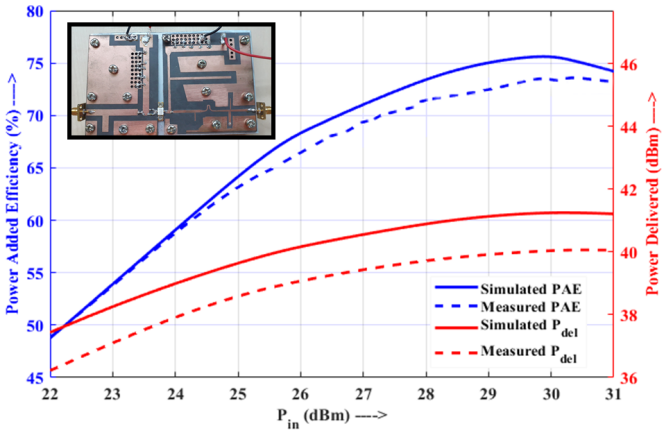

Fig. 5.11 The prototype, PAE and power delivered for input power sweep

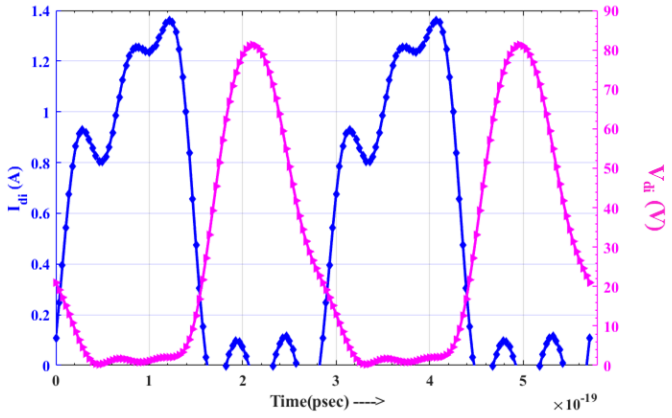

Fig. 5.12 Voltage and current waveforms at the intrinsic plane of transistor

5.3 Design of a Harmonically Tuned RF Power Amplifier - Design 2

In the previous design, we harmonically tuned the three harmonics concurrently, whilst this design reports the variation of efficiency of harmonic tuned PA by considering two harmonics only. An essential concept of this proposed design is to ease the mathematical equations while considering only two harmonics while optimizing the performance of the PA. The central aspect of designing a high-efficiency PA is to provide the optimum impedances at the drain of the transistor, which needs to be matched to a terminated load R_L, usually 50 Ω. Load-pull simulation is carried out at the packaged drain terminal of the non-linear transistor to estimate the value of the optimum load impedances [165]. As described in the former section, the first three harmonics affect the performance of the PA, while the other has a negligible effect.

The first step is to obtain the optimum drain impedance at the fundamental frequency to maximize the PAE and gain. Afterwards, the harmonics are tuned and observed to optimize the overall performance of the PA. The different cases have been studied to analyze the variation of the efficiency and other parameters, including the gain of the PA with the harmonic alteration at the drain of the transistor as discussed:

- ***Case - 1 :*** First, load-pull is carried out to calculate the impedance at fundamental frequency i.e. Z_{L1} @ f_0, while second harmonic is short-circuited with third harmonic open-circuited. For the second-harmonic to be short-circuited while fundamental and third-harmonic sees an open-circuit through the drain, the drain-bias network should follow the Design 1 depicted in Fig. 5.13 i.e., a quarter-wave transmission line at fundamental.

- ***Case - 2:*** The impedance at the fundamental frequency is kept fixed according to Case-1 and tuning the third harmonic impedance while keeping the second harmonic

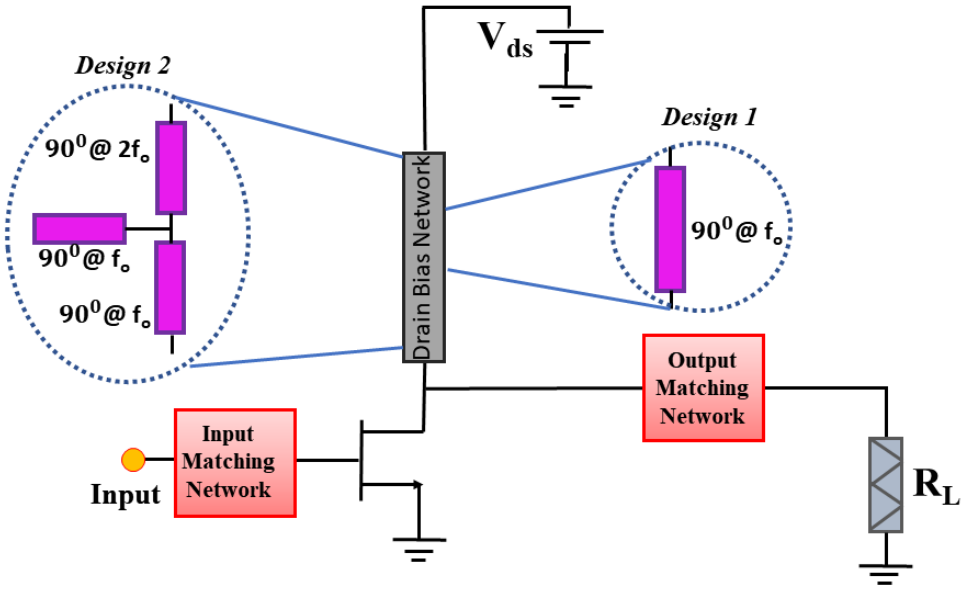

Fig. 5.13 Schematic of the PA with different drain bias network

short-circuited during load-pull simulation. The drain bias should also follow Design 1 shown in Fig. 5.13.

- ***Case - 3:*** Here, the fundamental and second-harmonic are considered only. The load-pull is performed to obtain the optimum fundamental impedance with a second-harmonic tunable. The drain-bias should follow the Design 2 [171] shown in Fig. 5.13. It ensures that the fundamental and second-harmonic impedances see an open circuit through the drain-bias network.

The different cases with impedances at the packaged drain terminal and the corresponding PAE obtained from load-pull at 3.5 GHz are tabulated in Table- 5.4. It can be observed that Case-2 corresponds to maximized efficiency. Hence, the necessary condition to design the two-port output network is to short the second harmonic while matching the fundamental and third harmonic impedance with the load R_L. The subsequent section will discuss the circuit design topology, analysis, and results.

Table 5.4 Impedances at the drain terminal with obtained PAE

Case	**Impedance Condition (Ω)**			**PAE (%) (obtained from Load-pull)**
1	Z_1 = 10.6+j*9.3 @ f_1	Z_2 = 0.0+j*0.0 @ f_2	-	71.9
2	Z_1 = 10.6+j*9.3 @ f_1	Z_2 = 0+j*0 @ f_2	Z_3 = 20-j*30 @ f_3	76.2
3	Z_1 = 10.6+j*9.3 @ f_1	Z_2 = 0.25+j*2.1 @ f_2	-	71.2

5.3.1 Circuit Design and Analysis

To obtain the high efficiency, it is required to terminate the drain with the optimal impedances at the fundamental and third harmonic frequency according to Table- 5.4 and match it with a load, 50 Ω. In the last decade, the different architectures for designing the dual-band matching network are available in the literature, including matching utilizing T-section, dual-band $\lambda/4$ lines, L-type network, two-section transmission line and more [40] - [44]. This section discusses the design of a dual-band output network to match the fundamental and third harmonic with the load R_L.

Circuit Topology

The schematic of the dual-band output network for matching the fundamental and harmonic impedances at the transistor's drain terminal to a resistive load R_L is presented in Fig. 5.14. Here, the output impedance is represented by Z_{L1} and Z_{L3} at the fundamental (f_0) and third $(3f_0)$ harmonics, respectively.

In Fig. 5.14, the output network consists two sections namely section-A and section-B. Section-A comprises of an all-pass coupled-line [134] denoted by $[Z_e, Z_o, \theta_1]$, a dual-band stub with characteristic impedance Z_{A1} and electrical length θ_2 [172]. Section-B consists of

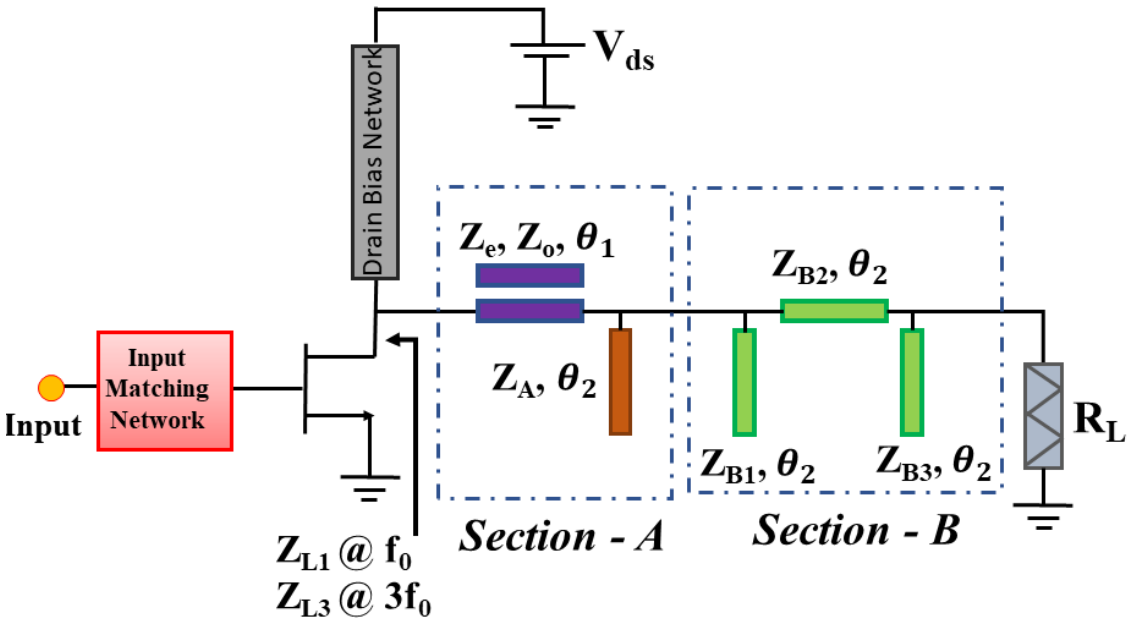

Fig. 5.14 Schematic of the proposed two-port output network

a $\pi-$ structure based real-to-real impedance transformer denoted by $[Z_{B1}, Z_{B2}, Z_{B3}, \theta_2]$ [29]. Each section of the dual-band output network along with their mathematical formulations is discussed below:

Section - A

The section - A depicted in Fig. 5.15 transforms the impedances Z_{L1} and Z_{L3} into a complex conjugate, i.e. $Y_A|_{f_0} = Y_A^*|_{3f_0}$, using coupled-line in its all-pass configuration [134]. The characteristic even/odd-mode impedance Z_{e1}, Z_{o1} related by M = Z_{e1}/Z_{o1} and electrical length θ_1 can be calculated using (5.8) [134].

$$Z_{e1} = \frac{2\sqrt{R_1R_3 + X_1X_3 + \frac{X_1+X_3}{R_1+R_3}(R_1X_3 - R_3X_1)}}{1+M} \tag{5.8a}$$

$$\theta_1 = \frac{n\pi + arctan(\frac{Z_{e1}(1+M)(R_1-R_3)}{2(R_1X_3-R_3X_1)})}{1+r_{31}} \tag{5.8b}$$

where, $r_{31} = 3f_0/f_0$.

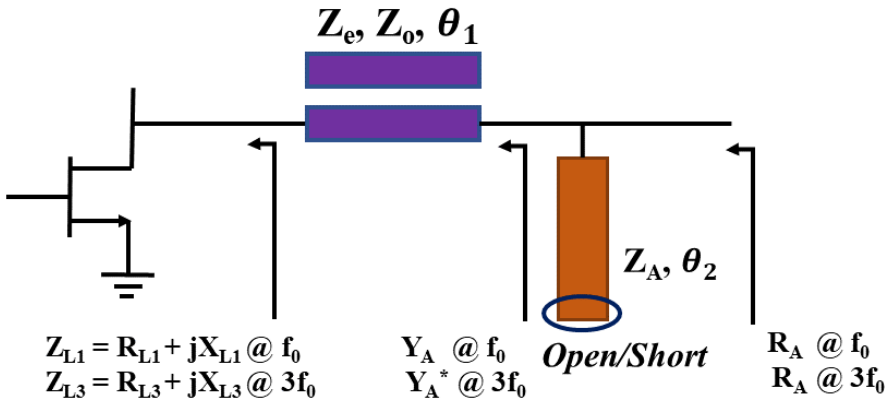

Fig. 5.15 Section - A: All-pass coupled line with dual-band stub

As illustrated in Fig. 5.15, the admittance looking into all-pass coupled line is complex conjugate of each other at two given frequencies i.e. $Y_A = 1/Z_A = G_A + jB_A$ @ f_0 and $G_A - jB_A$ @ $3f_0$. Subsequently, the susceptance B_A is cancelled using either open/short dual-band stub. The parameters $[Z_A, \theta_2]$ are calculated using (5.9)[172].

$$\theta_2 = \frac{n\pi}{1+r_{31}} = \frac{n\pi}{4} \tag{5.9a}$$

$$Z_A = \frac{-j\cot\theta_2}{B_A} \ (Short), \quad Z_A = \frac{j\tan\theta_2}{B_A} \ (Open) \tag{5.9b}$$

After cancelling the susceptance part, the real part of the impedance, i.e. $R_A = 1/G_A$ at fundamental and third harmonic frequency, remains. Now, Section-B is used to match this remaining real part to load R_L at two given frequencies.

Section - B

The $\pi-$ structure real-to-real dual-band impedance transformer as depicted in Fig. 5.16 is used to match the real part R_A with load R_L [29]. It consists of a transmission line and two open-circuit stubs in $\pi-$ configuration.

The design equations used to achieve the matching is defined in (5.10).

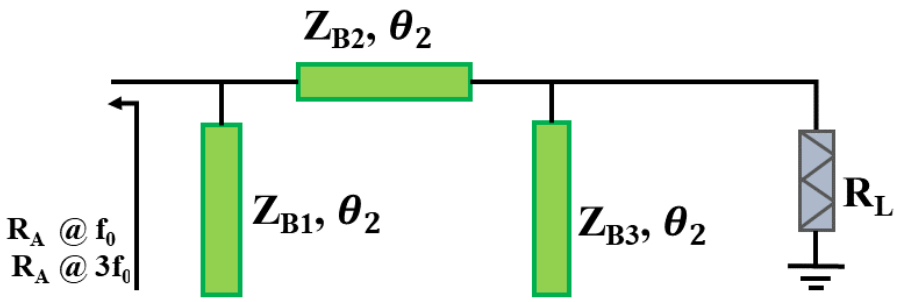

Fig. 5.16 Section - B: π-structure based real-to-real dual-band transformer

$$z_{b1} = \frac{k\alpha^2}{1+\sqrt{k}} \tag{5.10a}$$

$$z_{b2} = \sqrt{k} \tag{5.10b}$$

$$z_{b3} = \frac{\sqrt{k}\alpha^2}{1+\sqrt{k}} \tag{5.10c}$$

Here, k = R_L/R_A and the characteristic impedances of section-B in (5.10) are Z_{B1} = z_{b1}*R_L, Z_{B2} = z_{b2}*R_L, Z_{B3} = z_{b3}*R_L with electrical length θ_2 mentioned in (5.9a).

5.3.2 Experimental Validation and Results

A case study has been considered for verifying the theoretical formulations to design the harmonic-tuned PA with a dual-band output network. Initially, the standard 10W GaN HEMT was biased at a gate voltage of $V_{GS} = -2.7V$ and drain voltage of $V_{DS} = 28V$ for the drain current of $I_D = 61mA$. The impedances at fundamental and third harmonic frequencies are listed in Table - 5.5 below, obtained from the load-pull simulations to achieve the optimum efficiency and gain.

Subsequently, the proposed dual-band output network has been designed employing the concept discussed above. Table - 5.6 tabulates all the design parameters of the two-port output network, and it is evident that all the parameters are within the realizable limits of 20-150 Ω.

Table 5.5 Optimum impedances at the drain of the transistor

Frequency	**Output Impedances (Ω)**
$f_0 = 3.5GHz$	$10.669 + j9.393$
$3f_0 = 10.5GHz$	$20 - j30$

Table 5.6 Design parameters of the proposed output network

Section - A		**Section - B**	
Z_e	41.4252 Ω	Z_{B1}	40.5 Ω
Z_o	22.7839 Ω	Z_{B2}	69.64 Ω
θ_1	52.5002 °	Z_{B3}	29.1 Ω
Z_A	111 Ω		
θ_2	45 °		

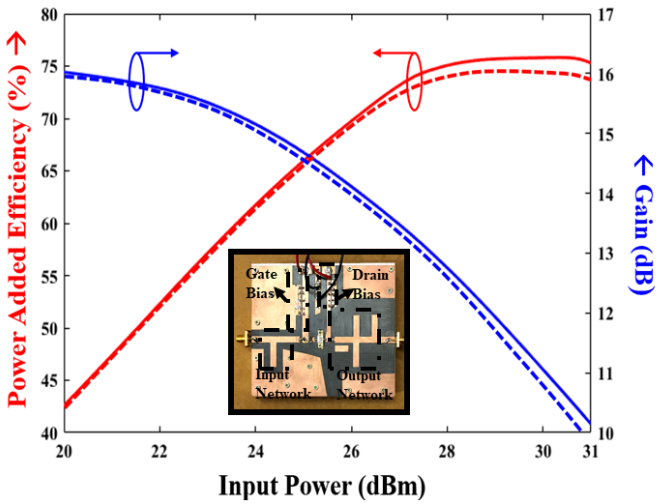

Fig. 5.17 Power added efficiency and gain vs input power(dBm) and prototype

The proposed 3.5GHz harmonic tuned PA using a dual-band output matching network has been fabricated on RO5880 substrate ($\varepsilon_r = 2.2$, thickness 1.575mm, 1oz Cu) with a 10W GaN Wolfspeed HEMT, shown in Fig.5.17. The current and voltage waveforms at the current generator (CG) plane of the transistor are illustrated in Fig. 5.19. The simulated and measured Power Added Efficiency (PAE), Gain, Drain Efficiency (DE), and Power Delivered are depicted in Fig. 5.17 and Fig. 5.18 respectively. For an input power of 30 dBm, the

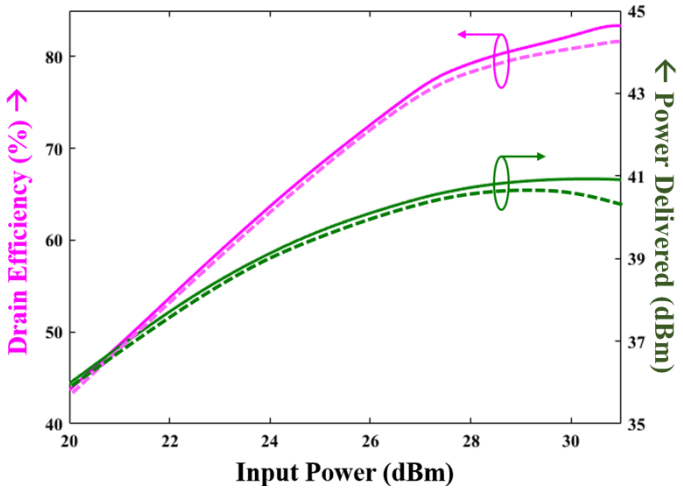

Fig. 5.18 Drain efficiency and power delivered vs input power(dBm)

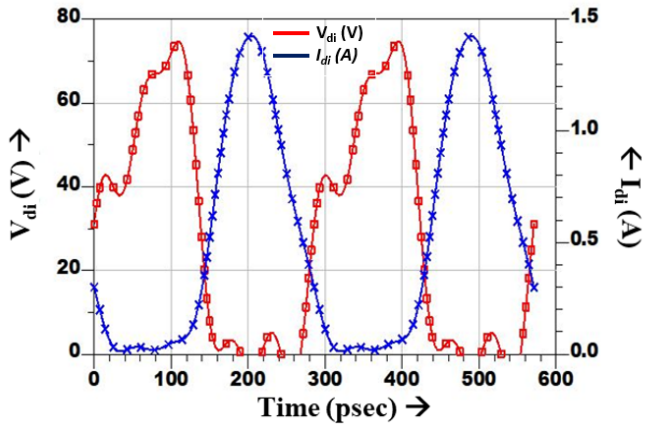

Fig. 5.19 Voltage and current waveform at the CG plane

Table 5.7 Comparison with previous high efficiency PAs

References	**Technique Used**	f_O **(GHz)**	**PAE (%)**	**DE (%)**	**Pout (dBm)**
(2009), [163]	2nd Harmonic Tuned	3.5	57.7	69.18	35.3
(2011), [149]	Class F	3.54	63	70	55
(2014), [173]	Resistive Loaded Harmonic Tuning	2.4	70	76	40.6
(2017), [174]	Low Pass Filter Matching Network	1.2	-	80	45
This Work	**Dual-band Output Network**	**3.5**	**75.1**	**79.4**	**40.7**

maximum measured PAE and DE are 75.1 % and 79.4 % respectively, while the gain is 10.8 dB. These are in good agreement with the corresponding simulation results.

5.4 Summary

RF power amplifier is a ubiquitous block, present in any RF front end, with various applications. This chapter discusses different classes of power amplifiers and their operation. The different traditional classes, including Class-A, B, AB and others, with their characteristics and performance, have been discussed with their pros and cons. Another class of power amplifiers is defined where harmonics at the drain of the transistor are tuned to reduce the overlap between current and voltage waveforms. This class, defined as Harmonic-tuned PA, can achieve theoretical efficiency of 100%. Although it is impossible to control an infinite number of harmonics, we propose a method that can tune either two or three harmonics of the amplifier to maximize the performance in terms of gain and efficiency. The two design methods to tune the three and two harmonics according to the load-pull have been presented. Design-1 described the technique to incorporate the tri-band impedance matching network to generate the desired impedance at the drain of the transistor. Similarly, design-2 utilizes the dual-band matching network to control the two harmonics to maximize performance. The closed-form design equations and mathematical formulations ease the design procedure with a reduction in form factor. Also, the prototype has been fabricated to validate the theoretical foundation with good agreement between simulated and measured results for both designs.

Chapter 6

Conclusions and Future Work

6.1 Conclusion

The exponential growth in the number of users increases the complexity of mobile devices because of the strong demand for high data rates. This results in more significant challenges from the engineering resource perspective. Communication based on the RF transceiver is one of the most significant examples of this challenging demand. Considering the RF front-end module with a multi-band platform is challenging as the constituent blocks have to operate on multiple frequencies simultaneously. With the evolution in telecommunication, researchers are moving from today's discrete solution toward multi-band or wideband solutions in which the RF transceiver module will support all available interface standards covering numerous frequency bands. In the multi-band RF front end, the design of multi-band or broadband modules, including matching networks, power amplifiers, dividers, couplers etc., is also challenging because it is tough to obtain optimum performance, and that too, at different frequencies of interest. This thesis demonstrates the design of passive and active circuits constituting the RF front end. The dual-band matching circuit and three design methodologies, including different scenarios, are discussed. The analysis, along with the closed-form design equations, is performed that ease the design part for easy fabrication. Unlike dual-

band matching networks, the broadband power dividers are focused. The few prominent characteristics of broadband power divider include simple and generalized mathematical analysis, fully Resistive isolation network, closed-form equations for determining the value of isolation resistor without involving optimization, flexible transmission bandwidth, sound isolation between two ports along with excellent port matching, ready scalability for DC blocking application that makes the design practical. The prototypes have been fabricated in both cases, demonstrating the effectiveness of the proposed design methods and several case studies. Another crucial active device, the power amplifier, is explored to achieve optimum performance in terms of gain, power added efficiency and drain efficiency. The multi-band matching network with its application in designing the output matching network of the power amplifier to achieve the optimum performance by tuning the harmonics is demonstrated. The designed output matching network can provide the performance well following the load-pull data, achieving good performance. The two design methods for designing a power amplifier by tuning either two or more harmonics are studied. The prototypes are developed along with measured results to verify the simulated design parameters and technique.

6.2 Future Work

The next-generation wireless system needs to accommodate new standards compared to the present scenario for providing more data rates with more standards. Therefore, the RF front end should be more complex than the present scenario. This thesis focuses on dual-band matching networks, broadband power dividers, and harmonically tuned power amplifiers with optimum performance. The future work of this research is discussed briefly:

- Designing of multi-band matching networks including tri/quad/penta-band designs. Since literature survey acknowledges the limitation of defined circuits with complicated mathematics and optimization algorithms. Hence, this area can be explored

further to improve the RF front end performance by reducing cost and form factor and simultaneously enhancing performance at multiple frequencies.

- The research can be focused on broadband designs for other circuits, including matching networks, power dividers, couplers etc, over a wide frequency range with excellent performance.

- The designing of the power amplifier is a challenging task as it is the most crucial block in any RF front end. The optimum efficiency, gain, and linearity performance are very demanding for any power amplifier. The multi-band power amplifiers are very limited in literature; hence multi-band matching networks can be the solution to design multi-band power amplifiers. These can be topics of interest for research since it is fascinating to obtain the optimum performance at different frequencies of operation simultaneously.

- Another vital area to be explored is to design a multi-band RF front end by cascading different multi-band circuitry with good performance.

References

[1] https://www.goodreads.com/quotes/1128396-this-change-in-the-conception-of-reality-is-the-most

[2] https://www.elon.edu/u/imagining/time-capsule/150-years/back-1870-1940/

[3] D. M. Pozar, "Microwave engineering", *John wiley & sons*, 2011.

[4] W. H. Hayt, J.E. Kemmerly, and S.M. Durbin, "Engineering Circuit Analysis (Eigth Edition)", 2006.

[5] A. A. Abidi,, "The path to the software-defined radio receiver", *IEEE Jour. of solid-state cir.*, vol.42, no. 5, pp. 954-966, 2007.

[6] J. Ryynanen, K. Kivekas, J. Jussila, A. Parssinen, and K. A. Halonen, "A dual-band RF front-end for WCDMA and GSM applications", *IEEE Jour. of solid-state cir.*, vol. 36, no. 8, pp. 1198-1204, 2008.

[7] https://www.nokia.com/networks/insights/spectrum-bands-5g-world/

[8] https://www.ceps.eu/5g-and-national-security/

[9] https://www.electronics-notes.com/articles/connectivity/wifi-ieee-802-11/channels-frequencies-bands-bandwidth.php

[10] J. Gubbi, R. Buyya, S. Marusic, and M. Palaniswami, "Internet of Things (IoT): A vision, architectural elements, and future directions", *Future generation computer systems*, vol. 29, no. 7, pp. 1645-1660, 2013.

[11] H. Okazaki, T. Furuta, K. Kawai, Y. Takagi, A. Fukuda, and S. Narahashi, "Reconfigurable RF circuits for future multi-mode multi-band mobile terminals", *IEEE Inter. Symp. on Electrom. Theory*, pp. 432-435.

[12] https://www.nxp.com/products/product- information/ip- blocklicensing/multiband-ism-transceiver-ip:MULTIBAND-ISM-TRANSCEIVER-IP.

[13] N. Cheng and J. P. Young, “Challenges and requirements of multimode multiband power amplifiers for mobile applications”, *IEEE Compound Semicond Integ Cir Symp (CSICS)*, pp. 1–4, 2011.
https://octopart.com/blog/archives/2019/10/rf-power-amplifiers-for-frequency-modulated-signals

[14] https://octopart.com/blog/archives/2019/10/rf-power-amplifiers-for-frequency-modulated-signals

[15] M. N. Sadiku, "Elements of electromagnetics", vol. 428. New York: Oxford university press, 2001.

[16] H.W. Bode, Network Analysis and Feedback Amplifier Design, Van Nostrand, 1945.

[17] S. Darlington, "Synthesis of Reactance 4-poles", *Bell Telephone*, 1939.

[18] R.M. Fano “Theoretical limitations on the broad-band matching of arbitrary impedances,” *J. Franklin Institute*, Vol. 249, Jan. 1950, pp. 57–83, and Feb. 1950, pp. 139-154.

[19] E. J. Wilkinson, "An N-Way Hybrid Power Divider", *IEEE Trans. Microw. Theory Tech.*, vol. 8, no. 1, pp. 116-118, Jan 1960.

[20] P. Colantonio, F. Giannini, and E. Limiti, "High efficiency RF and microwave solid state power amplifiers', *John Wiley and Sons*, 2009.

[21] Andrei Grebennikov, Nathan O Sokal, and Marc J Franco, "Switchmode RF and microwave power amplifiers", *Academic Press*, 2012.

[22] https://www.acquitek.com/product/403la-2/

[23] https://store.qorvo.com/products/amplifiers/rf-power-transistor

[24] J. J. Carr,"Secrets of RF circuit design", *McGraw-Hill Education*, 2001.

[25] Y. Chow and K. Wan, "A transformer of one-third wavelength in two sections-for a frequency and its first harmonic," *IEEE Microw Wireless Comp. Lett.*, vol. 12, no. 1, pp. 22–23, 2002.

[26] C. Monzon, "A small dual-frequency transformer in two sections," *IEEE Trans on Microw Th and Tech*, vol. 51, no. 4, pp. 1157–1161, 2003.

[27] J. O. Sophocles "A two-section dual-band Chebyshev impedance transformer", *IEEE Microw Wireless Comp. Lett.*, vol.13, no. 9, pp. 382–384, 2003.

[28] C. Giuseppe, V Fiumara, and I. M. Pinto. "A dual-band Chebyshev impedance transformer". *IEEE Microw Wireless Comp. Lett.*, vol. 39, no. 2, pp. 141–145, 2003. Dual-band impedance transformer using two-section

[29] Y. Wu, Y. Liu, and S. Li, "A compact pi-structure dual band transformer," *Progress In Electr. Research*, vol. 88, pp. 121–134, 2008.shunt stubs

[30] M. J. Park and B. Lee. “Dual-band design of single-stub impedance matching networks with application to dual-band stubbed T-junctions”. *IEEE Microw Wireless Comp. Lett.*, vol. 52, no. 6, pp. 1359 – 1362, 2010.

[31] M. A. Maktoomi and M. S. Hashmi. “A coupled-line based L-section DC-isolated dual-band real to real impedance transformer and its application to a dual-band T-junction power divider”. *Progress In Electr. Research*, vol. 55, pp. 95–104, 2014.

[32] R. K. Barik and S. Karthikeyan, “Dual-frequency impedance transformer using coupled-line for ultra-high transforming ratio,” *RADIO ENG.*, vol. 26, no. 4, p. 1067, 2017.

[33] X. Liu, Y.A. Liu, S. Li,F. Wu, and Y. Wu, ”A three-section dual-band transformer for frequency-dependent complex load impedance,” *IEEE Microw Wireless Comp. Lett.*, vol. 19, no. 10, 611-613, 2009.

[34] Y. Wu, Y. Liu, S.Li, C. Yu, and X. Liu, "A generalized dual-frequency transformer for two arbitrary complex frequency-dependent impedances", *IEEE Microw Wireless Comp. Lett.*, vol. 19, no.12, pp.792-794,2009.

[35] M.-L. Chuang, “Dual-band impedance transformer using two-section shunt stubs,”*IEEE Trans on Microw Theory and Tech*, vol. 58, no. 5, pp. 1257–1263, 2010.

[36] M. Nikravan and Z. Atlasbaf, “T-section dual-band impedance transformer for frequency-dependent complex impedance loads,” *Elect. Lett.*, vol. 47, no. 9, pp. 551–553, 2011.

[37] O. Manoochehri, A. Asoodeh, and K. Forooraghi. “π-Model Dual-Band Impedance Transformer for Unequal Complex Impedance Loads”. *IEEE Microw Wireless Comp. Lett.*, vol. 25, no. 4 pp. 238–240, 2015.

[38] X. Zheng, Y.A. Liu, S. Li, C. Yu, Z. Wang, and J. Li, "A dual-band impedance transformer using π-section structure for frequency-dependent complex loads", *Progress In Electr. Research*, vol. 32, pp.11-26, 2012.

[39] Y. Wu, W. Sun, S. W. Leung, Y. Diao, and K.H. Chan, "A novel compact dual-frequency coupled-line transformer with simple analytical design equations for frequency-dependent complex load impedance ", *Progress In Electr. Research*, 134, pp.47-62, 2013.

[40] M. A. Maktoomi, V. Panwar, M. S. Hashmi, and F. M. Ghannouchi,"A dual-band matching network for frequency-dependent complex loads suitable for dual-band RF amplifiers", *IEEE International Microwave and RF Conference (IMaRC)*, pp. 88-91, 2014.

[41] M. A. Maktoomi, M. S. Hashmi, and F. M. Ghannouchi. “A T-section dual-band matching network for frequency-dependent complex loads incorporating coupled line with DC-block property suitable for dual-band transistor amplifiers”. *Progress In Electr. Research*, vol. 54, pp. 75–84, 2014.

[42] M. A. Maktoomi, M. S. Hashmi, and V. Panwar. “A dual-frequency matching network for FDCLs using dual-band λ/4-lines”. *Progress In Electr. Research*, vol. 52, pp. 23–30, 2015.

[43] M. A. Maktoomi, R. Gupta, and M. S. Hashmi. “A dual-band impedance transformer for frequency-dependent complex loads incorporating an L-type network”. *Asia Pacific Microwave Conference (APMC)*, vol. 1, pp. 1–3, 2015.

[44] M. Maktoomi, M. Maktoomi, A. Yadav, M. Hashmi, and F. Ghannouchi, “Dual-frequency admittance property of two sections transmission-line and application,” *IEEE 59th International Midwest Symposium on Circuits and Systems (MWSCAS)*, pp. 1–4, 2016.

[45] M. Chongcheawchamnan, S. Patisang, M. Krairiksh, and I. D. Robertson, "Tri-band Wilkinson power divider using a three-section transmission-line transformer", *IEEE Microw Wireless Comp. Lett.*, vol. 16, no. 8, pp.452-454, 2006.

[46] S. Tanigawa, K. Hayashi, T. Fuji, T. Kawai, and I. Ohta," Tri-band/broadband matching techniques for 3-dB branch-line couplers", *European Microw. Conf. (EuMC)* pp. 560-563, 2007.

[47] W. Feng, Y. Zhao, W. Che, H. Chen, and W. Yang, "Dual-/tri-band branch line couplers with high power division isolation using coupled lines" *IEEE Trans on Cir and Sys II: Express Briefs*, vol. 65, no. 4, pp.461-465, 2017.

[48] X. H. Wang, L. Zhang, Y. Xu, Y. F. Bai, C. Liu, and X. W. Shi, "A tri-band impedance transformer using stubbed coupling line", *Progress In Electr. Research*, 141, pp.33-45, 2013.

[49] M. A. Maktoomi, R. Gupta, M. H. Maktoomi, M .S. Hashmi, and F. M . Ghannouchi, "A genaralized multi-frequency impedance matching technique", *16th Mediterranean Microwave Symposium (MMS)*, pp. 1-4, 2016.

[50] M. A. Maktoomi, M. S. Hashmi, A. P. Yadav, and V. Kumar, "A generic tri-band matching network", *IEEE Microw Wireless Comp. Lett.*, vol. 26, no.5, pp.316-318, 2016.

[51] S. Zhou, Y. Liu, X. Shen, Y. Wu, and W. Wang, "Dual-band impedance transformer using coupled line for arbitrary complex loads",IEEE Asia-Pacific Microwave Conference (APMC), Vol. 2, pp. 1-3, 2015.

[52] M. J. Park, B. Lee, "A dual-band Wilkinson power divider", *IEEE Microw. Wireless Compon. Lett.*, vol. 18, no. 2, pp.85-87, 2008.

[53] Y. Wu, Y. Liu, Y. Zhang, J. Gao, H. Zhou,"A dual band unequal Wilkinson power divider without reactive components", *IEEE Trans. Microw. Thry. Tech.*, vol. 57 , no. 1, pp.216-222, 2008.

[54] H. L. Zhang, B. J. Hu, X. Y. Zhang, "Compact equal and unequal dual-frequency power dividers based on composite right-/left-handed transmission lines," *IEEE Trans. Ind. Electron.*, vol. 59, no. 9, pp. 3464–3472, Sep. 2012.

[55] K. Al. Shamaileh, N. Dib, S. Abushamleh, "A dual-band 1:10 Wilkinson power divider based on multi-T-section characterization of high-impedance transmission lines," *IEEE Microw. Wireless Compon. Lett.*, vol. 27, no. 10, pp.897-899, 2017.

[56] L. Wu, Z. Sun, H. Yilmaz, M. Berroth,"A dual-frequency Wilkinson power divider, *IEEE Trans. Microw. Thry. Tech.*, Vol. 54, No. 1, p.p. 278 - 284, Jan. 2006.

[57] F. X. Liu, J. C. Lee, "Design of new dual-band Wilkinson power dividers with simple structure and wide isolation", *IEEE Trans. Microw. Thry. Tech.*, vol. 67, no. 9, pp.3628-3635, 2019.

[58] C. Pakasiri, S. Wang, “Dual-band compact wilkinson power divider using common inductor and complex load,” *IEEE Access*, vol. 8, pp. 97189–97195, 2020.

[59] N. Gao, G. Wu, Q. Tang, "Design of a novel compact dual-band Wilkinson power divider with wide frequency ratio", *IEEE Microw. Wireless Compon. Lett.*, vol. 24, no.2, pp.81-83, 2014.

[60] Y. Okada, T. Kawai, A. Enokihara, "Design Method for Multiband WPDs Using Multisection *LC*-Ladder Circuits", I*IEEE Microw. Wireless Compon. Lett.*, vol. 27, no. 10, pp.894-896, 2017.

[61] X. Wang, Z. Ma, M. Ohira, "Theory and experiment of two-section two-resistor Wilkinson power divider with two arbitrary frequency bands",*IEEE Trans. Microw. Thry. Tech.*, vol. 66, no.3, pp.1291-1300, 2017.

[62] W. Zhao, N. Zhang, B. Wu, X. Wang, Z, Ma, C.P. Chen," A Dual-Band Wilkinson Power Divider Using Dual Coupled Lines and Open Stubs", *IEEE MTT-S International Wireless Symposium (IWS)*, pp. 1-3, 2020.

[63] M. H. Maktoomi, D. Banerjee, M. S. Hashmi,"An enhanced frequency-ratio coupled-line dual-frequency Wilkinson power divider, *IEEE Trans. Circ. and Sys. II*, Vol. 65, No. 7, p.p. 888 - 892, Sep. 2017.

[64] A. Song, X. Wang, Z. Ma, M. Ohira, "Design theory of dual-band Wilkinson power divider with different frequency ratio ranges",*In IEEE Asia-Pacific Microwave Conference (APMC)*, pp. 1489-1491, 2020.

[65] Q.X. Chu, F. Lin, Z. Lin, Z. Gong, "Novel design method of tri-band power divider, *IEEE Trans. Microw. Thry. Tech.*, Vol. 59, No. 9, p.p. 2221 - 2226, Sep. 2011.

[66] B. M. Abdelrahman, H. N. Ahmed, A. I. Nashed, "A novel tri-band Wilkinson power divider for multiband wireless applications." *IEEE Microw. Wir. Compon. Lett.*, vol. 27, no. 10, 891-893, 2017.

[67] H. H. Chen, Y. H. Pang,"A tri-band Wilkinson power divider utilizing coupled lines," *IEEE Inter. Symp. on Ant. and Prop. (APSURSI)*, pp. 25-28, 2011.

[68] A. C. Papanastasiou, G. E. Georghiou, G.V. Eleftheriades, "A quad-band Wilkinson power divider using generalized NRI transmission lines", *IEEE Microw. Wir. Compon. Lett.*, vol. 18, no. 8, pp.521-523, 2008.

[69] H. J. Riblet, "General synthesis of quarter-wave impedance transformers", *IRE Trans. Microw. Thry. Tech.*, Vol. 5, No. 1, p.p. 36 – 43, Jan. 1957.

[70] P. K. Singh, S. Basu,Y. H. Wang, "Coupled line power divider with compact size and bandpass response" *Elect. Lett.*, vol. 45, no. 17, pp.892-894, 2009.

[71] Y. C. Li, Q. Xue, X. Y. Zhang, "Single-and dual-band power dividers integrated with bandpass filters", *IEEE Trans. Microw. Thry. Tech.*, Vol. 61, No. 1, p.p. 69 - 76, Jan. 2013.

[72] S. S. Gao, S. Sun, S. Xiao, "A novel wideband bandpass power divider with harmonic-suppressed ring resonator", *IEEE Microw. Wir. Compon. Lett.*, Vol. 23, No. 3, p.p. 119 – 121, Mar. 2013.

[73] K. Song, X. Ren, F. Chen, Y. Fan, "Compact in-phase power divider integrated filtering response using spiral resonator" *IET Microw., Ant. and Prop.*, vol. 8, no. 4, 228-234, 2014.

[74] J. Y. Shao, S.C.Huang, Y. H. Pang, "Wilkinson power divider incorporating quasi-elliptic filters for improved out-of-band rejection", *Elect. lett.*, vol. 47, no.23, 1288-1289, 2011.

[75] Q. Li, Y. Zhang, C.T.M. Wu, "High-selectivity and miniaturized filtering Wilkinson power dividers integrated with multimode resonators" *IEEE Trans. on Comp, Pack. and Manuf. Techno.*, vol. 7, no. 12, 1990-1997, 2017.

[76] X. Y. Zhang, K. X. Wang, B.J. Hu, "Compact filtering power divider with enhanced second-harmonic suppression", *IEEE Microw. Wir. Compon. Lett.*, vol. 23, no. 9 pp.483-485, 2013.

[77] Y. Liu, S. Sun, X. Yu, Y. Wu, Y. Liu, "Design of a wideband filtering power divider with good in-band and out-of-band isolations" *Inter. Jour. of RF and Micr. Comp.-Aided Engg.*, vol. 29, no.7, p.e21728, 2019.

[78] X. Wang, J. Wang, G. Zhang, J. S. Hong, W. Wu, "Dual-wideband filtering power divider with good isolation and high selectivity". *IEEE Microw. Wir. Compon. Lett.*, vol. 27, no. 12, pp.1071-1073, 2017.

[79] K. Song, Q. Xue, "Novel ultra-wideband (UWB) multilayer slotline power divider with bandpass response", *IEEE Microw. Wir. Compon. Lett.*, Vol. 20, No. 1, p.p. 13 - 15, Dec. 2009.

[80] X. Ren, K. Da. Xu, "Multilayer balanced-to-unbalanced power divider with wideband transmission characteristic and common-mode suppression", *IEEE Trans. Comp., Pack., Manf. Tech.*, Vol.9, No. 1, p.p. 72 - 79, Dec. 2018.

[81] H. Zhu, Z. Cheng, Y. J. Guo, "Design of wideband in-phase and out-of-phase power dividers using microstrip-to-slotline transitions and slotline resonators", *IEEE Trans. Micr. Th. Tech.*, Vol. 67, No. 4, p.p. 1412 – 1424, Apr. 2019.

[82] L. Guo, A. Abbosh, H. Zhu, “Ultra-wideband in-phase power divider using stepped-impedance three-line coupled structure and microstrip-to-slotline transitions,” *Elect. Lett.*, vol. 50, no. 5, pp. 383–384, Feb. 2014.

[83] J. X. Chen, C. H. K. Chin, K. W. Lau, Q. Xue, “180° out-of-phase power divider based on double-sided parallel striplines,” *Elect. Lett.*, vol. 42, no. 21, pp. 1229–1230, Oct. 2006.

[84] M. E. Bialkowski, A. M. Abbosh, “Design of a compact UWB outof-phase power divider,” *IEEE Microw. Wireless Compon. Lett.*, vol. 17, no. 4, pp. 289–291, Apr. 2007.

[85] U. T. Ahmed, A. M. Abbosh, “Wideband out-of-phase power divider using tightly coupled lines and microstrip to slotline transitions", *Elect. Lett.*, vol. 52, no. 2, pp. 126–128, 2016.

[86] Y. Liu, L. Zhu, S. Sun, "Proposal and Design of a Power Divider With Wideband Power Division and Port-to-Port Isolation: A New Topology", *IEEE Trans. Micr. Th. Techn.*, Vol. 68, No. 4, p.p. 1431 - 1438, Apr. 2020.

[87] D. Chen, L. Zhu, C. Cheng, “Dual-resonant-mode (DRM) impedance transformer and its application to wideband 3 dB power divider,” *IEEE Microw. Wireless Compon. Lett.*, vol. 23, no. 9, pp. 471–473, Sep. 2013.

[88] M. Weng, Y. Song, J. Zhao," Design of compact microstrip UWB power divider using square ring multiple-mode resonator" *Asia-Pacific Microw. Conf. (APMC)*, Vol. 1, pp. 1-3, Dec. 2015.

[89] H. Zhu, A. M. Abbosh, L. Guo, "Wideband four-way filtering power divider with sharp selectivity and wide stopband using looped coupled line structures", *IEEE Micr. Wir. Let.*, Vol. 26, No. 6, p.p. 413 – 415, Jun. 2016.

[90] L. Jiao, Y. Wu, Y. Liu, Q. Xue, Z. Ghassemlooy, "Wideband filtering power divider with embedded transversal signal-interference sections", *IEEE Microw. Wir. Compon. Lett.*, Vol. 27, No. 12, p.p. 1068 - 1070, Oct. 2017.

[91] K. Song, Y. Mo, Y. Fan, “Wideband four-way filtering-response power divider with improved output isolation based on coupled lines,” *IEEE Microw. Wireless Compon. Lett.*, vol. 24, no. 10, pp. 674–676, Oct. 2014.

[92] C.W. Tang, J. T. Chen, "A design of 3-dB wideband microstrip power divider with an ultra-wide isolated frequency band", *IEEE Trans. Microw. Thry. Tech.*, Vol. 64, No. 6, p.p. 1806 – 1811, Jun. 2016.

[93] L. Li, Z.F.Li, “Side-coupled shorted microstrip line for compact quasi-elliptic wideband bandpass filter design,” *IEEE Microw. Wireless Compon. Lett.*, vol. 20, no. 6, pp. 322–324, Jun. 2010

[94] K. D. Xu, Y. Bai, X. Ren, Q. Xue, "Broadband filtering power dividers using simple three-line coupled structures", *IEEE Trans. Compon., Packg., Manf. Tech.*, Vol.9, No. 6, p.p. 1103 - 1110, Sep. 2018.

[95] T.S. Dang, C. W. Kim, S. W. Yoon, "Ultra-wideband power divider using three parallel-coupled lines and one shunt stub", *Electr. Lett.*, vol. 50, no. 2 pp.95-96, 2014.

[96] L. Guo, H. Zhu, A. M. Abbosh, "Wideband tunable in-phase power divider using three-line coupled structure", *IEEE Microw. Wireless Compon. Lett.*, Vol. 26, No. 6, p.p. 404 – 406, Jun. 2016.

[97] X. Yu, S. Sun, "A novel wideband filtering power divider with embedding three-line coupled structures", *IEEE Access*, Vol. 6, p.p. 41280 – 41290, Jul. 2018.

[98] H. Oraizi, A. R. Sharifi, "Optimum design of asymmetrical multisection two-way power dividers with arbitrary power division and impedance matching," *IEEE Trans. Microw. Theory Techn.*, vol. 59, no. 6, pp. 1478–1490, Jun. 2011.

[99] S. W. Wong, L. Zhu, "Ultra-wideband power divider with good in-band splitting and isolation performances", *IEEE Microw. Wir. Compon. Lett.*, Vol. 18, No. 8, p.p. 518 – 520, Aug. 2008.

[100] Y. Xu, R. Bosisio, "Design of multiway power divider by using stepped-impedance transformers", *IEEE Trans. Microw. Thry. Tech.*, Vol. 60, No. 9, p.p. 2781 – 2790, 2012.

[101] M. A. Maktoomi, M. S.Hashmi, F. M. Ghannouchi, "Theory and design of a novel wideband DC isolated Wilkinson power divider", *IEEE Microw. Wir. Compon. Lett.*, Vol. 26, No. 8, p.p. 586 - 588, Jul. 2016.

[102] J. C. Kao, Z. M. Tsai, K. Y. Lin, H. Wang, "A modified Wilkinson power divider with isolation bandwidth improvement", *IEEE Trans. Microw. Thry. Techn.*, Vol. 60, No. 9, p.p. 2768 – 2780, Sep. 2012.

[103] V. Tas, A. Atalar, "An optimized isolation network for the Wilkinson divider", *IEEE Trans. Microw. Thry. Techn.*, vol. 62, no.12, pp.3393-3402, 2014.

[104] T. Yu, J. H. Tsai, Y. Chang, “A radial four-way power divider with the proposed isolation network,” *IEEE Microw. Wireless Compon. Lett.*, vol. 28, no. 3, pp. 194–196, Mar. 2018.

[105] X. Wang, I. Sakagami, A. Mase, M. Ichimura, “Wilkinson power divider with complex isolation component and its miniaturization,” *IEEE Trans. Microw. Theory Techn.*, vol. 62, no. 3, pp. 422–430, Mar. 2014.

[106] https://www.leedeforest.org/Home.html

[107] G. D. Ewing, "High-Efficiency Radio-Frequency Power Amplifiers", *Oregon State University*, 1964.

[108] N. O. Sokal and A. D. Sokal, "Class E – A New Class of High-Efficiency Tuned Single-Ended Switching Power Amplifiers", *IEEE Journal of Solid-State Circuits,* vol. SC-10, pp. 168–176, 1975.

[109] F. H. Raab, "Class-F power amplifiers with maximally flat waveforms", *IEEE Trans. Microw. Theory Techn.*, vol. 45, no. 11, 2007-2012, 1997.

[110] F. H. Raab, "Class-E, class-C, and class-F power amplifiers based upon a finite number of harmonics", *IEEE Trans. Microw. Theory Techn.*, vol. 49, no. 8, pp. 1462-1468, 2001.

[111] S. D. Kee, I. Aoki, A. Hajimiri, and D. Rutledge, "The class-E/F family of ZVS switching amplifiers", *IEEE Trans. Microw. Theory Techn.*, vol. 51, no. 6, pp. 1677-1690, 2003.

[112] S. Goto, T. Kunii, A. Ohta, A. Inoue, Y. Hosokawa, R. Hattori, and Y. Mitsui,"Effect of bias condition and input harmonic termination on high efficiency inverse class-F amplifiers", *IEEE Europ. Microw. Conf. (EuMC)* pp. 1-4, 2001.

[113] S. Gao, P. Butterworth, S. Ooi, and A. Sambell, "High-efficiency power amplifier design including input harmonic termination" *IEEE Microw. Wire. Compo. Lett.*, vol.16, no. 2, pp. 81-83, 2005.

[114] L. El Maazouzi, P. Colantonio, A. Mediavilla, and F. Giannini, "A 3.5 GHz 2nd harmonic tuned PA design", *IEEE Europ. Microw. Conf. (EuMC)*, pp. 1090-1093, 2009.

[115] A. Inoue, T. Heima, A. Ohta, R. Hattori, and Y. Mitsui, "Analysis of class-F and inverse class-F amplifiers", *IEEE MTT-S Inter. Microw. Symp. Digest (Cat. No. 00CH37017)*, Vol. 2, pp. 775-778, 2001.

[116] J. Moon, S. Jee, J. Kim, J. Son, S. Kim, J. Lee, and B. Kim," Investigation of a class-F-1 power amplifier with a nonlinear output capacitor", *IEEE 6th Euro. Microw. Integ. Cir. Conf.*, pp. 124-127, 2011.

[117] J. Moon, S. Jee, J. Kim, J. Kim, and B. Kim, "Behaviors of Class-F and Class-F^{-1} Amplifiers" *IEEE Trans. Microw. Theory Techn.*, vol. 60, no. 6, pp. 1937-1951, 2012.

[118] A. Dupuy, K. M. Leong, and T. Itoh, "Class-F power amplifier using a multi-frequency composite right/left-handed transmission line harmonic tuner" *IEEE MTT-S Inter. Microw. Symp. Digest*, pp. 2023-2026, 2005.

[119] A. Dupuy, A., Leong, K. M., R. Staraj, G. Jacquemod, and T. Itoh, "Inverse class-F power amplifier using composite right/left-handed transmission lines as a harmonic trap", *Euro. Microw. Conf.*, pp. 360-363, 2006.

[120] S. H. Kam, M. W. Lee, and Y. H. Jeong, "A high-efficiency inverse class-E power amplifier using double CRLH-TL for 3.5 GHz WiMAX applications", *IEEE Asia-Pacific Microw. Conf.*, pp. 279-282, 2011.

[121] X. P. Xiong, Y. L. Luo, Y. Zhang, X. L. Ma, P. C. Wu, and L. Chen, "A high-efficiency Class-F power amplifier using double CRLH-TL for LTE application", *15th Inter. Conf. Electr. Pack. Tech.*,pp. 1312-1315, 2014.

[122] F. M. Ghannouchi, M. M. Ebrahimi, and M. Helaoui, "Inverse class F power amplifier for WiMAX applications with 74% efficiency at 2.45 GHz", *IEEE Inter. Conf Comm. Workshops*, pp. 1-5, 2009.

[123] M. Helaoui, and F. M. Ghannouchi, "Optimizing losses in distributed multiharmonic matching networks applied to the design of an RF GaN power amplifier with higher than 80% power-added efficiency", *IEEE Trans. Microw. Theory Techn.*, vol. 57, no. 2, pp. 314-322, 2009.

[124] P. Saad, H. M. Nemati, M. Thorsell, K. Andersson, and C. Fager, "An inverse class-F GaN HEMT power amplifier with 78% PAE at 3.5 GHz",*Euro. Microw. Conf. (EuMC)*, pp. 496-499, 2009.

[125] K. Chen, and D. Peroulis, "A 3.1-GHz class-F power amplifier with 82% power-added-efficiency", *IEEE Microw Wireless Comp. Lett.*, vol. 23, no.8, pp. 436-438, 2013.

[126] M. Seo, H. Lee, J. Gu, H. Kim, J. Ham, W. Choi, and Y. Yang, "High-efficiency power amplifier using an active second-harmonic injection technique under optimized third-harmonic termination", *IEEE Trans. Cir. Sys. II: Express Briefs*, vol. 61, no. 8, pp. 549-553, 2014.

[127] M. Hayati, A. Sheikhi, and A. Grebennikov, "Class-F power amplifier with high power added efficiency using bowtie-shaped harmonic control circuit", *IEEE Microw Wireless Comp. Lett.*, vol. 25, no. 2, pp. 133-135, 2015.

[128] V. Carrubba, A. L. Clarke, M. Akmal, J. Lees, J. Benedikt, P. J. Tasker, S. C. Cripps, "The continuous class-F mode power amplifier", *40th Euro. Microw. Conf.*, pp. 1674-1677, 2010.

[129] N. Tuffy, L. Guan, A. Zhu, and T. J. Brazil, "A simplified broadband design methodology for linearized high-efficiency continuous class-F power amplifiers", *IEEE Trans. Microw. Theory Techn.*, vol. 60, no. 6, 1952-1963, 2012.

[130] V. Carrubba, M. Akmal, R. Quay, J. Lees, J. Benedikt, S. C. Cripps, and P. J. Tasker, "The continuous inverse class-F mode with resistive second-harmonic impedance", *IEEE Trans. Microw. Theory Techn.*, vol.60, no. 6, pp. 01928-1936, 2012.

[131] M. Yang, J. Xia, Y. Guo, and A. Zhu, "Highly efficient broadband continuous inverse class-F power amplifier design using modified elliptic low-pass filtering matching network",*IEEE Trans. Microw. Theory Techn.*, vol. 64, no. 5, pp. 1515-1525, 2016.

[132] W. Shi, S. He, and Q. Li, "A series of inverse continuous modes for designing broadband power amplifiers",*IEEE Microw. Wire. Compo. Lett.*, vol. 26, no. 7, pp. 525-527, 2016.

[133] P. H. Smith, "Electronic Applications of the Smith Chart: In waveguide, circuit, and component analysis", *SciTech Publishing*, 1995.

[134] D. Banerjee, A. Saxena, M. Hashmi and F. Ghannouchi, “A Compact Dual-Band Impedance Matching Network Based on All-Pass Coupled Lines,” *IEEE 61st Inter. Midwest Symp. on Cir. and Sys. (MWSCAS)*, pp. 937-939, 2018.

[135] R. Gomez-Garcia, F. M. Ghannouchi, N. B. Carvalho, H.C. Luong, "Guest editorial advanced circuits and systems for CR/SDR applications. *IEEE Trans. Emerg. Sel. Topics Circuits Syst.*, vol. 3, no. 4, pp. 485-488, Dec. 2013.

[136] W. Hallberg, M. Ozen, D. Kuylenstierna, K. Buisman, C. Fager, “A generalized 3-db wilkinson power divider/combiner with complex terminations,” *IEEE Trans. Microw. Theory Techn.*, vol. 66, no. 10, pp. 4497-4506, Oct. 2018.

[137] Y. Liu, "Synthesis techniques on multiband impedance matching networks for frequency-dependent complex loads" *IEEE Trans Microw. Theory Techn*, vol. 66, no. 10, pp.4507-4519, 2018.

[138] M .A. Maktoomi, M.S. Hashmi and F. M. Ghannouchi, "A dual-band port-extended branch-line coupler and mitigation of the band-ratio and power division limitations," *IEEE Trans. Comp., Pack., Manf. Tech.*, 2017; 7(8): 1313-1323.

[139] M. A. Maktoomi, M. S. Hashmi, "A performance enhanced port extended dual-band Wilkinson power divider", *IEEE Access* 2017; 5: 11832-40.

[140] B. Li, X. Wu, J. Yang, and W. Wu, "A defected-ground coupled line section with two shorts for wideband balun application", *IEEE Asia Pacific Micro. Conf.*, 2009; 2030-2032.

[141] J. S. Lim, C. S. Kim, D. Ahn, Y.C. Jeong, and S. Nam, "Design of low-pass filters using defected ground structure",*IEEE Trans. Microw. Thry. Tech.*, 2005; 53(8): 2539-2545.

[142] H. Oraizi, and M.S. Esfahlan, "Miniaturization of Wilkinson power dividers by using defected ground structures", *Prog. In Electro. Research*, 2008; 4: 113-120.

[143] M. A. Maktoomi, M. S. Hashmi, and F. M. Ghannouchi, "Theory and design of a novel wideband DC isolated Wilkinson power divider", *IEEE Microw. Wir. Compon. Lett.*, vol.26, no. 8, pp. 586-588, 2016.

[144] X. Yu, and S. Sun, "A novel wideband filtering power divider with embedding three-line coupled structures" *IEEE Access*, vol. 6, pp. 41280-41290, 2018.

[145] C. W. Tang, and J. T. Chen, "A design of 3-dB wideband microstrip power divider with an ultra-wide isolated frequency band", *IEEE Trans. Microw. Theory Techn.*, vol. 64, no. 6, pp. 1806-1811, 2016.

[146] K. Da Xu, Y. Bai, X. Ren, and Q. Xue, "Broadband filtering power dividers using simple three-line coupled structures" *IEEE Trans. Comp., Pack., Manf. Tech.*, vol. 9, no. 6, pp. 1103-1110, 2018.

[147] Y. Liu, L. Zhu, and S. Sun, "Proposal and design of a power divider with wideband power division and Port-to-Port isolation: A new topology", *IEEE Trans. Microw. Thry. Tech.*, vol. 68, no. 4, pp. 1431-1438, 2019.

[148] A. Grebennikov, and N. O. Sokal, "Switchmode RF Power Amplifiers", *Newnes, Newton*, MA, USA, 2007.

[149] J. H. Kim, G. D. Jo, J. F. Oh, Y. H. Kim, K. C. Lee, and J. H. Jung, “Modeling and design methodology of high-efficiency class-F and class-F^{-1} power amplifiers,” *IEEE Trans. Microw. Theory Techn.*, Vol. 59, No. 1, 153–165, 2011.

[150] A. A. Tanany, A. Sayed, and G. Boeck, “Analysis of broadband GaN switch mode class-E power amplifier", *Progress In Electro Research Lett.*, Vol. 38, 151–160, 2013.

[151] F. H. Raab, “Maximum efficiency and output of class-F power amplifiers,” *IEEE Trans. Microw. Theory Techn..*, Vol. 49, No. 6, 1162–1166, 2001.

[152] Y. Xu, J. Wang, and X. Zhu, “Analysis and implementation of inverse class-F power amplifier for 3.5 GHz transmitters", *Proc. Asia-Pacific Microw. Conf.*, 410–413, 2010.

[153] Y. S. Lee, and Y. H. Jeong, “A high-efficiency class-E GaN HEMT power amplifier for WCDMA applications,” *IEEE Microw Wireless Comp. Lett.*, Vol. 17, No. 8, 622–624, 2007.

[154] S. Gao, P. Butterworth, S. Ooi, and A. Sambell, "High-efficiency power amplifier design including input harmonic termination," *IEEE Microw Wireless Comp. Lett.*, Vol. 16, No. 2, 81–83, 2006.

[155] G. Liu, S. Li, Z. Cheng, H. Feng, and Z. Dong, "High efficiency broadband GaN HEMT power amplifier based on harmonic tuned matching approach," *Inter Jour of RF and Microw Comp Aided Engg*, Vol. 30, No. 2, e22097, 2020.

[156] A. Dani, M. Roberg, and Z. Popovic, "PA efficiency and linearity enhancement using external harmonic injection," *IEEE Trans. Microw. Theory Tech.*, Vol. 60, No. 12, 4097–4106, 2012.

[157] S. Jee, J. Moon, J. Kim, J. Son, and B. Kim, "Switching behavior of class-E power amplifier and its operation above maximum frequency," *IEEE Trans. Microw. Theory Tech.*, Vol. 60, No. 1, 89–98, Dec. 2011.

[158] Y. S. Lee, M. W. Lee, and Y. H. Jeong, "High-efficiency class-F GaN HEMT amplifier with simple parasitic-compensation circuit," *IEEE Microw Wireless Comp. Lett.*, Vol. 18, No. 1, 55–57, 2008.

[159] D. Banerjee, A. Saxena, and M. Hashmi, "A novel independent harmonic tuned two port output network for efficiency enhanced RF power amplifiers," *Microw. and Opt Techn. Lett.*, vol. 63, no. 2, pp.426-431, 2020.

[160] M. Kamiyama,I. Ryo, and H. Kazuhiko, "5.65 GHz high-efficiency GaN HEMT power amplifier with harmonics treatment up to fourth order," *IEEE Microw Wireless Comp. Lett.*, Vol. 22, No. 6, 315–317, 2012.

[161] P. Saad, H. M. Nemati, K. Andersson, and C. Fager, "Highly efficient GaN-HEMT power amplifiers at 3.5 GHz and 5.5 GHz," *Proc. IEEE WAMICON Conf.*, pp. 1–4, 2011.

[162] P. Colantonio, F. Giannini, R. Giofre, and L. Piazzon, "A design technique for concurrent dualband harmonic tuned power amplifier," *IEEE Trans. Microw. Theory Techn.*, Vol. 56, No. 11, pp. 2545–2555, 2008.

[163] L. El Maazouzi, P. Colantonio, A. Mediavilla, and F. Giannini, "A 3.5 GHz 2nd harmonic tuned PA design," *IEEE European Microw. Conf. (EuMC)*, 1090–1093, 2009.

[164] P. Saad,C. Fager, H. M. Nemati, H. Cao, H. Zirath, and K. Andersson, "A highly efficient 3.5 GHz inverse class-F GaN HEMT power amplifier," *Inter. Journal of Micro. Wireless Techno.*, Vol. 2, No. 3–4, pp. 317–24, 2010.

[165] F. M. Ghannouchi, and M. S. Hashmi, Load-pull Techniques with Applications to Power Amplifier Design, *Springer Series in Advanced Microelectronics*, 2013.

[166] F. Lin, C. X. Qing, and L. Zhe, "A novel tri-band branch-line coupler with three controllable operating frequencies," *IEEE Microw Wireless Comp. Lett.*, Vol. 20, No. 12, 666–668, 2010.

[167] L. Piazzon, P. Saad, P. Colantonio, F. Giannini, K. Andersson, and C. Fager, "Branch-line coupler design operating in four arbitrary frequencies," *IEEE Microw Wireless Comp. Lett.*, Vol. 22, No. 2, 67–69, 2012.

[168] D. Banerjee, A. Saxena, and M. S. Hashmi, "A novel concept of virtual impedance for high frequency tri-band impedance matching networks," *IEEE Trans. Circuits Syst. II, Exp. Briefs*, Vol. 65, No. 9, 1184–1188, 2018.

[169] X. Tang, and K. Mouthaan, "Compact dual-band power divider with single all pass coupled lines sections," *IET Elect. Lett.*, Vol. 46, No. 10, 688–689, 2010.

[170] M. W. Lee, Y. S. Lee, and Y. H. Jeong, "A high-efficiency GaN HEMT hybrid class-E power amplifier for 3.5 GHz WiMAX applications," *IEEE European Microw. Conf. (EuMC)*, 436–439, 2008.

[171] A. Saxena, and M. S. Hashmi, "A Tri-Band Impedance Transformer Based Output Network for Efficient RF Power Amplifiers", *Progress In Electrom. Research C*, vol. 106, pp.177-186, 2020.

[172] R. Gupta, A. Saxena, M. A. Maktoomi, and M.S. Hashmi, “An high impedance transformation ratio dual-band matching network with DC isolation capability,” *In 2017 IEEE Asia Pacific Microwave Conference (APMC)*, pp. 1069-1072, 2017.

[173] S. Preis, Z. Zhang, and M. T. Arnous, “Design of a GaN HEMT power amplifier using resistive loaded harmonic tuning,” *IEEE 9th European Microwave Integrated Circuit Conference*, pp. 552-555, 2014.

[174] K. Rabbi, J. Zhou, Y. Huang, Y. Zhuang, N. McEwan, A. Rayit, and R. Rayit. ”Highly efficient wideband harmonic-tuned power amplifier using low-pass matching network,” *IEEE 47th European Microwave Conference (EuMC)*, pp. 292-295, 2017.

Publications

- **A. Saxena**, M. Hashmi, D. Banerjee, and M.A. Chaudhary, “Theory and Design of a Flexible Two-Stage Wide band Wilkinson Power Divider”, Electronics, 10(17), p.2168, 2021.
- **A. Saxena**, D. Banerjee and M. S. Hashmi, " Theory and Design of a Coupled-Line Based Ultra-Wideband Wilkinson Power Divider" Journal of Communications Technology and Electronics, Vol. 66, Suppl. 2, pp. S69–S78, 2021.
- **A. Saxena** and M.S. Hashmi, “A Tri-Band Impedance Transformer Based Output Network for Efficient RF Power Amplifiers”, Progress In Electromagnetics Research C, vol. 106, pp. 177-186, 2020.
- **A. Saxena** and M.S. Hashmi, “A Simple Design Topology for a Harmonically Tuned RF Power Amplifier with Dual-band Output Network”, (submitted).
- **A. Saxena**, D. Banerjee, M.S Hashmi, “A Dual-Band Impedance Transformer for Matching Frequency Dependent Complex Source and Load Impedances”, 15th IEEE PRIME 2019, July 15 - 19,2019, Lausanne, Switzerland.
- **A. Saxena**, D. Banerjee, M.S Hashmi and F. Ghannouchi, “Design of Compact Dual-Band Matching Network using Single Unequal Susceptance Cancellation Stub”, 30th IEEE Asia-Pacific Microwave Conference (APMC), Feb. 6 - 9, 2018, Kyoto, Japan.

- **A. Saxena**, D. Banerjee, M.S. Hashmi, "Design of π-structure Dual-Band Matching Network with Unequal Susceptance Cancellation Stubs", IEEE MTT S International Microwave and RF Conference (IMaRC), Nov. 28-30, Kolkata, India.

Other contributions: Publications not included in this thesis

- **A. Saxena**, D. Banerjee, and M.S Hashmi, "A Novel Meandered Coupled-Line TriBand Impedance Matching Network", 24th IEEE National Conference on Communication (NCC), Feb. 25 - 28, 2018, Hyderabad, India.

- D. Banerjee, **A. Saxena**, and M. Hashmi, "A novel independent harmonic tuned two port output network for efficiency enhanced RF power amplifiers.," Microwave and Optical Technology Letters, 2020.

- D. Banerjee, **A. Saxena** and M.S. Hashmi, "A Novel Concept of Virtual Impedance for High Frequency Tri-Band Impedance Matching Networks", IEEE Transactions on Circuits and Systems-II: Express Briefs, Vol. 65, Iss.9, pp. 1184 - 1188, Sept. 2018.

- D. Banerjee, **A. Saxena** and M.S Hashmi, "A Novel Compact Tri-band Matching Network Utilizing Two Dual - Band Transformers at a Common Reference Frequency",29th IEEE Asia-Pacific Microwave Conference(APMC), Nov. 13 - 16, 2017, Kuala Lumpur, Malaysia.

- R. Gupta, **A. Saxena**, M.A Maktoomi and M.S Hashmi, "A High Impedance Transformation Ratio Dual-Band Matching Network with DC Isolation Capability", 29th IEEE Asia-Pacific Microwave Conference (APMC), Nov. 13 - 16, 2017, Kuala Lumpur, Malaysia.

- D. Banerjee, **A. Saxena** and M.S Hashmi, "A Novel Compact Tri-band Matching Network with Enhanced Frequency Ratios", IEEE-MTTS International Microwave and RF Conference (IMaRC), Dec. 11-13, 2017, Ahmedabad, India.

- D. Banerjee, **A. Saxena**, M.S Hashmi and F.M Ghannouchi, "A Compact DualBand Impedance Matching Network Based on All-Pass Coupled Lines", 61st IEEE Mid-West Symposium on Circuits and Systems (MWSCAS), Aug. 06 - 08, Windsor, Ontario, Canada.